

***The influence of epigenetic alterations on synaptic
function and memory***

Dissertation

for the award of the degree
“Doctor rerum naturalium”
of the Georg-August-Universität Göttingen

within the doctoral program Cellular and Molecular Physiology of the Brain,
GGNB of the Georg-August University School of Science (GAUSS)

submitted by
Henning Schroeder

from Aix-en-Provence

Göttingen 2021

Thesis Committee

Prof. Dr. André Fischer, Epigenetic mechanisms in brain diseases, Dep. of Psychiatry and Psychotherapy, University Göttingen

Dr. Camin Dean, Synaptic Dysfunction, DZNE/Charité, Berlin University of Medicine

Prof. Dr. Tiago Fleming Outeiro, Neurodegeneration and Neurorestoration, University Medical Center, Göttingen

Members of the Examination Board

Referee: Prof. Dr. André Fischer, Epigenetic mechanisms in brain diseases, Dep. of Psychiatry and Psychotherapy, University Göttingen

2nd Referee: Dr. Camin Dean, Synaptic Dysfunction, DZNE/Charité, Berlin University of Medicine

Further members of the Examination Board

Prof. Dr. Ralf Heinrich Dept. of Cellular Neurobiology, Schwann-Schleiden Research Center Georg-August-Universität, Göttingen

Prof. Dr. Tiago Fleming Outeiro, Experimental Neurodegeneration, University Medical Center, Göttingen

Prof. Dr. Thomas Dresbach, Dept. of Anatomy and Embryology, University Medical Center, Göttingen

Dr. Jan Clemens, Neural Computation and Behavior, European Neuroscience Institute, Göttingen

Date of oral examination 15.10.2021

Abbreviations	1
1. INTRODUCTION	2
1.1 <i>The physiological basis of memory</i>	2
1.2 <i>Epigenetic Influences on Transcription</i>	4
1.3 <i>BET chromatin readers in epigenetics and cognition</i>	10
1.4 <i>Scope of this thesis</i>	13
2. MATERIALS AND METHODS	13
2.1 <i>Mice</i>	13
2.1.1 Animal welfare	13
2.1.2 Brd2 and Brd4 cKO mice	14
2.1.3 Stereotactic intracranial injections	15
2.1.4 JQ1 injections	16
2.1.5 Intracardial perfusion	16
2.2 <i>Behavior</i>	16
2.2.1 General notes	16
2.2.2 Morris water maze	17
2.2.3 Fear conditioning	17
2.2.4 Open field test	18
2.2.5 Novel object recognition	18
2.2.6 Elevated plus maze	19
2.3 <i>Cell Culture</i>	19
2.3.1 Cell culture conditions	19
2.3.2 Etching and coating of coverslips	19
2.3.3 Coating of plates for cell culture	20
2.3.4 Primary hippocampal cultures	20
2.3.5 Calcium phosphate transfection	21
2.3.6 Viral transduction	21
2.3.7 RNA extraction from cell culture	22
2.3.8 Live cell calcium imaging	22
2.4 <i>Immunocytochemistry (ICC)</i>	23
2.4.1 Fixation	23
2.4.2 Immunostaining	24
2.4.3 Analysis of imaging data	24
2.4.4 Analysis of calcium imaging data	25
2.4.5 Perineuronal net (PNN) staining and analysis	25
2.5 <i>RNAseq</i>	26
2.5.1 RNA sequencing and mapping	26
2.5.2 Differential gene expression analysis and visualization of RNA sequencing data	26
2.6 Molecular Lab Work	27
2.6.1 Subcloning	27
2.6.2 qPCR	28
2.6.3 Nuclei FAC sorting using NeuN labeling and RNA extraction from tissue	29
2.6.4 Protein purification and western blots	29
2.6.5 Immunohistochemistry (IHC)	30

2.6.6 AAV preparation	31
3. RESULTS	32
3.1 Chapter 1 - cell culture optimization	32
3.1.1 Acquisition of neuronal enriched cultures	34
3.1.2 Optimization of cell health following GCaMP transduction	36
3.1.3 Automation of Ca ²⁺ imaging analysis	40
3.2 Chapter 2 – Brd2 KO in primary hippocampal cell culture	47
3.3 Chapter 3 – Behavior of Brd2 cKO and OE mice	57
3.4 Chapter 4 – Brd2 OE in primary hippocampal cell culture	70
3.5 Chapter 5 – Brd4 cKO and OE	84
3.6 Chapter 6 – Miscellaneous	94
3.6.1 TRPC6 forms condensed structures on the neurites of cultured primary hippocampal neurons	94
3.6.2 JQ1 could be a general stimulant independent of its BET-inhibiting properties	98
4. DISCUSSION	103
5. SUMMARY	116
References	119
Appendix	126
Acknowledgements	128
Curriculum Vitae	129

Abbreviations

AD	Alzheimers Disease	KO	Knock Out
BD	Bromodomain	LTD	Long-term depression
BET	Bromodomain and extra-terminal proteins	LTM	Long-term memory
Brd	Bromodomain-containing protein	LTP	Long-term potentiation
CA	Cornu Ammonis	MAPK	Mitogen-activated protein kinases
caMKII/IV	Ca ²⁺ /calmodulin-dependent protein kinase II/IV	mass spec	Mass spectrometry
ChIPseq	Chromatin immunoprecipitation sequencing	MWM	Morris Water Maze
cKO	conditional Knock Out	NOR	Novel Object Recognition
DG	Dentate Gyrus	OE	Over Expression
DIV	Day in vitro	OF	Open Field
DMEM	Dulbecco's modified Eagle medium, high-glucose	PCR	Polymerase Chain Reaction
DNA	Deoxyribonucleic acid	PM	Plating Medium
Dnmt	DNA methyltransferase	PRMT	Arginine methyltransferase
DPBS	Dulbecco's phosphate buffered saline	PT	Probe Test
ET	Extra-terminal domain	P-TEFb	Transcription elongation factor b complex
EtOH	Ethanol	qPCR	quantitative PCR
FC	Fear Conditioning	RNA	Ribonucleic acid
GluA1	Glutamate receptor 1	RNAseq	Ribonucleic acid sequencing
GO	Gene Ontology	ROI	Region of interest
H3, H4	Hsitone 3, Histone 4	STM	Short-term memory
HAT	Histone acetylase	TF	transcription factor
HDAC	Histone deacetylase	TSS	Transcription start site
HDM	Histone demethylase	vh	vehicle
HMT	Histone methyltransferase	WB	Western Blot
HPC	Hippocampus	WT	Wild Type
IP	intraperitoneal		

1. INTRODUCTION

1.1 The physiological basis of memory

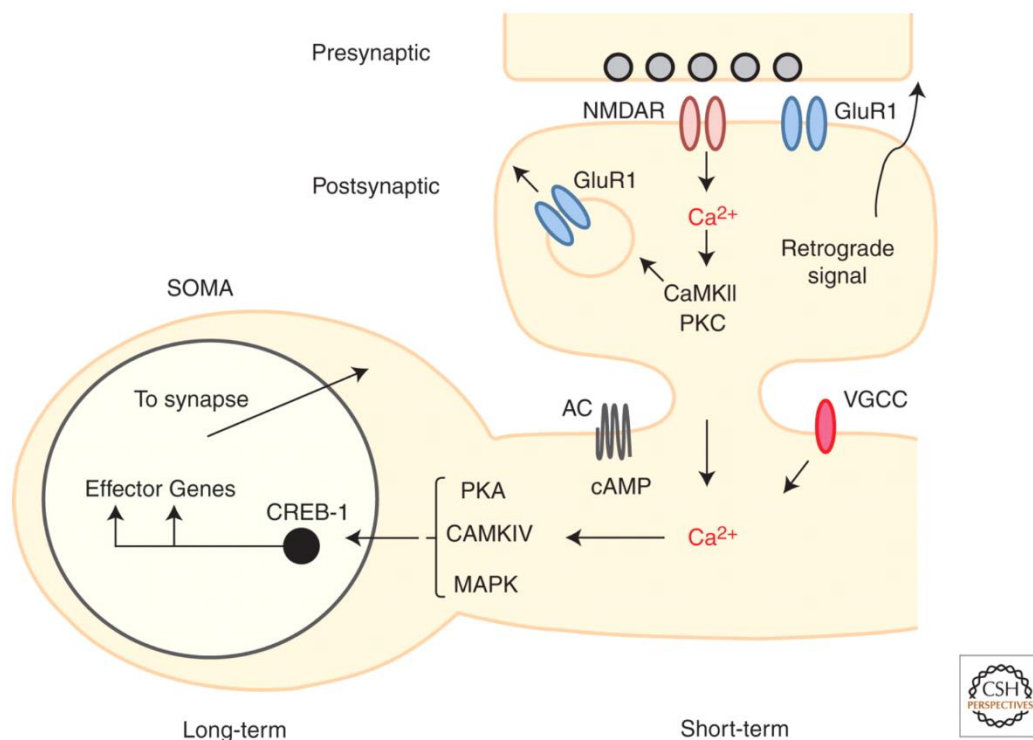
The physiological basis of memory formation and forgetting and therefore the phenomena known as learning are based on changes in synaptic strength. These changes depend on the synapse's activity and the resulting changes of its makeup. Changes in synaptic activity or inhibition of active synapses by other neurons (inhibitory synapses) can either increase or decrease synaptic strength which in turn means synapses are in a constant state of change in strength that allows for the modulation of memory formation and memory recall. This system is known as synaptic plasticity and allows neurons to retain, remove and modify information. For a memory to form and be retained different cascades must be activated in a stimulated neuron. The initiation of this process is dependent on two kinds of ionotropic receptors, namely α -amino-3-hydroxy-5-methyl-4-isoxazolepropionic acid (AMPA) and *N*-methyl-D-aspartate receptor (NMDA) receptors.

For the formation of an initial memory that can be recalled for several seconds, so-called „short term memory” (STM), relatively small-scale changes have to be made. These consist of the relocation of extra synaptic GluA1 (formerly GluR1) subunit-containing AMPA receptors to the postsynaptic density (PSD). For the transformation of STM into long term memory (LTM), which can be stored indefinitely, the strengthening of the synapse must be made permanent. This process, known as long term potentiation (LTP) depends on several cascades both in the post synapse itself and in the soma of the neuron. On the synaptic level the initial strengthening is caused by the release of glutamate by the pre-synapse into the synaptic cleft. Upon binding glutamate GluA1 changes conformation, allowing the influx of cations such as potassium, sodium, and calcium for about 1 ms. If this happens with a high enough frequency, the post synaptic membrane depolarizes, which then leads to the dispelling of Mg^{2+} ions from the NMDA receptors, leading to a conformational change and allowing influx of cations, most notably Ca^{2+} via NMDA receptors.

The repeated influx of Ca^{2+} ions upon stimulation and the resulting depolarization of the cell membrane at the PSD, leads to the phosphorylation of Ca^{2+} /calmodulin-dependent protein kinase II (CaMKII). CaMKII is, as its name suggests, is sensitive to calcium. When a CaMKII subunit binds a calcium ion (or calmodulin molecule), it is

phosphorylated at Threonine 286 which in turn raises the probability of neighboring subunits phosphorylating without binding a ligand first. Consequently, when a certain threshold is reached and enough of its subunits are phosphorylated, the complete protein autophosphorylates and switches to a permanently activated state. Activated CaMKII migrates to the PSD where it phosphorylates GluA1. This raises the sensitivity of affected AMPA receptors which in turn keeps the post synapse more excitable and therefore increases synaptic strength. While the autophosphorylation of CaMKII is reversible, higher sensitivity AMPA receptors leads to a higher probability of calcium influx, causing a higher rate of phosphorylated and therefore active CaMKII.

However, this process by itself is not sufficient for maintenance of LTP and therefore LTM. In order to strengthen a synapse permanently, synthesis of new protein is required. Mainly to replace the extra synaptic GluA1 that migrated to the PSD during the initial stage of LTP but also to provide further vesicle and receptor subunits as well as other proteins required for the strengthening of the PSD (Tao-Cheng, 2019). This in turn requires changes in transcription levels of the respective genes. While all involved pathways and mechanisms are not fully revealed yet, certain cascades have been identified and partly understood giving an insight into the connection between synaptic stimulation and transcriptional responses. The increase of Ca^{2+} influx and the resulting increase in adenylate cyclase (AC) activity in the neuron raises the levels of cyclic adenosine monophosphate (cAMP) in the cell. cAMP acts as a second messenger in CaMKII-containing neurons through recruitment of mitogen-activated protein kinase (MAPK) through protein kinase A (PKA). High levels of cAMP therefore lead to increased MAPK activation which causes the kinase to relocate to the nucleus where it is involved in the activation of transcription via the cAMP response element binding protein (CREB) mediated pathways (Fig. 1) (Bacskai et al. 1993; Martin et al. 1997; Kandel, 2001). This simplified example, while just depicting an aspect of what is required for LTP formation, shows that the function of synapses and therefore neurons are tightly bound to transcriptional activation and regulation. Without the appropriate changes in transcription LTM cannot form (Leal et al 2014; Leal et al. 2017) which makes transcriptional regulation an important field of research with respect to learning and memory and disturbances thereof.



Mark Mayford et al. Cold Spring Harb Perspect Biol 2012;4:a005751

©2012 by Cold Spring Harbor Laboratory Press

Figure 1: A schematic representation of LTM and STM on the cellular level. (source: <http://cshperspectives.cshlp.org/content/4/6/a005751/F3.expansion.htm>)

1.2 Epigenetic Influences on Transcription

In short, the term transcription refers to the process of transcribing the information found on DNA into RNA. In the case of gene transcription, which is as mentioned above necessary for LTP, the resulting RNA is referred to as messenger RNA (mRNA) that can be transported outside of the nucleus and translated into functional proteins (Fig. 2). In order for this to happen some basic requirements need to be fulfilled. In general, the gene and its promoter need to be accessible so transcription factors (TF) can bind. TFs are a group of mostly highly conserved molecules that fulfill a variety of DNA binding triggered functions. TFs recognize specific sequences on the DNA. In the case

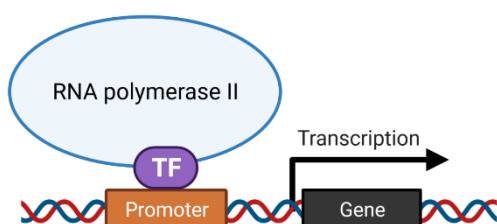


Figure 2: A representation of transcriptional activation through transcription factor (TF) binding. (Created with BioRender.com)

of initiating gene transcription this would be a promotor, a sequence physically close to a related gene body. The TF binding initiates transcription via facilitating the recruitment of RNA Polymerase II (Pol II) -the protein responsible for synthesizing RNA based on the respective gene out of loose nucleic acids -to the transcription start side (TSS) of the gene. TFs can require activation, removal of inhibition, or targeted localization to function and, like all proteins, their abundance is bound to the expression level of their respective genes. Taking into account that the term TF, besides proteins that facilitate the transcription of certain genes, also encompasses repressors that fulfill the opposite function, together with the many ways they can be regulated in their function, it is unsurprising that they play a central role in the regulation of gene expression and the influence thereof by outside factors such as stimulation.

Processes and factors that surround the DNA and govern gene expression in a tight and precise manner without changing the genes sequences themselves are summarized under the term „Epigenetics“, a chimera of the word „epi“ (greek for upon, around, on top) and genetics. Since the expression levels and timepoints of certain genes determine cell identity and fate, epigenetic regulation represents the keystone on which a multi-cellular organism is built and maintained. Epigenetic regulation happens on different levels of complexity with very direct and monocausal as well as very general effects on the expression of a few, very specific or several genes.

The first epigenetic mechanisms discovered were the methylation of DNA itself which is governed by two classes of proteins called DNA methyltransferases (Dnmts). Dnmts either facilitate the de novo methylation of DNA (e.g. Dnmt3a and b) or „copy“ the methylation of a site onto the daughter strand of DNA during replication (Dnmt1), which means the DNA methylation pattern is inherited by the new cell (Moore et al. 2013).

This process is always carried out on the fifth carbon of cytosine residues, by transferring a methyl group from the donor S-adenyl methionine (SAM) and plays a major role in repression of gene expression by preventing the binding of TFs to DNA. In the mammalian genome it represents an essential mechanism to silence potentially harmful genetic regions such viral transposable elements the DNA acquired over the course of an organism's evolution. These regions are often hyper methylated throughout an organism's life cycle. DNA methylation drastically raises the chance of deamination of the affected cytosine. This in turn raises the probability of point mutation drastically which can potentially render these viral transposable elements harmless

over time. The repressive function of DNA methylation is not limited to promoter methylation which prevents TF binding. It can also be recognized by reader proteins (MBD, UHRF and the zinc-finger proteins) with additional transcription repressing or DNA methylation facilitating features. DNA methylation patterns and the proteins governing it have been shown to play a role in learning and memory in the adult brain. Due to their influence on transcription and the changes required therein for synaptic strengthening this points to a strong connection between epigenetics and LTM. This line of thought is supported by the fact that DNA methylation levels in the human brain are the highest of any tissue, underlining their relevance for neuronal cell function.

On the most basic level the accessibility of genes themselves are also regulated epigenetically. In the cell nucleus of eukaryotes, such as humans, DNA is stored in a condensed supercoiled structure called chromosomes which consists of chromatin (Fig. 2). Chromatin in turn consists of DNA and associated proteins such as histones, barrel shaped protein octamers (Fig. 3A). One histone with the associated DNA wrapped around it (approximately 1.7 turns or 150bp) is referred to as a nucleosome (Fig. 3B). When nucleosomes are tightly packed, chromatin is referred to as heterochromatin. In this state genes are not accessible by Pol II and cannot be transcribed (Fig. 3A).

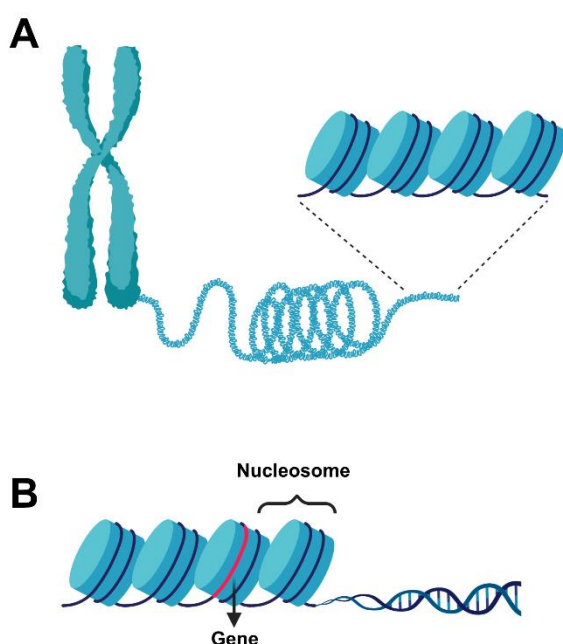


Figure 3: A: A chromosome and its subunits, the nucleosomes. **B:** Nucleosomes consisting of histones and DNA. (Created with [BioRender.com](https://www.biorender.com))

By methylating certain histone tails - long, linear sections of the protein - the positive charge of the histone is neutralized which cancels the attraction between it and the negatively charged DNA. This allows TFs and Pol II access to genes silenced this way, enabling transcription (Fig. 4). This „open“ chromatin state is referred to as heterochromatin.

Since cells must constantly produce certain proteins to maintain their homeostasis, chromosomes are usually partially in an open and closed state at the same time with the exception of mitosis or meiosis.

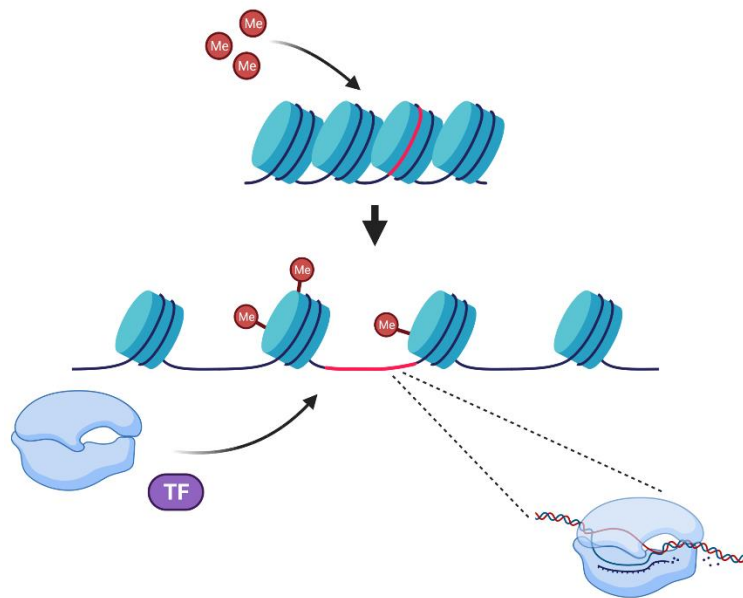


Figure 4: Histone methylation can negate the attraction between histones and DNA, allowing transcription factors (TFs) to bind, leading to transcription of otherwise inaccessible genes by RNA Pol II. (Created with [BioRender.com](https://www.biorender.com))

It must be mentioned that not all histone methylations have the same effect. Based on which histone tail is methylated and if it is mono or poly methylated, gene transcription may also be repressed (e.g. dimethylation of H3K9 or trimethylation of H3K27 Gupta et al. 2010, Hyun et al. 2017) as well as enhanced (e.g. trimethylation of H3K4). This can additionally be influenced by the methylation or acetylation state of surrounding histone tails. Acetylation represents another kind of histone tail modification that works to a similar effect of methylation with the difference that acetylation only occurs on lysine residues and only in the form of monoacetylation.

The addition or removal of histone modifications is regulated by protein classes named after their functions, histone methyltransferases (HMT), demethylases, histone deacetylases (HDACs) and histone acetyltransferases (HATs). In contrast to methylases which are classified by their affinity for either lysine or arginine residues, HATs are roughly separated into class A, whose members are found in the nucleus and class B, whose members are located in the cytoplasm of the cell. In general, class B HATs exclusively recognize their target lysine residues in newly translated histones

and acetylate those before the protein enters the nucleus where it is integrated into the chromatin. Certain class A HATs are additionally able to bind acetylated lysines via a specific domain (bromodomain) enabling them to acetylate target lysine residues in the periphery of their binding site. This hints at an interplay of class A and class B HATs allowing for a very versatile and fine regulation of chromatin marks, structure and state, driven by factors outside and inside the nucleus. Like DNA methylation, histone acetylation and methylation patterns, while subject to constant change, are inherited by the next generation of cells after cell division. The fact that certain HMTs and Dnmts as well as DNA methylation readers, HDACS, and HATs have been shown to associate in order to regulate gene expression further underlines that epigenetic mechanisms do not exist in isolation but are strongly dependent on each other.

The cause of differences in effects propagated by different levels and kinds of histone modifications does not lie only in the neutralization of histone charge and therefore attraction to the backbone of DNA in direct proximity. In fact, many histone modifications do not change the overall charge of the affected histone.

The reason the finely regulated and highly diverse epigenetic code is maintained and changed by the above-mentioned writers and erasers is the existence of chromatin readers (Fig 5).

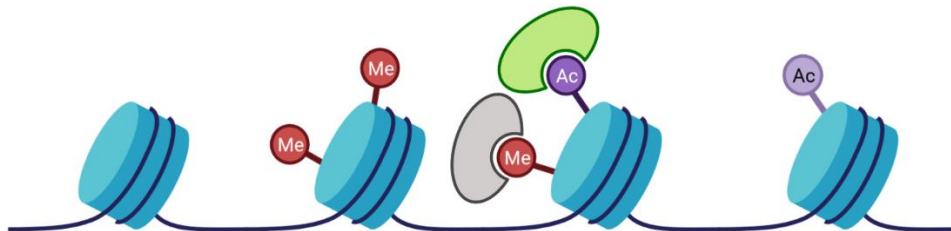


Figure 5: Histone modifications can be bound or “read” by specific proteins called chromatin readers. (Created with [BioRender.com](https://www.biorender.com))

These proteins recognize specific methylated or acetylated residues, therefore „reading“ the epigenetic code. While they themselves are not necessarily enzymatically active, they can facilitate, among other things, the enhancement or repression of transcription by functioning as a tether or scaffold between the transcriptional machinery and the respective histone mark (Fig 6). Even though their binding sites are specific one should keep in mind that the overall structure of chromatin can allow

interaction from bound proteins with elements on the DNA hundreds of bp up- or downstream from their own position (Crump et al. 2021).

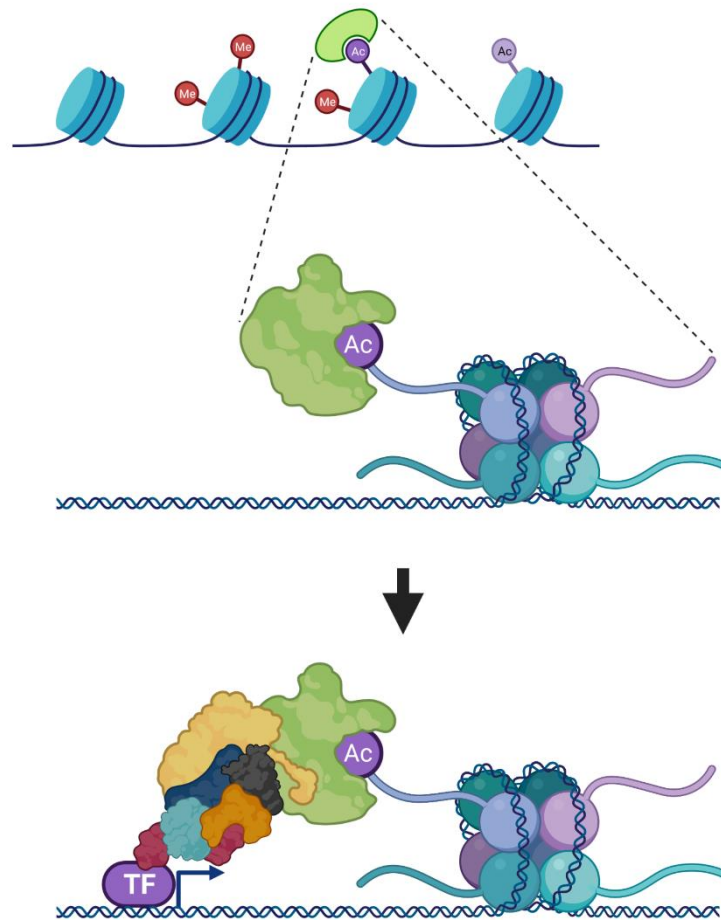


Figure 6: Facilitation of a transcription activating protein complex by a chromatin reader. (Created with [BioRender.com](https://www.biorender.com))

Due to their mode of action the function and activity of chromatin readers, as with the other classes of epigenetically relevant proteins mentioned above, are dependent on the chromatin state and interconnected with the other factors influencing it, which adds a regulatory layer to the complex machinery governing transcription (Fig. 7). The fact that they act as translators of the epigenetic code has made chromatin readers potential targets for drug-based intervention over the last decade, mostly in their relation to the expression of cancer related genes. Their role in neurological diseases in relation to memory formation however remains only partly understood despite their known function of linking outside stimuli to transcriptional changes.

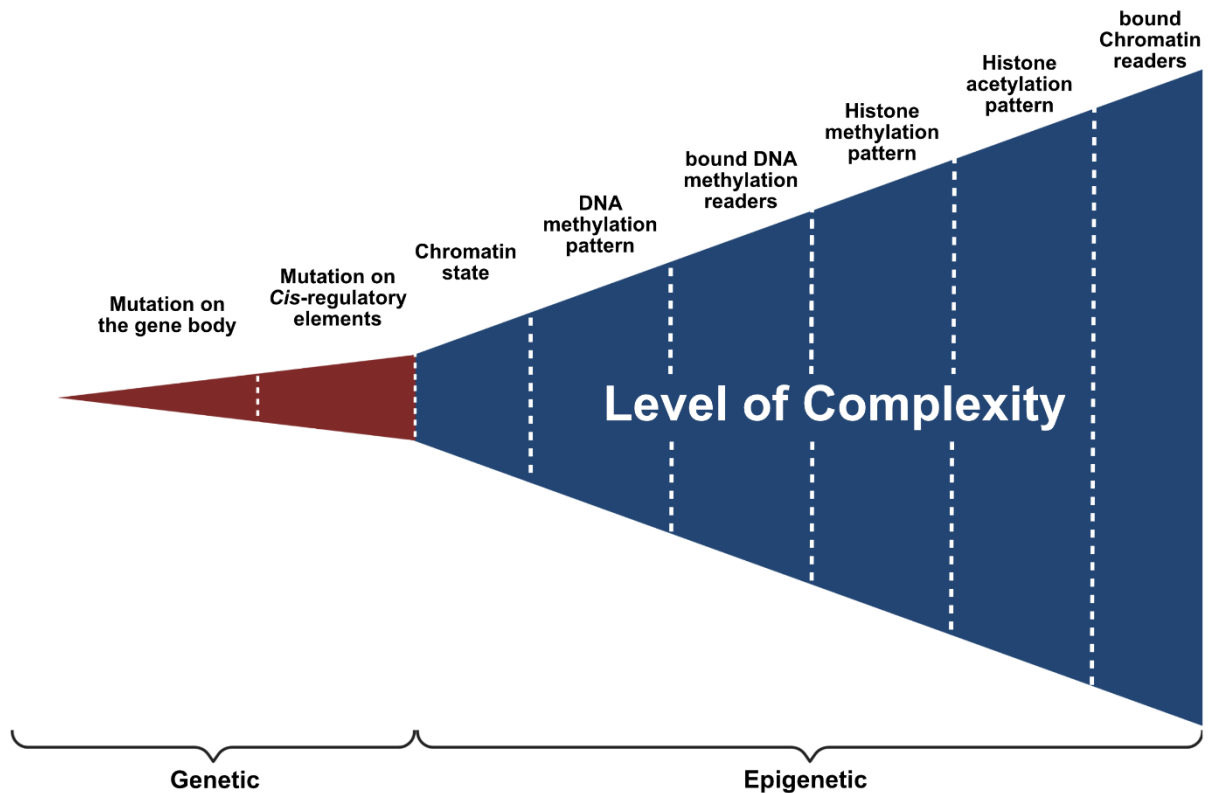


Figure 7: Depiction of the different enhancing or suppressing influences on gene transcription at the chromatin level.

1.3 BET chromatin readers in epigenetics and cognition

The main focus of this work is the role of a specific group of chromatin readers, named Bromodomain and Extra-Terminal motif (BET) proteins. Like certain HATs, BETs bind specific lysine residues via their bromodomain. Unlike HATs, as chromatin readers, they do not influence the surrounding chromatin directly, but indirectly through interaction with other proteins. Their histone interacting regions, twin bromodomains (BDs), are evolutionarily conserved, 110 amino acid motifs, which are found in a variety of chromatin-associated proteins, such as HATs (GCN5, PCAF), methyltransferases (MLL, ASH1L), helicases (SMARCA), ATP-dependent chromatin remodeling complexes (BAZ1B), transcriptional mediators (TAF1) transcriptional co-activators (TRIM/TIF1) as well as nuclear-scaffolding proteins (PB1) (Muller et al. 2011). Their unique structure consists of two N-terminal bromodomains, an extra-terminal domain (ET), a C-terminal recruitment motif also called C-terminal domain (CTM or CTD) as well as a small, conserved region called motif B (Fig. 8).

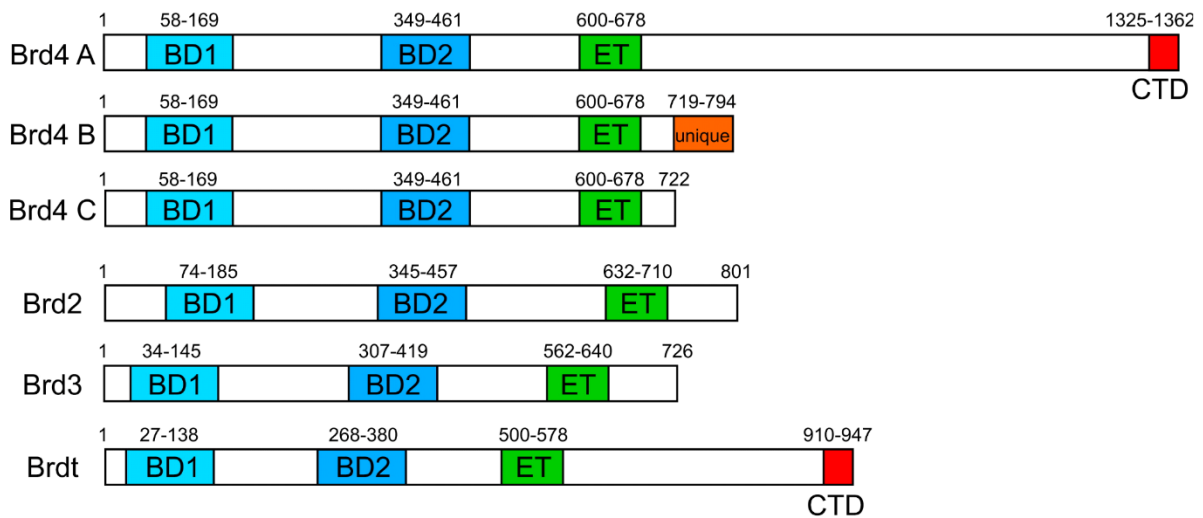


Figure 8: Depiction of the primary structure of different BET chromatin readers (from Molecular Cell 2014 54728-736DOI: (10.1016/j.molcel.2014.05.016)). All members share two bromodomains (BD) and an extra-terminal domain.

While the two bromodomains recognize certain acetylated lysine sites in histones (Filippakopoulos et al. 2010; Muller et al. 2011), the CTD binds different interaction partners that are able to influence or interact with the surrounding chromatin structure. Examples of BET interaction partners from the literature are transcription factors (e.g. P-TEF β , E2F, ERG), members of mediator complexes (e.g. CDK8) as well as polymerases (e.g. Pol II) as well as HDACs (e.g. HDAC1). Motif B is required but not sufficient for BET proteins to form hetero- or homodimers and is indicated to be essential for BD function with respect to chromatin association (Garcia-Gutierrez et al. 2012).

With this overall structure it is unsurprising that BET-binding sites are often found on or in close proximity to highly and moderately expressed genes. Four members of the BET family are described in *homo sapiens* and *mus musculus* at the point of this work, namely Brd2, Brd3, Brd4 and the testis-specific Brdt (Fig. 8). While BET gene bodies look distinctively different between species, the primary structures of the proteins are highly conserved and over 95% identical for some of the family members with up to 100% sequence similarity in the active regions.

BET proteins are important cell cycle proteins and have been shown to play a major role in cancer, inflammatory response, diabetes, and apoptosis. Some reports have linked them to autism spectrum disorder (ASD) and formation of addiction (Nicodeme et al. 2010; Muller et al. 2011; Sartor et al. 2015; Sullivan et al. 2015). Despite some

hints of their fundamental importance for brain development (Houzelstein et al. 2002; Shang et al. 2009), the exact function of BET proteins in cognition remains understudied to this date.

In a previous mouse study (Benito et al. 2017) we investigated the effect of inhibition of BET histone binding, specifically in Brd4 and to less extent in Brd2, on memory formation. By injecting the small molecule BET inhibitor JQ1 or vehicle solution after training sessions we could show that JQ1 injected mice had a better memory recall in spatial and fear memory tasks, suggesting a link between BET chromatin interaction and memory formation. This was further supported by RNAseq showing changes in the expression of synaptic genes and an LTP enhancing effect of JQ1 in hippocampal brain slices from mice, suggesting that BET inhibition influences brain function on a transcriptional as well as a physiological level. For this reason, our further investigations presented here are focussed on these BET members. Relatively recent studies by other groups had implied that Brd4 does play a role in formation of memory (Korb et al. 2015). The exact mechanisms by which the BET proteins govern this effect in neurons, however, were not identified. It is also unclear in which specific brain regions and which cognitive tasks Brd4 would be relevant. Another BET protein present in the brain, Brd2, is highly expressed in many developing tissues of the mouse nervous system and plays a crucial role in neuronal development most specifically the formation of the neuronal tube in mouse embryos (Gyuris et al. 2009; Shang et al. 2009). It is therefore unsurprising, that full body Brd2 knockout mice do not survive embryogenesis (Gyuris et al. 2009; Shang et al. 2009). This is also true for Brd4 (Houzelstein et al. 2002).

There are a few reported cases of polymorphisms in the human Brd2 gene that could be linked to common juvenile myoclonic epilepsy (Cavalleri et al. 2007; Layouni et al. 2010) and photoconvulsive response on EEGs (Lorenz et al. 2006). Both Brd2 and Brd4 bind more than one acetylated histone mark; more specifically the acetylated lysine residues H4K5, H4K12, H4K14 for Brd2 and H3K14, H4K5 as well as H4K12 for Brd4. There is experimental evidence for both Brd2 and Brd4 playing a crucial roles in transcriptional activation and RNA polymerase II elongation (LeRoy et al. 2008; Umehara et al. 2010), therefore connecting external influences to transcriptional changes. Since changes in H4K12 acetylation levels, a mark both BETs bind, have been linked to age-associated memory impairments in mice (Peleg et al. 2010), Brd2

or Brd4 or both are possible options for at least partially tying synaptic stimulation to transcription and phenotypic changes that drive LTP and consequently LTM formation.

1.4 Scope of this thesis

In earlier studies we found the application of a BET inhibitor enhanced learning performance in mice. However, JQ1, the inhibitor in question, is neither suited for clinical application due to its limited shelf life nor specific for a single BET chromatin reader. Consequently, the aim of this thesis was to identify the role single BETs play in learning and memory contexts in mice, how this is tied to the effect they have on transcriptional regulation, and finally to find out if one of them could serve as a potential specific candidate for targeted inhibition to recreate the learning enhancement effect we observed with JQ1 treatment. To test this we performed behavioral experiments with conditional KO lines of Brd2 and Brd4 in combination with qPCR, next generation sequencing, as well as phenotypic analysis performed on primary hippocampal neurons via ICC and calcium imaging.

2. MATERIALS AND METHODS

2.1 Mice

2.1.1 Animal welfare

Animals used in all studies related to this thesis were bred and housed under standard laboratory conditions in a 12 h light cycle with food and water available ad libitum. KO lines were bred in-house and mice were kept in groups of up to five with same sex littermates until used for experiments. In preparation for behavioral studies animals were separated into single cages and relocated to a separate holding room at least one week before experimental onset. If not stated explicitly otherwise in the results, mice used for experiments were 12 weeks of age and male. Pregnant females intended for hippocampal primary cultures were housed in groups of two until dissection. All experiments performed in the course of this thesis complied with national animal care guidelines and were approved by the animal welfare office in the state of lower saxony (LAVES).

2.1.2 Brd2 and Brd4 cKO mice

All animals were backcrossed to a B6J background (Charles River) for ten generations before being used in experiments. Conditional knockout mice were created in-house by crossing B6J mice expressing cre recombinase or a tamoxifen activatable ERTcre fusion construct (B6;129S6-Tg (Camk2a-cre/ERT2)1Aibs/J; JAX) under the CaMKII promoter with mouse lines generated by TACONIC BIOSCIENCES, INC. that had loxP sites flanking either exon 2 and 3 (Brd2) or exon 3 and 4 (Brd4) of the respective BET. Transgenic mice were genotyped at P21. DNA for genotyping was acquired from a piece of tissue from ear punches used for animal identification. The tissue was lysed by adding 50 μ l Alkaline Lysis Buffer (25mM NaOH, 0.2 mM EDTA in ddH₂O) and incubating at 95°C while shaking at 1000 rpm for 10 minutes on a Eppendorf Thermomixer. Subsequently, samples were put on ice and 50 μ l of neutralization buffer (40mM Tris HCl in ddH₂O) was added. 1 μ l of the resulting solution was then either directly used for genotyping or stored at -20 °C for later use. Animals with inducible ERTcre were given one gram Tamoxifen (MedChemExpress) per ten grams of bodyweight dissolved in sunflower oil and administered via oral gavage three times equally distributed over the course of five days at nine weeks of age.

Reagent	Amount in μ l
H ₂ O	13.4
5X Ph. Reaction Buffer	4
10mM dNTPs	0.4
primer F (10 μ M)	0.5
primer R (10 μ M)	0.5
DNA Template	1
Phire Hot Start II	0.2

Step	Temp. in °C	Time (min)	
Initial Denaturation	98	2:00	
Denaturation	98	0:10	40x
Amplification	55	0:15	
Elongation	72	0:30	
Final Elongation	72	5:00	

Name	Sequence
Brd2 FW hs 3	TGCTTCCTTTTCGTTTAGTTGAG
Brd2 RV hs 2	AAACCCTGTCTCCATAACAAG
Brd4 FW hs 2	GACTTGCTGTCATTCCATCTG
Brd4 RV hs 3	AACTCCTCACTCAGATACAGAC
Cre FW hs 3	CGATGCAACGAGTGATGAG
Cre RV hs 2	CCCAGAAATGCCAGATTACG

Table 1: Genotyping PCR protocol for BET cKO mice and primers.

2.1.3 Stereotactic intracranial injections

Injection of adeno-associated virus (AAV) for Brd2 OE experiments were made into the lateral ventricle ventral to the dentate gyrus (DG) of ten-week-old male mice. The animals were anesthetized via intraperitoneal injection (IP) (NaCl 0.9 % 164 μ l, Ketamin 20 μ l, Xylarem 16 μ l; 100 μ l/10g bodyweight) and given Buprenorphine as analgesic via the same delivery method (NaCl 0.9 % 470 μ l, Buprenorphine 30 μ l; 50 μ l/mouse). After testing the paw withdrawal response, the head of the mouse was fixated in a 3-point stereotaxic setup. To expose the skull, the cranial skin was removed in a longitudinal incision, followed by the drilling of holes for injection bilateral symmetrically relative to the bregma (mediolateral: +/- 1mm; anteroposterior: - 1.75mm). The solution containing viral particles was injected via glass capillaries. To minimize gas compression during injection, capillaries were first filled with mineral oil, then washed with 2100 nl DPBS before being loaded with 2000 nl viral solution (AAV in DPBS). The capillary was then lowered 2 mm at 0.01mm/s on the dorsoventral axis into the brain until the lateral ventricle was reached. After three minutes to let the tissue settle and engulf the foreign body, 900 nl viral solution was injected at a rate of 250 nl/min. After another three-minute pause to allow diffusion of the virus, the capillary was retracted at the same speed as insertion. The process was then repeated on the other hemisphere after which the cranial skin was reattached and sealed using polyacryl glue and the mouse placed on a heating mat to ensure body temperature would not drop. After the glue dried an anti-Sedative (NaCl 0.9% 190 μ l, Antipemazol 10 μ l, 50 μ l/10g bodyweight) was injected intraperitoneally to terminate the anaesthesia. Animals were housed in single cages post operation to avoid fights for dominance that occur between male mice after longer separation periods.

2.1.4 JQ1 injections

JQ1 passes through the blood brain barrier (Korb et al. 2015), therefore all injections could be carried out by IP. The injections were prepared by dissolving JQ1 in DMSO and diluting this solution 1:10 in 10% beta-cyclodextrin. Injection amount was adjusted to the individual weight of the mouse at 50 ng/g of bodyweight.

2.1.5 Intracardial perfusion

Animals were IP injected with a lethal dose of Ketamine solution (NaCl 0.9% 30 µl, Ketamine 20 µl, Xylarem 150 µl) at 100µl/10g body weight. As soon as the paw withdrawal reflex test was negative, the animal was pinned to a dissection board, its ribcage sprayed with 70% EtOH and opened via a V-cut to expose the heart. The right ventricle was then carefully nicked to the point that blood could exit. The left ventricle was penetrated with a butterfly cannula (Braun Melsung) to allow for perfusion via peristaltic pump (Heidolph, Pumpdrive 5201). Initial perfusion solution consisted of ice cold DPBS injected into the ventricle at 5 rpm for up to 5 minutes. When the liquid exiting the right ventricle was clear, PBS was switched with ice cold 4% PFA in DPBS and the perfusion continued for another 5 minutes, then ended. The brain was extracted and submerged in 4% PFA for 24h at 4°C. To avoid damage by ice crystal formation during cryosection brains were kept in 10%, 20%, and 30% Sucrose/PBS for 24 h each before being embedded in Jung tissue freezing medium (Leica Microsystems) and cut into 30 µm slices in a Leica CM 1850 UV cryostat at -20 °C then stored in DPBS with 0.5% PFA at 4°C until further use.

2.2 Behavior

2.2.1 General notes

All behavior experiments were performed double-blinded to avoid experimenter bias. Animal cage positions were rearranged in the holding racks by a colleague. The identification cards were then covered, and animals were given numbers from 1 to n to serve as identifiers during experiments. The experimenter did not know which animals belonged in each group until the end of the respective test or if required to decide to progress to the next phase (e.g. in the Morris Water Maze), a colleague with access to the unblinded data decided whether to proceed or not. When the statistical

analysis was finished the identity of the groups was revealed and the experimenter unblinded.

If applicable, in order to prevent other animals from being influenced, surfaces were cleaned with 70% EtOH after each animal's trial to ensure no olfactory trace remained.

2.2.2 Morris water maze

To test spatial memory, we performed a version of the well-established Morris Water Maze (MWM) test (Morris, 1981). A pool 120 cm in diameter was filled with opaque water and surrounded by cues every 90° (here a star, a circle, a triangle and a square) visible from the water's surface. An acrylic glass platform (10x10 cm) was submerged in the water 1 cm below the surface, invisible to the mouse, to serve as the escape. On training days the test animal was placed carefully in the water beside one of the cues (entry point changed for every trial) facing the wall. The experimenter then left the room for one minute during which the animal's movement was recorded. If the animal found the platform and remained there for two seconds the trial was ended. If the time ran out without the animal finding the escape, the experimenter placed it on the platform and left it for 15 seconds to allow it to consolidate the position. This was repeated four times per training day. When animals showed a plateau in escape latency between 15-20sec for several days in a row (usually three) a probe test was performed (PT). For this the platform was removed and the animal was placed in a position it had not entered the maze in before, between two cues, facing the wall. The animal was given one minute to swim then returned to its homecage. For analysis the pool was divided into 4 quadrants. Time spent in the target quadrant (quadrant that had contained the platform) and the number of platform region crossings were used for analysis. Animals which showed "floating" behavior were removed from the trials and the statistical analysis. Recordings were performed using TSE VideoMot 2.

2.2.3 Fear conditioning

To assess differences in associative fear memory we performed Fear Conditioning (FC) a classical Pavlovian conditioning paradigm. A mouse is placed in a dark chamber with an electrifiable grid as flooring. The animal is given three minutes of undisturbed exploration, then exposed to a mild footshock via the grid (0.5 mA for 2s), upon which a healthy animal will associate the shock (unconditioned stimulus) to the context, in

this paradigm being the dark chamber (conditioned stimulus). When exposed to the context again 24 h later, animals that associate the context with the shock should display “freezing” behavior, defined as the absence of movement (with the exception of breathing). Freezing in experiments performed here was recorded using VideoFreeze (Med Associates) and defined as motion threshold < 30, episode duration > 2s. To minimize influence of outside sounds white background noise was played in the chamber during training and testing sessions.

2.2.4 Open field test

In order to assess overall motility and potential anxiety-like behavior, we performed the Open Field test. Animals were individually placed in a featureless, grey plastic arena (40 x 50 x 40 cm) and given three minutes to explore their environment freely. For analysis purposes recordings were made and the arena was virtually divided into 16 squares with TSE VideoMot 2. The four center squares were labeled as „exposed“. Percentage of time spend in the center was then compared to time spend in the areas close to the wall, where more time spent near the wall indicates higher anxiety and more time spent in the center indicates lower anxiety. Additionally, movement speed and distance were recorded. To determine if an increased or decreased anxiety level is evident in one of the groups a comparison of center to wall area ratio can be calculated.

2.2.5 Novel object recognition

To determine potential differences in short term memory (STM) and long-term memory (LTM) between BET cKO and WT mice, Novel Object Recognition (Ennaceur and Delacour 1988) was performed subsequently to the Open Field test. The same arena was prepped by placing two identical objects (here black plastic cubes) about 12 cm from the walls. Individual animals were then again placed in the arena and allowed to explore. Their interactions with the individual objects were recorded over three minutes. Animals were then placed back in their home cage for five minutes while the arena was cleaned with EtOH to remove olfactory cues followed by the replacement of one of the objects with a new one (here blue bottle cap). Since mice are curious by nature, they should generally spend more time investigating the new object if they have learned both previous objects. The animals were then placed back in the arena for three minutes and their interaction with the objects was again recorded. The rate of

interactions with the new compared to the old object can then be used to measure differences in STM. To test LTM the other object was also replaced with a new one (here a plastic star mold) 24 hours after the first test. Again, animals were given three minutes to explore. Interactions and durations of these interactions were again recorded and scored using VideoMot 2 and the amount of exploration of the new object was used as an indicator for LTM.

2.2.6 Elevated plus maze

As a test for anxiety vs explorative behavior the elevated plus maze experiment was performed (Pellow, Chopin et al. 1985). Individual mice were placed in the center of a cross-shaped maze made out of plastic (10 x 40 cm) with two open and two closed arms. While the open arms consisted only of floor plates, the closed arms had 20 cm high walls surrounding them. On entry the mice faced a closed arm, away from the experimenter. Animals remained in the maze for three minutes and the time they spent in the open vs. the walled areas of the maze were recorded in VideoMot 2. The ratio of open (low anxiety) to closed (high anxiety) arm exploration was then calculated as an indicator for anxiety levels.

2.3 Cell Culture

2.3.1 Cell culture conditions

All cultures were kept under standard S1 cell culture conditions with 5% CO₂ at 37°C. All experiments on cultures were performed under S1 sterile hoods if not explicitly stated otherwise.

2.3.2 Etching and coating of coverslips

12mm coverslips (Thor labs) were etched via submerging them in 70% nitric acid while shaking (here in a 50 ml falcon while turning horizontally) for at least 24h. The acid was then removed and stored for further usage. The coverslips were washed for 20 minutes under slow running ddH₂O. Subsequently, a 1 h incubation while shaking coverslips in 70% EtOH was performed (here in a 50 ml falcon while turning horizontally). The coverslips were then stored in fresh 70% EtOH. The day before use the coverslips were washed five times with sterile ddH₂O under a sterile hood and transferred into the wells of a sterile 24-well plate (Thermo Fisher). Wells containing

coverslips were then filled with 250 μ l of a 0.5 mg/ml Poly-D-lysine (PDL) solution (Millipore), and wells not containing coverslips were filled with the same amount of sterile ddH₂O. Plates were sealed with parafilm (Merck) and incubated overnight in a cell culture incubator at 37°C. PDL was removed the next day and stored at 4°C for further usage, the coverslips were washed four times with sterile ddH₂O before being seeded with cells.

2.3.3 Coating of plates for cell culture

For cultures intended for RNA extraction and subsequent RNAseq and qPCR, 12-well plates (Thermo Fisher) were coated by covering wells with 500 μ l of a 0.5 mg/ml PDL solution (Millipore). Wells not intended for seeding were covered with the same amount of sterile ddH₂O instead. The plates were then sealed with parafilm (Merck) and incubated overnight in a cell culture incubator at 37°C. PDL was recovered the next day and stored at 4°C for further usage. The coated wells were washed four times with sterile ddH₂O before being seeded.

2.3.4 Primary hippocampal cultures

All cell culture experiments were performed using primary hippocampal neurons. Cultures were produced by dissecting E17.5 embryonic mouse brains and digesting their hippocampi for 45 min using the Papain Dissociation System (Worthington) following the manufacturer's instructions. If not explicitly stated otherwise cells were seeded and maintained exclusively in serum free medium consisting of Neurobasal Plus (Gibco) containing 2% B27 Plus (Gibco), 1% Pen/Strep (PanReac AppliChem) and 1x GlutaMAX (Gibco) that was prepared and sterile filtered in a cell culture hood, to ensure minimal glial contamination and optimal neuronal health. For immunocytochemistry (ICC) and live imaging approaches cells were seeded with a density of 80k per 12 mm coverslip, in 500 μ l medium per well in 24-well plates. 12-well plates intended for RNA preparation were seeded with 200k cells in 1 ml medium per well. To ensure optimal health in the cultures, 50% medium swaps with pre-warmed (37°C) medium were performed every 3 days starting on DIV5. For co-culturing astrocytes and neurons, primary neuronal cells were initially plated in filter-sterilized plating medium (DMEM (Gibco), 10% FBS (Gibco), 1% Pen/Strep) which was switched for Neurobasal Plus the next day.

2.3.5 Calcium phosphate transfection

To transfect neurons with plasmids, conditioned medium was removed and collected on DIV3 and replaced with an equal amount of pre-warmed Opti-MEM (Gibco). Cultures were then placed back in the incubator for 30 minutes. During this time the collected medium was sterile filtered using a 0.22 μm syringe driven filter (Millipore), then stored at 37°C and 10% CO_2 to increase the acidification of the medium. An equal amount of Neurobasal (Gibco) was pipetted into a 10 cm petri dish (Thermo Fisher) and also incubated at 37°C and 10% CO_2 .

The transfection solution was prepared by first mixing 1 μg plasmid DNA and 1.87 μl 2 M CaCl_2 and then adding up to 15 μl total volume ddH₂O per well of a 24-well plate. An equal volume of transfection buffer (274 mM NaCl, 10 mM KCl, 1.4 mM Na_2HPO_4 , 15 mM glucose, 42 mM HEPES in dH₂O; pH 7.05 - 7.12, 0.22 μm sterile filtered) re was then added drop-wise while gently vortexing, and this mixture incubated for 20 minutes under light exclusion at room temperature. This transfection solution was then added drop-wise to the cells (30 μl per well for a 24-well plate) which were then placed back in the incubator for another 45 minutes. Subsequently, the transfection solution / Opti-MEM mix was removed and the stored conditioned medium was applied back to the cells, which were placed in a standard S1 37°C, 5% CO_2 incubator for the rest of the experiment.

2.3.6 Viral transduction

All viral transductions were performed on DIV3. For this purpose, 110 μl of medium were carefully pipetted out of each well to be transduced using a 200 μl pipette (Eppendorf) and pooled in a 2 ml Eppendorf tube. The adjusted amount of the respective AAV (Table 2 below) was then added to the medium and the mixture pipetted up and down five times with a 1000 μl pipette (Eppendorf) to ensure equal distribution of viral particles. 100 μl of the resulting solution was then added back to the respective wells using a 200 μl pipette. For viral concentrations see Table 2 below.

	Original conc.	Per 100k cell final conc.	Provided by
AAV8-CaMKIIa-GFP	4.5×10^{12}	3.375×10^{12}	UNC vector core
AAV8-CaMKIIa-GFP-Cre	8.0×10^{12}	3.36×10^{12}	UNC vector core
AAV1-CaMKIIa-GCaMP6f	2.3×10^{13}	5.75×10^{12}	UNC vector core
AAV1-CW3SL-EGFP			
AAV1 flagBrd4 CW3SL		variable	In house
AAV1/2 Brd2-myc		1 μ l	In house

Table 2: AAVs serotypes and concentrations

2.3.7 RNA extraction from cell culture

RNA extraction from cultured cells in 12-well plates was performed using the NucleoSpin TriPrep kit (Macherey-Nagel) at DIV16. The appropriate amount of Lysis Buffer was prepared according to the manufacturer's instructions (here 350 μ l RP1, 15mM TCEP). The cell cultures were taken out of the incubator, medium was removed under the sterile hood and immediately replaced with 350 μ l room temperature Lysis Buffer. The cells were then scraped off using a cell scraper (Sarstedt) and the resulting cell/buffer mix was collected with a 1ml pipette and transferred to individual 1.5 ml DNase & RNase free Eppendorf tubes where the solution was pipetted up and down five times to lyse cells. Scrapers were washed with ddH₂O between samples and changed between conditions. From that point on the NucleoSpin TriPrep kit instructions were followed: the lysate was added to columns, which were washed with ethanol and then DNA wash buffer, treated with DNase, washed, and RNA was eluted in 40 μ l sterile ddH₂O and stored at -80°C until further use.

2.3.8 Live cell calcium imaging

In our live imaging experiments, we used primary hippocampal DIV15 neurons of the Brd2 fl/fl genotype that were cultured on 12 mm coverslips. Cells had beforehand been transduced with AAV1 CaMKIIa:GCaMP6f only (WT), AAV1 CaMKIIa:GCaMP6f + AAV8 CaMKIIa:GFP-Cre (Brd2 KO) or AAV1 CaMKIIa:GCaMP6f + AAV1 CaMKIIa:GCaMP6f + AAV1/2 6P-Brd2-myc according to the viral transduction protocol see 2.3.6). For the imaging itself we used a Zeiss Axio Observer Z1 TIRF scope equipped with a Photometrics Evolve EMCCD camera (kindly provided by the European

Neuroscience Institute). Images were acquired at 550 ms intervals (exposure time 120 ms), using 488 nm laser excitation and a 63X oil objective.

Coverslips with neurons were removed from the 24-well plate and fixed onto a custom-made chamber (provided by the European Neuroscience Institute workshop) containing 200 μ l ACSF TTX/0 Mg solution (1 μ M TTX, 140 mM NaCl, 5 mM KCl, 2 mM CaCl₂, 5.5 mM D-glucose, 20 mM HEPES, pH = 7.3). If the cell health looked adequate, 3.5 minute videos from four different areas of the coverslip were taken to record synaptic events. The ACSF TTX/0 Mg solution was then removed and replaced with normal ACSF (140 mM NaCl, 5 mM KCl, 2 mM CaCl₂, 2 mM MgCl₂, 5.5 mM D-glucose, 20 mM HEPES, pH = 7.3). After two minutes to ensure washout of TTX, dendritic regions of interest were determined and 30 second baseline recordings were acquired before stimulation of the cells by adding 200 μ l of high potassium ACSF buffer (100 mM NaCl, 45 mM KCl, 2 mM CaCl₂, 2 mM MgCl₂, 5.5 mM glucose, 20 mM HEPES, pH = 7.3) while recording for another three minutes. After stimulation the solution was removed and replaced with 200 μ l ACSF again. This process was repeated three times for three different fields of view.

2.4 Immunocytochemistry (ICC)

2.4.1 Fixation

Cells on coverslips intended for ICC were fixed on DIV16. Medium was removed under a sterile cell culture hood; the cells were then washed with 4°C DPBS (PAN Biotech) once and then immediately covered in a solution consisting of DPBS with 4% PFA (Merck) and 4% sucrose (Roth) and incubated for 30 minutes at room temperature. Subsequently, PFA solution was removed, and coverslips were washed once with DPBS, then covered in a quenching solution consisting of DPBS plus 100 mM NH₄Cl to neutralize unreacted aldehydes, for another 30 min at room temperature. After removal of the quenching solution, the cells were washed three times with 4°C DPBS, then covered with 1 ml DPBS for storage or transport. Afterwards the 24-well plate was sealed with parafilm to be stored at 4°C or the coverslips were directly processed.

2.4.2 Immunostaining

For permeabilization, the DPBS covering the coverslips was replaced by T-PBS (DPBS with 0.3% Triton X-100 (Sigma Aldrich)). They were then incubated gently rocking on a shaking plate for 30 minutes at room temperature, followed by a blocking step of 1 h in 5% BSA (Carl Roth) T-PBS on the rocking plate. Primary antibodies were applied in their respective concentration (see table 3) diluted in T-PBS and incubated overnight at 4°C while rocking.

The next day primary antibody solution was removed and replaced with T-PBS to avoid the drying of coverslips. Five washing steps with T-PBS each lasting 5 minutes on a rocking plate were performed. Secondary, fluorophore-associated antibodies specific for the species of the primary antibodies were applied in T-PBS (at 1:400) for 2 h while rocking. The 24-well plate was protected from light during this time to avoid photobleaching. If applicable, DAPI was applied after the removal of the secondary antibodies. After five more washing steps coverslips were mounted: coverslips were taken out of the well using a pair of forceps, and most of the liquid clinging to them was removed by holding the side of the coverslip gently against a Kimwipe (Kimtech). The coverslips were then mounted on a slide (Marienfeld) in 5 µl Fluoromount (Thermo Fisher) per 12 mm coverslip, then stored horizontally at 4°C protected from light for at least 24 h before imaging. Imaging was performed using a Zeiss LSM 800 confocal microscope, kindly provided by the European Neuroscience Institute, with 405 nm, 488 nm, 561 nm, and 640 nm, laser lines, using either 20x, 40x, or 63x objectives.

Target	Identifier	Supplier	Host species	Dilution
PSD95	MABN68	Millipore	Ms	1:300
Synaptophysin	101 004	Synaptic Systems	Gp	1:1000
Map2	C-1382-50	Biosensis	Ch	1:2500
GFAP	173-004	Synaptic Systems	Gp	1:1000
myc	MA1-980	Thermo Fisher	Ms	1:50
TRPC6	T6442	Sigma	Rb	1:400

Table 3: List of primary ICC antibodies

2.4.3 Analysis of imaging data

Imaging analysis was performed with custom made pipelines in CellProfiler (Lamprecht et al., 2007). Pipelines and included thresholds were adjusted to the specific

experiment and can be found in the Appendix with reference to the results section in which they were used.

2.4.4 Analysis of calcium imaging data

A detailed description of the calcium imaging analysis workflow is located in Results Chapter 1. The respective codes and pipelines can be found in the Appendix ordered by chapter.

2.4.5 Perineuronal net (PNN) staining and analysis

After blocking for 1 h in 5% BSA (Carl Roth) T-PBS, the neurons were incubated at 4°C overnight with 1:500 biotinylated Wisteria floribunda agglutinin WFA (#L8258; Merck), an aggrecan binding molecule and 1:500 anti-VGlut1 nanobodies conjugated to STAR580 (#N1602; NanoTag), applied in blocking solution. The next day cells were washed three times for five minutes, and then incubated with 1:500 streptavidin-Atto647N (#AD 647-61; ATTO-TEC GmbH) for one hour at room temperature in blocking solution. This was followed by three more five-minute washing steps with DPBS, followed by embedding in Mowiol (Calbiochem).

Two-color STED imaging was performed with an Abberior easy3D STED microscope (Abberior GmbH) equipped with a UPlanSApo 100×, 1.4 NA oil objective (Olympus Corporation) and an EMCCD iXon Ultra camera (Andor). Excitation was provided by pulsed 561 nm and 640 nm lasers. Depletion was done with an easy3D module 775 nm laser. The pinhole was set to 1 Airy unit for each channel.

For analysis a custom script was written in Python (Python Software Foundation). Synaptic puncta were identified by manually thresholding the VGlut1 channel. Sub-images of 2 x 2 μm centered around individual VGlut1 puncta, corresponding to synapses, were extracted from the image. These sub-images were then averaged in order to visualize the distribution and intensity of the PNN protein aggrecan at synapses for each of the three conditions (WT, Brd2 cKO, Brd2 OE). After background subtraction (5x5 median filter of the original image) the mean fluorescence intensity was calculated for each sub-image. The values were normalized to the median of each individual experiment and then plotted.

2.5 RNAseq

2.5.1 RNA sequencing and mapping

Whole transcriptome RNA sequencing was performed by creating single-end libraries prepared from 250 ng total RNA using the TruSeq RNA Library Preparation Kit v2 (Illumina) according to manufacturer's instructions. Library quality was determined with a Bioanalyzer 2100 (Agilent Technologies) using the RNA 6000 Nano Kit (Thermo Fisher) according to manufacturer's instructions. Libraries were sequenced using a HiSeq2000 machine (Illumina). The resulting reads were analyzed by our bioinformatics unit using an in-house pipeline developed by our former colleague Dr. Gaurav Jain. In brief, Illumina's bcl2fastq was used to convert base calls the machines output (BCL) to FASTQ. Base calling, adapter trimming, as well as demultiplexing were performed followed by quality control of raw data using FastQC (<https://www.bioinformatics.babraham.ac.uk/projects/fastqc/>). Reads were mapped using STAR aligner (Dobin, Davis et al. 2013) to the mouse transcriptome (mm10 Mus_musculus.GRCm38.86). Read counting on coding regions was done with HTSeq (htseq-count, intersection-non-empty) (HTSeq, <http://www-huber.embl.de/users/anders/HTSeq>).

2.5.2 Differential gene expression analysis and visualization of RNA sequencing data

For determining differential expression of genes between groups (here Brd2 cKO and WT) we used DESeq2 version 1.32.0 (Anders, Reyes et al. 2012). Transcripts were considered differentially expressed if p adjusted value (Benjamini-Hochberg) < 0.05 and basemean \geq 25.

For further analysis additional cut-offs were applied: log2fold > 0.8 or log2fold < - 0.8 (at least 75% relative transcript increase or decrease) and basemean > 75. Analysis for enriched GO categories in the resulting gene list was performed using Cytoscape version 3.5.1 (Shannon et al. 2003) with the plug-in ClueGO 2.5.7 (Bindea et al. 2009). Chosen selection criteria were tested against a randomly generated gene list (<https://www.molbiotools.com/randomgenesetgenerator.php>) to ensure resulting GO categories were reliable. Resulting selection criteria are listed here:

Statistical Test Used = Enrichment/Depletion (Two-sided hypergeometric test)

Correction Method Used = Bonferroni step down

Min GO Level = 5

Max GO Level = 15

Cluster #1

Sample File Name = File selection: ManuallyAddedOrModifiedIDs

Number of Genes = 4

Min Percentage = 3.0

GO Fusion = true

GO Group = true

Kappa Score Threshold = 0.4

Over View Term = SmallestPValue

Group By Kappa Statistics = true

Initial Group Size = 1

Sharing Group Percentage = 50.0

The resulting list of enriched GO category was then visualized using a custom R script with the ggplot2 version 3.3.5 plug-in.

2.6 Molecular Lab Work

2.6.1 Subcloning

All plasmid digestions were performed with Fast Digest enzymes (Thermo Fisher) according to the manufacturer's instructions. Plasmids were transformed into NEB[®] Stable Competent E. coli (High Efficiency) to prevent unintended recombinations. Minipreps were performed using the Zyppy[™] Plasmid Miniprep Kit (Zymo Research), and Maxipreps were performed using the NucleoBond Xtra Maxi kit (Macherey Nagel). To create an AAV1 to overexpress Brd4 we performed an oligo cloning following a protocol provided by Addgene (<https://www.addgene.org/protocols/annealed-oligo-cloning/>). First, we created an oligo carrying the digestion sites Bsp119I and XmaJI and the sticky ends from NheI and XhoI. We then replaced the EGFP in pAAV-CW3SL-

EGFP with said oligo. Subsequently, we digested RSV-Flag-Brd4 and pAAV-CW3SL-oligo with Bsp119I and XmaJI, purified the backbone and insert using the QIAEX II Gel extraction kit (Qiagen) according to the manufacturer's instructions and ligated them (ratio 1:3) using Blunt/TA Ligase (NEB) according to the manufacturer's instruction.

pAAV-CW3SL-EGFP was a gift from Bong-Kiun Kaang (Addgene plasmid # 61463 ; <http://n2t.net/addgene:61463> ; RRID:Addgene_61463).

RSV-Flag-Brd4 was a gift from Mario García-Domínguez (Addgene plasmid # 86616 ; <http://n2t.net/addgene:86616> ; RRID:Addgene_86616).

pAAV1/2 6P-NoTB-SEWB was a gift from Sebastian Kügler, University Medicine Göttingen, Dept. of Neurology

2.6.2 qPCR

cDNA was generated from RNA using the Transcriptor First Strand cDNA Synthesis Kit Version 09 (ROCHE) according to the manufacturer's instructions. The amount of input RNA was dependent on the respective experiment. qPCRs were performed on a Light Cycler 480 II (ROCHE) using LightCycler 480 SYBR Green (ROCHE) according to the manufacturer's instructions. Primer sequences were either designed using the freeware ApE version 3.0.5 (M. Wayne Davis; <https://jorgensen.biology.utah.edu/wayned/ape/>) or taken from publications (see Table below). In all instances of qPCRs in this work expression levels were normalized to GAPDH with the exception of qPCRs with nuclear samples in which 18s served as the control.

Name	Sequence	Ref if applicable
ACAN_F_B1	CTCCTGGGTGTAAGGACTGTCTATC	
ACAN_R_B1	CTTTGCTGTAAGGATCACGCTGC	
BDNF_F_C2	GAGCCTCCTCTACTCTTTCTGCTG	
BDNF_R_C1	GACCCACTCGCTAATACTGTACACAC	
Brd2 recomb val r1	GTTAGCACAAAGCACACATC	
Brd2 recomb val r2	ACAATATCATCGGTGGGCTG	
Brd2_e2 Mm F	CTGAGGTCAAGATGCTGCAA	
Brd2_e2 Mm R	GAATCCTTTTCCCTGGTGCT	
Fos_F_A2	GAATGGTGAAGACCGTGTCAGG	
Fos_R_A1	GTTCCCTTCGGATTCTCCGTTTCTC	
Gapdh_mm_mRNA_F2	GACACTGAGCAAGAGAGGC	
Gapdh_mm_mRNA_R2	GATGGAAATTGTGAGGGAGAT	
mm Npas4_F1	CAGAGTTCAGGAAACAAACTGG	
mm Npas4_R1	ACACTTTCAGAAACGTCCAGTA	
MmBrd4_e3_e4_F	GGAAACACCAGTTTGCCTGG	
MmBrd4_e3_e4_R	AGTTGTTTTCCAAGCGCTTCTT	
Myob5b_F_B2	GACCTCATAGAGGCAAAGCTGG	
Myob5b_R_B1	GGAGTGTCTGTTTCGTAGAGTTTCTGG	
Ryr1_F_C1	ACCGGGTCGTCTTCGACATC	
Ryr1_R_C2	CCATGTCTTCCTTCACTTGCTCTTG	
s18s-Fwd	CTTAGAGGGACAAGTGGCG	BMC Res Notes. 2011; 4: 410
s18s-Rev	ACGCTGAGCCAGTCAGTGTA	BMC Res Notes. 2011; 4: 410
Trpc6 SYBR F	GCAGCTGTTCAGGATGAAAAC	Zhang et al. 2016
Trpc6 SYBR R	TTCAGCCCATATCATGCCTA	Zhang et al. 2016

Table 4: List of qPCR primers

2.6.3 Nuclei FAC sorting using NeuN labeling and RNA extraction from tissue

Nuclei sorting and subsequent RNA extraction was performed by Sakib Sadman according to <https://www.biorxiv.org/content/10.1101/2020.08.07.240853v1>.

2.6.4 Protein purification and western blots

Proteins were separated into membrane, cytoplasmic, cytoskeletal, nuclear, and chromatin-bound fraction upon isolation using the Pierce Subcellular Protein Fractionation Kit for Tissues (Thermo Fisher) protein concentrations were determined using the Pierce™ BCA Protein Assay Kit (Thermo Fisher), both following the manufacturer's instructions.

For western blots 10 µg protein was mixed 1:5 with loading buffer (250 mM Tris-HCl, pH 6.8, 10% SDS, 30% Glycerol, 10 mM DTT, 0.05% Bromophenol Blue) and incubated at 95°C for five minutes. Samples were then loaded onto a 4–20% Mini-PROTEAN® TGX™ gel system (BioRad) with either ten or 15 chambers and electrophoresis was performed for 45 minutes at 150V. The separated proteins were then blotted on a nitrocellulose membrane using a Trans-Blot® Turbo™ Mini Nitrocellulose Transfer Pack (BioRad) and the Trans-Blot® Turbo™ (BioRad) with pre-programmed High molecular weight (HMW) settings. Membranes were then blocked for one hour at room temperature with 4% BSA (Roth) in 0.22 µm filtered (Millex syringe filter, Millipore) TBS-T (136.89 mM NaCl, 2.68mM, 23.11 mM Tris base, 0.1% Tween, pH 7.4). Primary antibodies were applied in the same blocking solution (for concentrations see Table 5) overnight. The next day, the antibody solution was removed and stored at 4°C for further use. The blot was washed five times for five minutes with T-BST. Secondary antibodies (IRDye 800CW goat anti-rabbit and IRDye 680RD goat anti-mouse) were then applied at 1:10000 in blocking solution protected from light for one to two hours at room temperature while gently (70 rpm) shaking on a rocking plate. After five more T-BST washing steps, the membrane was stored in a dark plastic box filled with TBS until it was scanned on a Li-COR Odyssey infrared fluorescence scanner.

Target	Identifier	Supplier	Host species	Dilution
Brd2	D89B4	Cell Signaling	Rb	1:250
Brd4	ab128874	abcam	Rb	1:250
Actin (pan)	ACTN05 (C4)	Novus	Ms	1:1000

Table 5: Primary antibodies for WB

2.6.5 Immunohistochemistry (IHC)

To remove PFA, brain slices were washed three times for five minutes in DPBS. This was followed by a permeabilization step consisting of a ten-minute incubation in 0.1% Triton-X in PBS followed by a 60 minute blocking step (in DPBS, 0.3 % Triton-X and 5% goat serum) while gently rocking. Primary antibodies were applied in fresh blocking buffer overnight at 4°C while gently rocking.

The following day samples were washed three times for 10 min in DPBS containing 0.2% Triton-X and 1% goat serum., followed by application of fluorophor associated secondary antibodies in blocking buffer at room temperature at a dilution of 1:1000 for

2 hours at room temperature in the dark while rocking. After three five-minute washing steps with DPBS, a DAPI solution was added to the slices (1:10000 in DPBS) for 30 min. Subsequently, they were washed twice in DPBS and mounted in Mowiol (Roth) and stored at 4°C in the dark until imaging.

target	Identifier	Supplier	Host species	Dilution
Brd4	ab75898	abcam	Rb	1:250
Map2	C-1382-50	Biosensis	Ch	1:1000
NeuN	MAB377	Merck	Ms	1:150
myc	9E10	Santa Cruz	Ms	1:50

Table 6: Primary antibodies for IHC

2.6.6 AAV preparation

Viral preps were performed as described in the PhD thesis of Dr. Hendrik Urbanke Section 3.3.4. (<http://hdl.handle.net/11858/00-1735-0000-002E-E53E-2>):

“Adeno-associated virus preparation was adapted from McClure and colleagues (McClure, Cole et al. 2011) with several adjustments. Required plasmids (pRV1, pH21, pFΔ6) were amplified and extracted by Midiprep and digested for sequence validation (pRV1(XbaI) 7.5 kb, 3.8 kb; pH21(EcoRI) 4.5 kb, 2.8 kb, 0.2 kb; pFΔ6 (HindIII) 5.5 kb, 3 kb, 3 kb, 2.3 kb, 1.5 kb). For viral particle assembly five HEK293T 15 cm dishes were grown to 70-80% confluence in standard DMEM with low glucose containing 10% fetal bovine serum (Gibco) and 100 U/ml penicillin/ 100 µg/ml streptomycin. Three hours before transfection, medium was removed and replaced with fresh medium. For one batch (five 15 cm dishes) 62.5 µg AAV plasmid, 125 µg pFΔ6, 31.25 µg pRV1, 31.25 µg pH21 and 1650 µl 2.5 M CaCl₂ were mixed in 12 ml dH₂O and sterile filtered. While vortexing, 13 ml 2x HEPES (250 mM NaCl, 1.5mM Na₂HPO₄, 50 mM HEPES, pH 7.05) was quickly added to the solution. The solution was allowed to stand for 2 min until a white precipitate started to form. Then 5 ml of the transfection solution was added to each 15 cm culture dish. Depending on expression, cells were incubated for 48 h - 72 h. For harvest, the supernatant was removed from plates. Cells were then washed and scraped from the dish. Samples were then centrifuged for 5 min at 1000 g, 4°C and resuspended in lysis buffer (20 mM Tris, 150 mM NaCl, pH 8.0, 0.5 % NaDOC, Benzonase). The slurry was then incubated for 30 min at 37°C and occasional vigorous shaking. The reaction was quenched by adding 21.63 mg/ml NaCl and

incubating at 56°C for 30 min. After one freeze-thaw cycle (-80°C freezing O/N, 37°C thawing) the sample was centrifuged for 30 min at 4000 g and subsequently layered onto a discontinuous Iodixanol (Sigma) gradient (top to bottom 6.5 ml, 15%; 4 ml, 25%; 3 ml, 40%; 3 ml, 54%) in an ultracentrifuge tube. To avoid collapse of the ultracentrifuge tubes, any air volume was filled with with PBS-MK. Then the viral preparation was centrifuged for 1.5h at 60,000 rpm (rotor: Ti 70, Beckmann). Subsequently, the 40/54% interphase was removed, diluted to 10 ml with PBS- MK and concentrated in an Amicon 100K filter (Millipore) at 2000g at room temperature. The samples were centrifuged repeatedly for 5 min until 500 µl resided in the concentration unit. The concentration was repeated 3 times by refilling the concentrator to 10 ml with PBS-MK. Subsequently, the viral solution was sterile filtered and stored at 4°C and -80°C for long-term storage.”

3. RESULTS

3.1 Chapter 1 - cell culture optimization

When studying neuro-specific knockouts, especially respective changes in gene expression, one faces certain challenges. In brain tissue neurons are surrounded by different glia fulfilling a multitude of tasks such as immune response (microglia), myelination (oligodendrocytes), production of cerebral spinal fluid (ependymal cells), maintenance of the blood brain barrier and synaptic support and modification (astrocytes) or serving as neuronal and glial progenitor cells (radial glia). To fulfill these functions all of these types of glia must have vastly different epigenetic and transcriptional profiles (Khakh and Sofroniew 2015; Khakh and Deneen 2019). This in turn means that if one sequences RNA from brain tissue, one must not only consider masking effects but also the direct or indirect influence that glia, especially astrocytes, have on the function and therefore transcriptional profiles of the neurons they surround.

Single cell sequencing addresses some of these problems by enabling separation of the transcriptional profiles of cells. Single cell sequencing approaches for neuronal tissues faces an additional problem, since neurons are difficult to isolate intact due to their strong arborization. One can therefore use nuclear isolation and sorting approaches to sequence nuclei. However, these approaches have certain drawbacks. Sequencing performed on samples generated via nuclei sorting can, by their nature,

only provide transcription information from a very limited timeframe due to the quick transport of mature RNAs out of the nucleus. Single cell and nuclei sequencing additionally have the drawback of low sequencing depth.

If one intends to study certain neuron-specific behaviors under certain conditions, it also has to be taken into account that in tissue the overall phenotype observed may be influenced by surrounding glia. This might be suitable for purely pharmacological approaches where the main focus is on the effect a pharmaceutical has on the system as a whole but can be less suitable to study finer aspects of neuron behavior and structure, especially in scenarios where one tries to manipulate and study single genes, RNAs or proteins. For these reasons cell culture approaches are often used. In the case of very directed scientific questions, they provide an easier and faster system compared to animals, combined with options for generally easier optical readouts.

For our studies on BET KO mice we used primary cell cultures: First to get basic information on what the absence of a BET chromatin reader does to the transcriptome of affected cells, and second, to determine the effect those transcriptional changes had on the overall physiology and function of neurons (see Chapter 2). In order to achieve this, we had to overcome several technical challenges and develop custom analysis tools, some of which are suitable for common use by other labs. Their purpose and function are explained in this chapter.

The challenges we encountered were the following:

1. Use a cell culture system that is as purely neuronal as possible with minimal interference from other cell types to allow specific observation of the phenotypes in neurons as unmasked as possible.
2. Ensure best possible cell health under the respective stress conditions the cells undergo in experiments, for optimal data quality.
3. Automatize the analysis of all collected data to avoid experimenter bias and accelerate or enable analysis of specific parameters.

3.1.1 Acquisition of neuronal enriched cultures

There are several published and widely used approaches for primary cell culture preparations. Their usage is dependent on such factors as: the age of the embryo or pup when dissected, survivability of the culture, and finally, not to be disregarded, user preference. The standard approach our lab used was based on culturing the primary neurons in serum containing DMEM (see "Plating Medium" in Materials & Methods) to encourage the growth of astrocytes for the first day after plating (Fig. 1A1)). This

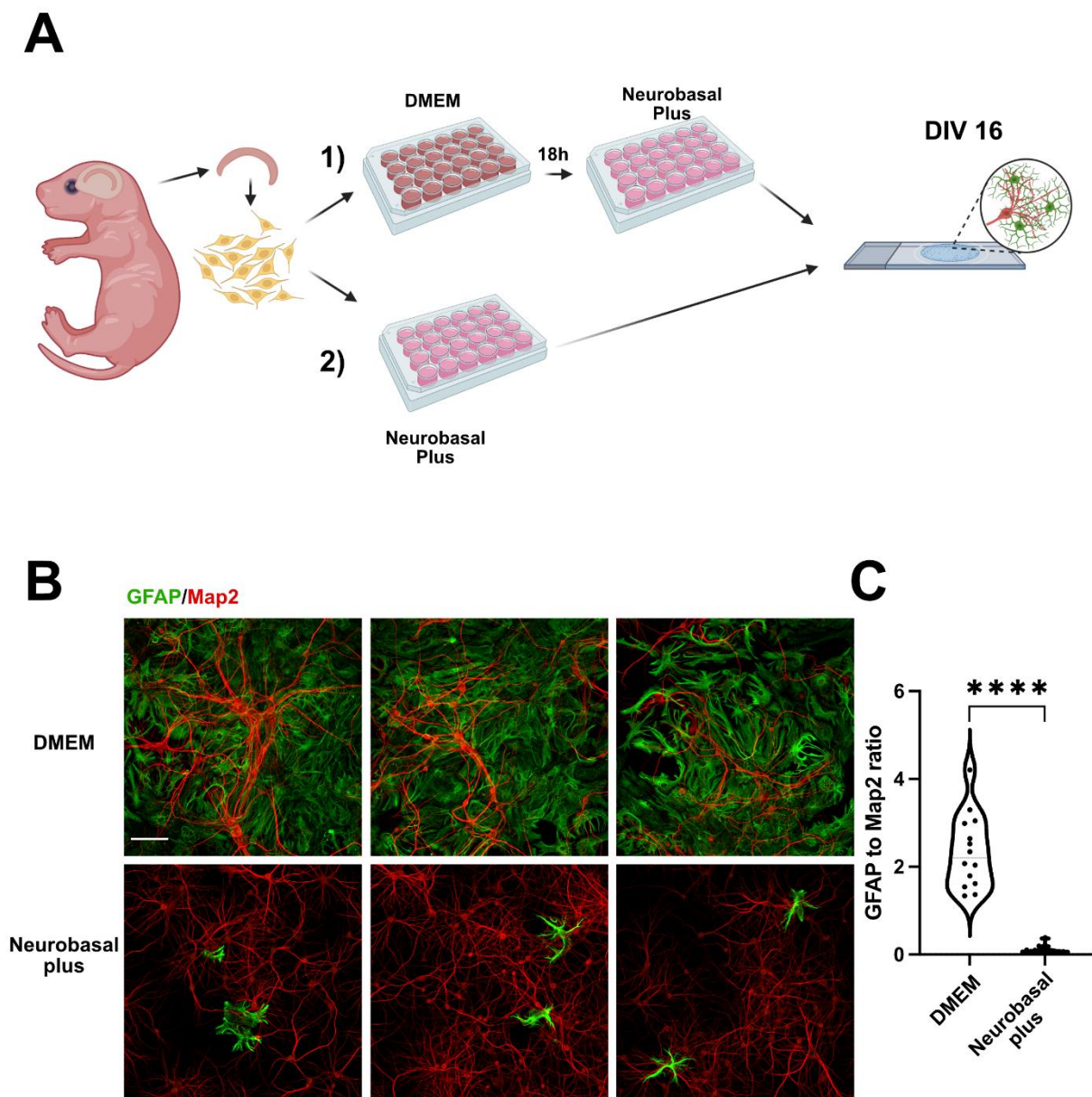


Figure 1: **A:** Schematic of the experimental workflow. Primary cells were prepared with two different approaches before being fixed, stained and imaged. (Created with BioRender.com) **B:** Representative images collected from cultures created by the methods in **A** stained with GFAP (to mark astrocytes) and Map2 (to mark neurons). **C:** Quantitation of the ratio of GFAP to Map2 signal in the two conditions. (Significance determined by Student's t-test).

provides the neurons with a support/feeder layer of astrocytes. However, astrocytes are known to influence synaptic signaling and other aspects of neuronal function and development (Lin and Bergles 2004; Robichaux et al. 2014; Allen et al. 2018; Wilton et al. 2019). Additionally, they have a high transcriptional diversity due to the multiple functions they fulfill. To avoid contamination of our future samples with astrocytic RNAs and minimize the influence non-neuronal cells could have on neuronal signaling and development, we aimed for an astrocyte free culture. Gibco's optimized Neurobasal Plus media in combination with the B27 Plus supplement was tested for this purpose in parallel with our classic approach for comparison (Fig 1A). On DIV16 we fixed the cells and stained for the neuronal marker microtubule associated protein 2 (MAP2) and the astrocytic marker glial fibrillary acidic protein (GFAP). Examples images of these staining can be found in Figure 1B. The number of GFAP positive astrocytes is strongly decreased in the Neurobasal Plus approach. We quantified the ratio of GFAP to MAP2 with a custom CellProfiler pipeline that performed the following steps:

For both channels:

1. Separate the desired channels (GFAP and MAP2 in this case) and designate respective names using the **ColorToGray** function.
2. Globally apply a manual threshold of 5% of the maximum intensity for both signals using the **Threshold** function with maximum smoothing scale (1.3488) to remove background fluorescence.
3. Measure the area (in pixels) occupied by the thresholded areas using the **MeasureAreaOccupied** function
4. List and export the results to a spreadsheet via the **ExportToSpreadsheet** function

We then divided the GFAP value by the MAP2 value for each picture and plotted the result (Fig. 1C). Unsurprisingly, the ratio of GFAP to MAP2 was significantly reduced in Neurobasal Plus cultures when an unpaired T-test was performed.

We concluded that the Neurobasal Plus approach would provide cultures with minimal astrocytic contamination and therefore used it for all future experiments.

3.1.2 Optimization of cell health following GCaMP transduction

One of the experiments performed in this thesis included calcium imaging using a GCaMP6f construct (see Materials & Methods for details). Initial transfection approaches using calcium phosphate led to suboptimal cell health and resulted in poor image and data quality. A picture taken before and during a 45 mM KCl stimulus is shown in Figure 2A. In the video on the right, it is clearly visible that the cell takes several frames (1 frame = 500 ms) after the stimulus is applied at frame 30 to react. Together with the high amount of debris and the poor and unpredictable survivability of these culture to DIV15 we concluded that this approach was not suitable for our experiments.

The detrimental effect on neuron health might have been caused by the relatively high concentration of GCaMP6f (compared to GFP or GFPcre, which we used similar amounts of before without a clear negative effect on cell health). It is also possible that the calcium binding properties of GCaMP6f itself, especially when expressed in high amounts, deprive neurons of some of the calcium necessary for synaptic/neuronal growth and survival. Visual inspection of the transfected cells with high GCaMP expression (Fig. 2A; to view video, focus your smart phone camera on the QR code) seems to support this hypothesis, since the neurites of GCaMP6f positive cells apparently lack mushroom spines at DIV14. We therefore switched to a viral approach. Since the first cultures transduced with AAV1 CamKII-driven GCaMP6f in addition to the Brd2 KO or WT constructs perished, while cultures exclusively transfected with either AAV8 CamKII-driven GFP or AAV8 CamKII-drive GFP-cre survived, we titrated GCaMP6f AAV concentrations. Figure 2-B shows image of cultures transduced with a 10-fold lower titer compared to our first trial. While the cells looked overall healthier, upon stimulation the reaction was delayed and the signal decayed slowly. Together with the occurrence of deformities on the neurite after the stimulus and the overall high background fluorescence, we concluded that the cell integrity was compromised. We also noted that the seeding density used here (100k cells per 24-well plate) seemed too high, which made differentiation between axons and dendrites, and therefore proper analysis, impossible. By halving the GCaMP6f AAV concentration and lowering seeding density to 80k per 24-well plate, we achieved stable and reliable cultures that could be stimulated several times without apparent reductions in cell health (Fig. 2C).

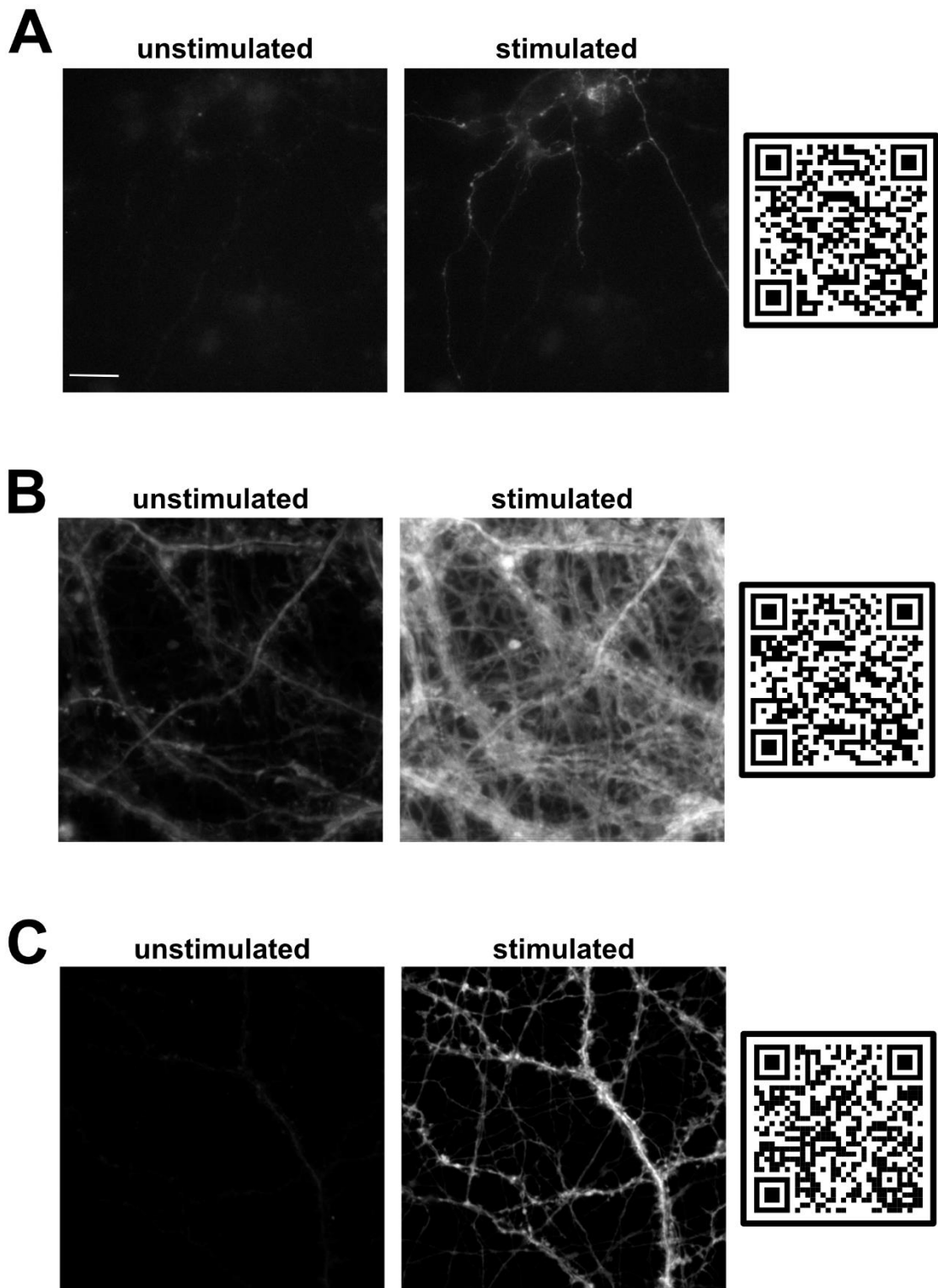
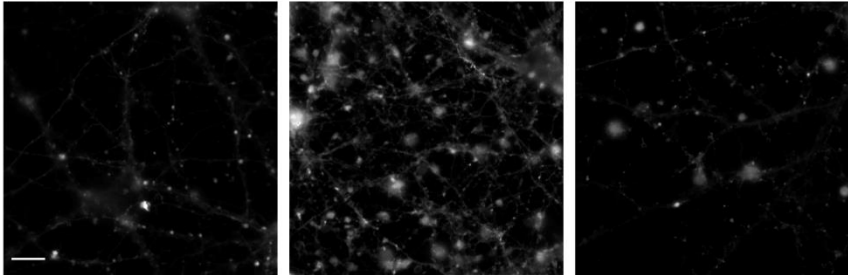


Figure 2: **A:** Example of a culture transfected with GCaMP6f using calcium phosphate, before and after stimulation with 45mM KCl. The QR code can be scanned with the camera of a mobile phone and leads to a video of the recording. Scale bar: 10 μ m. **B:** Example of a culture transduced with a high amount of GCaMP6f AAV1, before and after stimulation with 45mM KCl. **C:** Example of a culture transduced with a four-fold reduced amount of GCaMP6f AAV1, which was used for later experiments, before and after stimulation with 45mM KCl.

Cultures with high amounts of debris (Fig. 3A) still occurred in this approach occasionally, which provided us with an easy optical clue of which cultures to exclude from the final experiment, we also noted that cultures that did not display overt signs of damage could still decline in health upon stimulation. This manifested in the formation of vacuoles (Fig. 3B, red arrows) after the first or later KCl stimulations. We used this as a suitable indicator of overall cell health and only proceeded with cultures that did not display any indication of disintegration or delay of fluorescence response when stimulated multiple times (Fig. 3B bottom panels). The differences in response can easily be observed in the videos (QR codes to the right).

A



B

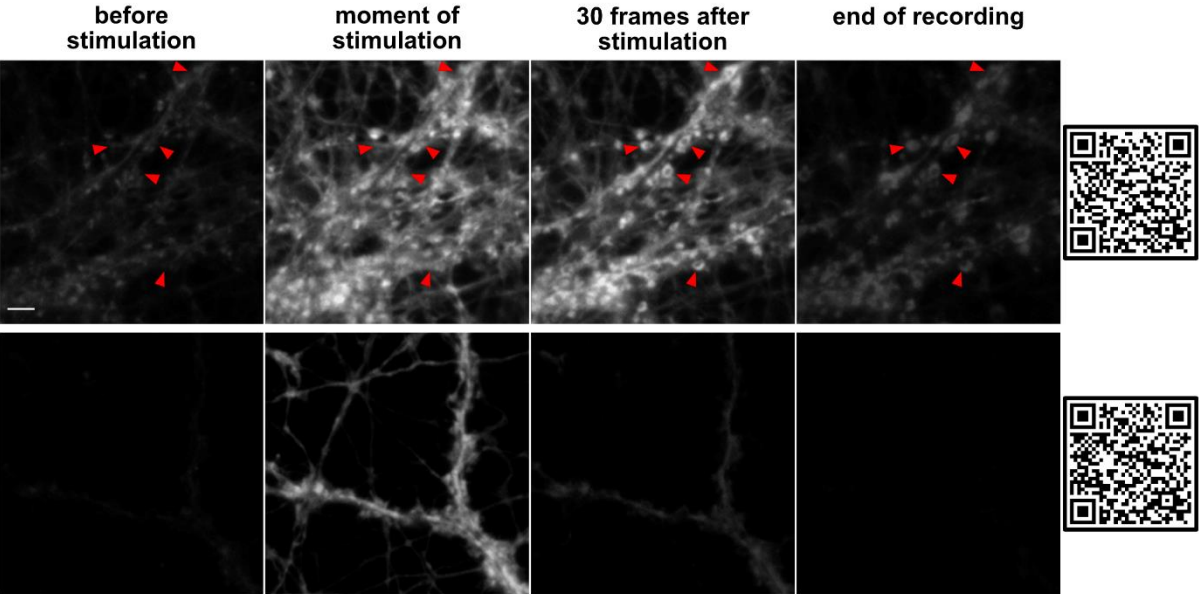


Figure 3: A: Three example pictures of unhealthy cultures, where fluorescent cell debris is clearly visible. Scale bar: 10 μm . **B:** Zoomed in pictures taken from recordings of two cultures before, during, and shortly after stimulation, and at the end of recording. Red arrows indicate vacuoles characteristic of unhealthy cultures unsuited for experiments. Scale bar: 2.5 μm . The QR code can be scanned with the camera of a mobile phone and leads to a video of the recording.

Further lowering of the GCaMP6f virus titer resulted in expression that was too dim to adequately quantify. In general, we would recommend lowering the viral concentration of GCaMP6f AAV to the lowest possible level that still provides signal in basal conditions.

Under physiological conditions NMDA receptors are bound by Mg^{2+} which prevents them from opening, preventing influx of cations such as Ca^{2+} through NMDA receptors. Upon depolarization of the membrane, Mg^{2+} is dispelled, opening the receptor and allowing cation influx (Fig. 4A).

To record single spine events, we used conditions in which action potentials were blocked by TTX and NMDA receptors were kept permanently open via the absence of magnesium (Fig. 4B). Figure 4C shows two images obtained through such a recording. A single frame picture (left) shows no discernable calcium signal. If the maximum fluorescence values of all frames are overlaid, one can easily see single calcium transients in mushroom spines during the recording. Further 4D shows the corresponding three-and-a-half-minute video accelerated two-fold to give an impression of the overall frequency of events.

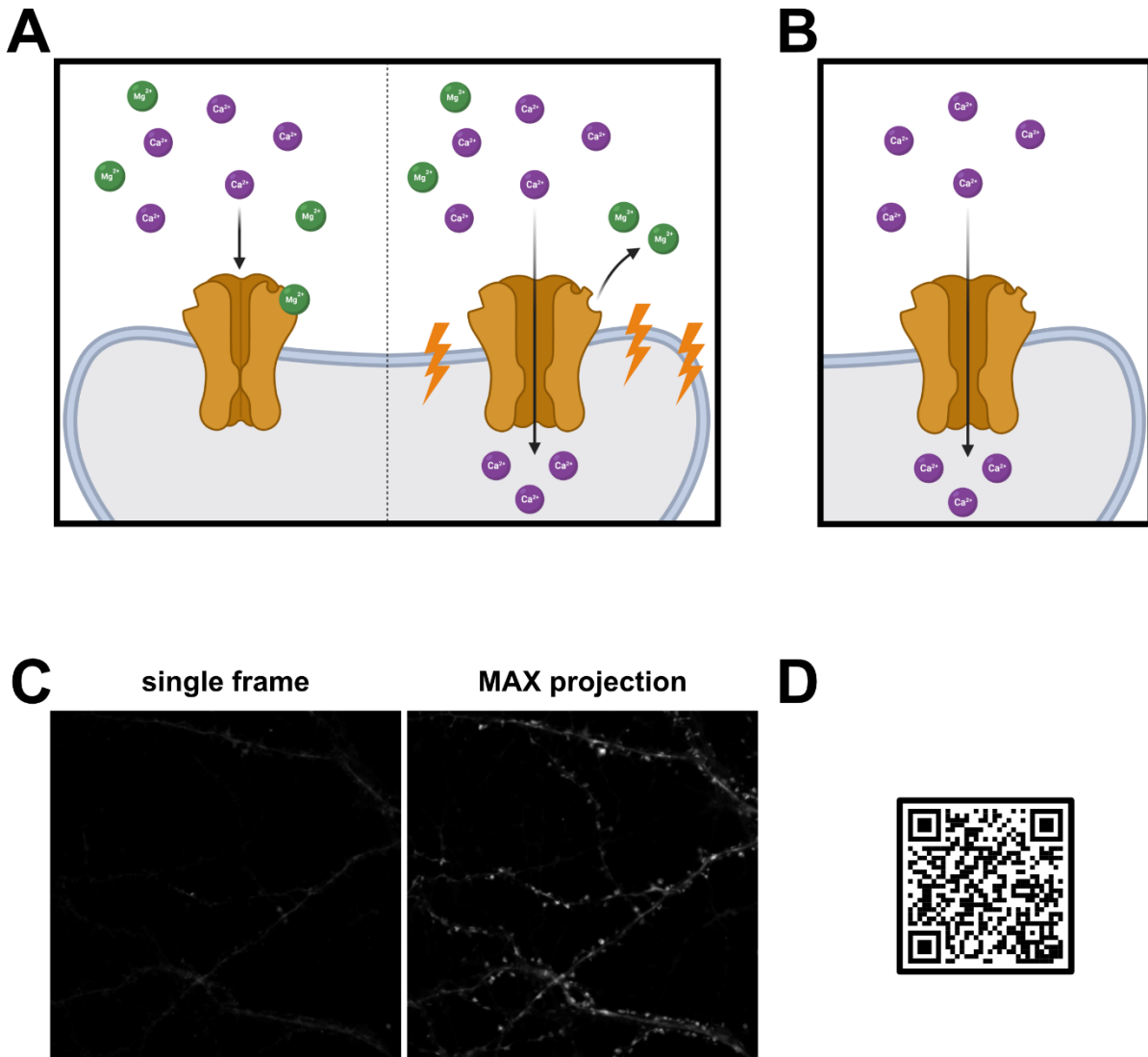


Figure 4: **A:** Simplified depiction of the function of NMDA receptors. In basal (left) and depolarized (right) conditions. **B:** NMDA receptor function in the absence of Mg²⁺ ions. **C:** Single frame (left) and maximum projection of all 379 frames (right) of a recording of single spine calcium events. The QR code can be scanned with the camera of a mobile phone and leads to a video of the recording.

3.1.3 Automation of Ca²⁺ imaging analysis

To avoid experimenter bias, reduce analysis time and reduce the influence of human mistakes in the analysis, one can aim to automatize the process. Recently the user-friendly tool CellProfiler has become more and more powerful, allowing the analysis of multichannel images and the performance of more and more complex analysis tasks. However, this tool was primarily developed to analyze static images or time-lapse recordings consisting of a low number of frames. As of the time point of this work (CellProfiler Version 4.2.1) the software is not optimized for recordings consisting of several hundred frames such as videos, especially in high number. This results in

simple analysis steps, such as the creation of overlays, taking several hours to days. Fiji, a version of ImageJ including additional plugins, offers a variety of functions and is suitable to handle videos with the computing power a personal computer provides. While less user-friendly with respect to more complex „ready to use“ functions that perform complex tasks without much user input, Fiji/ImageJ is very versatile and has its own programming language which allows one to chain single functions into integratable scripts called macros. We combined the usage of pipelines created with CellProfiler and self-coded, user-friendly, Fiji macros to allow for fast and reliable analysis of calcium imaging data.

Figure 5 shows the workflow of the analysis process. The code of the Fiji macros and CellProfiler pipelines are included in the Appendix. To measure dendritic calcium signaling upon KCl stimulation, we proceeded as follows. After recording the videos and sorting for acceptable cell health by the criteria described above (Fig. 5,1)) we used a custom Fiji macro to create maximum intensity overlays of all frames in a video file and removed background fluorescence by subtracting the corresponding minimum intensity overlay. The resulting images were then run through a CellProfiler pipeline which created a mask of the respective image (Fig 5, 2)) by:

1. Evening out the illumination along fluorescent objects in the image (here axons and dendrites) using the **CorrectIlluminationCalculate** and the **CorrectIlluminationApply** functions to ensure created masks cover the whole object and not just the regions of highest fluorescence.
2. Rescaling the fluorescence intensity based on the maximum in the image to prevent threshold-based mistakes due to low maximum intensity in some samples or conditions later in the pipeline, using the **RescaleIntensity** function.
3. Separating background from real signal via the **Threshold** function with a 12.5% cut-off in signal strength.
4. Converting the image into an object for further processing with the **ImageToObjects** function.
5. Filtering out small puncta as well as axons (for measurement from dendrites only) via the **MeasureObjectSizeShape** followed by the **FilterObjects** function.

6. Creating a mask based on the isolated dendritic signal using the **MaskImage** function.
7. Adding the prefix **_MaskDendrites** to the respective name of the original video and saving the mask in the determined output folder via the **SaveImages** function.

Subsequently we used a custom Fiji macro which, upon directory input by the user, matches masks and videos by name, creates regions of interest (ROIs) based on the masks, measures the pixel values inside the ROI over all frames of the respective video (Fig. 5,3)) calculates an average and adds the values together with the video name to an excel file which is extended until all videos with corresponding masks have been processed.

The resulting .xlsx file can then directly be used for further analysis and the creation of plots (Fig. 5, 4)).

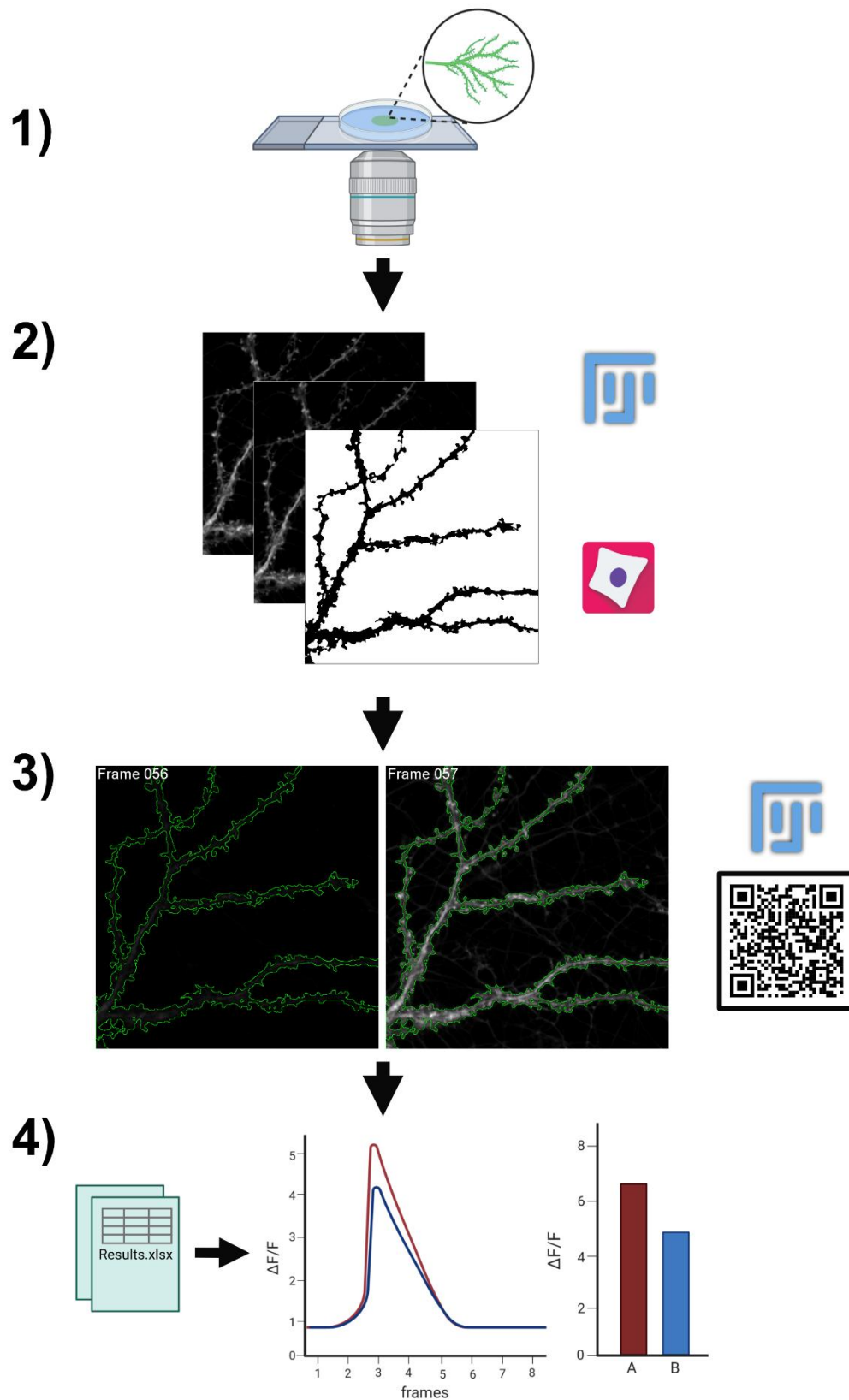


Figure 5: Workflow of the imaging and analysis process for calcium imaging data from stimulated cultures. After recording (1) masks were created using custom Fiji macros and CellProfiler pipelines (2) and dendritic signal was measured using a custom macro (3) creating excel files for downstream analysis (4). The QR code can be scanned with the camera of a mobile phone and leads to a video of the recording.

The analysis of synaptic events proved more challenging (Fig. 6). The initial steps were similar. We again used a custom CellProfiler pipeline which created a mask of synapses that signaled during the recording (Fig. 6,1),2)) by:

4. Rescaling the fluorescence intensity based on the maximum in the image to prevent threshold-based mistakes due to low maximum intensity in some samples or conditions later in the pipeline, using the **RescaleIntensity** function.
1. Evening out the illumination along fluorescent objects in the image using the **CorrectIlluminationCalculate** and the **CorrectIlluminationApply** function to ensure created masks cover the whole object and not just the region of highest fluorescence.
2. Identifying synapses with **IdentifyPrimaryObjects** and applying a size (2 pixel minimum diameter) and an intensity threshold (10%).
3. Separating synapses which were positioned close to each other to avoid them wrongly appearing as one object in the mask using the **ExpandOrShrinkObjects** function.
4. Filtering out objects that were too small (here <10 pixels) or too big (here >115 pixels) to be synapses via the **MeasureObjectSize** and **FilterObjects** functions.
5. Creating a mask based on the isolated dendritic signal using the **MaskImage** function.
6. Adding the prefix **_MaskSynapses** to the respective name of the original video and saving the mask in the determined output folder via the **SaveImages** function.

For further analysis we used the same Fiji macro mentioned above. When launching the macro, the user can specify if a measurement should be performed with one ROI for the provided mask or create separate ROIs for separate objects (Fig. 6,3)). The following processing of the videos is identical to the above-described steps used to measure dendritic calcium signaling upon KCl stimulation, with the difference that instead of one list of values, as many lists as there are objects in the mask are created and added to the excel file. For recordings containing a small number of different

objects (such as cells) the resulting excel file is sufficient for further analysis as long as the required information only concerns average/max/min intensity or similar values that Fiji's **measure** function offers. In our case we had to further process this file, since we were also interested in event frequency and length.

To do this we used a custom R script that was able to read and transform the format of the created .xlsx files and used a peak calling approach to determine when peak signals rose above a certain fluorescence value (here 112.5% of the average) and dropped below it again (Fig. 6,4)). The script outputs an excel file containing the frequency and duration of these peaks, which could then be used for further processing (Fig. 6,5)). In the final analysis non-synaptic fluorescent particles were filtered out by applying cut-offs based on the duration of peak signal and by removing every object that shows a peak number of 0.

In conclusion the combination of these tools and especially the Fiji script allows a user friendly, fast and reliable tool to analyze calcium imaging data, since they only require user input on the thresholds and location of the files.

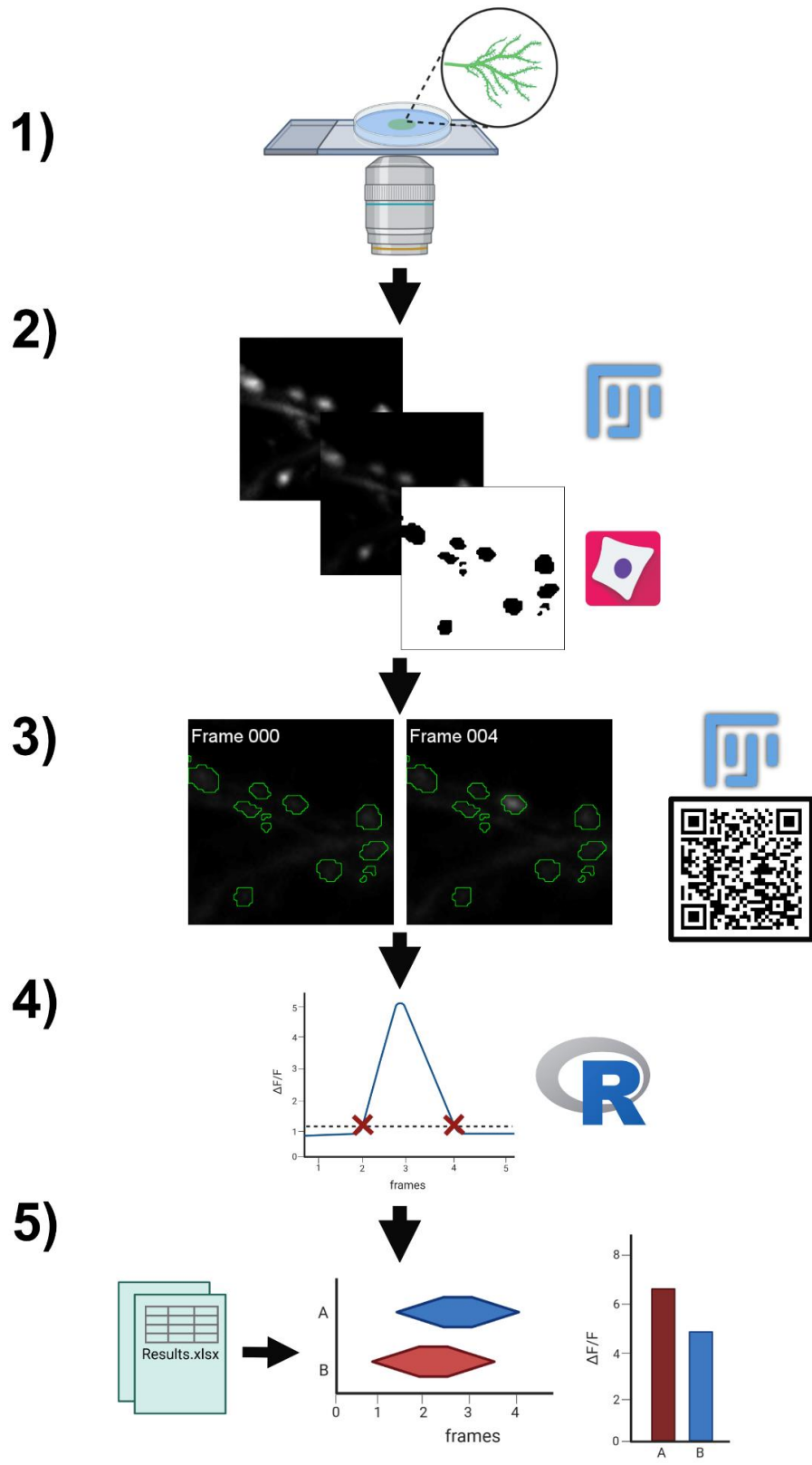
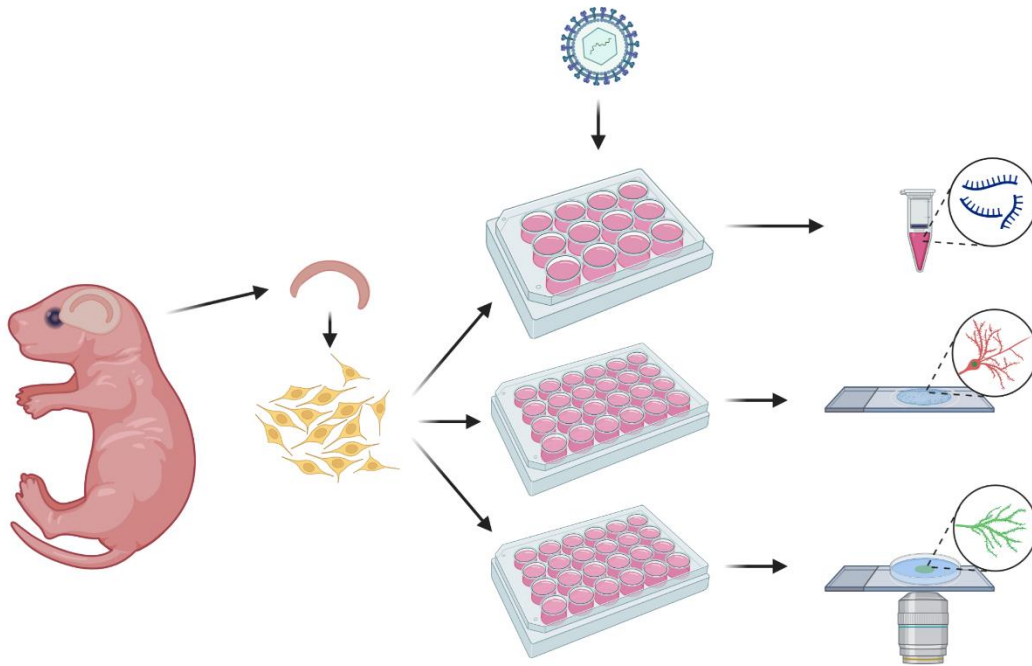


Figure 6: Workflow of the imaging and analysis process for calcium imaging data from single spine events. After recording (1) masks were created using custom Fiji macros and CellProfiler pipelines (2) and individual synapses measured using a custom macro (3). Data was then further processed with a custom R script to identify peak length and amplitude (4) creating excel files for downstream analysis (5). The QR code can be scanned with the camera of a mobile phone and leads to a video of the recording.

3.2 Chapter 2 – Brd2 KO in primary hippocampal cell culture



Graphical Abstract: A depiction of the experimental procedure. We dissected the brains of E17.5 Brd2 flox/flox embryos and isolated the hippocampi. The resulting tissue was digested with papain to isolate primary neurons that were plated either on 12 well plates, for later RNA extraction, or onto glass coverslips in 24 well plates for either immunostaining or calcium imaging. AAVs to express GFP (as a control) or Cre (to knockout Brd2) under control of the CamKII promoter were applied on DIV3. Cells were harvested for RNA extraction or fixed for immunostaining at DIV16. Calcium imaging was performed at DIV15.

To identify the role of Brd2 in the development and function of primary hippocampal neurons, we took an unbiased investigative approach. After validating that Brd2 was knocked out in our AAV:Cre transduced cultures using qPCR (Fig. 1A), we prepared libraries from 125 μ g of isolated RNA and used next generation sequencing (TruSeq) to observe the resulting deregulation of gene expression. After applying strict cuts-offs (\log_2 Fold 0.8), we found 296 genes deregulated (118 up, 179 down), in the Brd2 KO cultures (Fig.1B). A ClueGo analysis revealed deregulated genes in GO biological function categories linked to signaling of chemical synapses, calcium signaling and calcium homeostasis (Fig.1C). The proteins encoded by the deregulated genes were unsurprisingly mainly located at the neuronal projections, specifically the synaptic membrane (Fig. 1 D). We designed qPCR primers and validated several key genes of the respective categories (Fig. 1 E). Intriguingly we found the neuron-specific immediate early genes Brain Derived Neurotropic Factor (BDNF), Npas4 and Fos

down-regulated, which would point towards reduced synapse strengthening in response to neuronal activity (Okuno 2011). Contradictive to this, we found genes that would indicate increased strengthening of the synapse: Myo5b (a protein responsible for transporting GluA1 subunits to dendritic spines) (Lise et al. 2006) and Ryr1 (a receptor responsible for releasing Ca²⁺ from the ER in neurons) (Johanning et al. 2015) were highly upregulated.

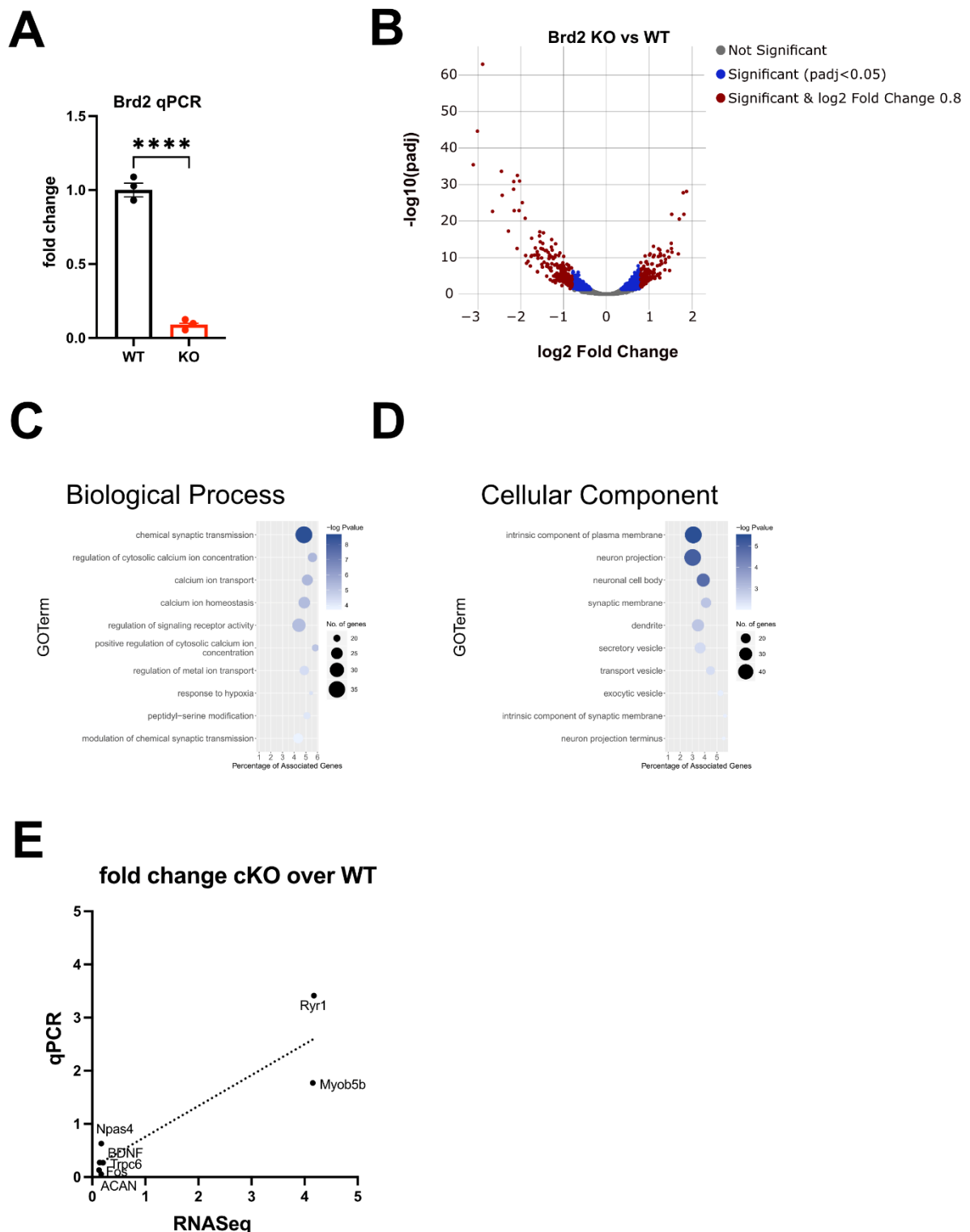


Figure 1: **A:** A qPCR performed with primers spanning the 5' intron exon boundary junction of Brd2s exon 2 on cDNA synthesized from Brd2 fl/fl primary hippocampal neurons either transduced with AAV8 GFP-cre or AAV8 GFP. (Significance determined by Student's t-test). **B:** A volcano plot of differentially expressed genes between Brd2 KO and WT identified by RNAseq. Only genes with a log₂ fold change > 0.8 or < -0.8 (red dots) were considered in downstream analysis. **C:** A depiction of Biological Process GO categories enriched with a 0.8 log₂ fold cut-off. **D:** A depiction of Cellular Component GO categories enriched with 0.8 log₂

To investigate synapse strength in Brd2 KO cultures, we performed ICC stainings of the pre- and postsynapse using the synaptic markers Synaptophysin (Syp) and postsynaptic density protein 95 (PSD95), respectively (Fig. 2A). The signal strength of these markers is indicative for the strength of the respective part of the synapse (Masliah et al.1990; Ehrlich et al. 2007). We found no difference in synapse size (Syp signal area; Fig. 2B), number of synapses (Syp puncta per length dendrite; Fig. 2C) or Syp signal strength (Fig. 2D) between conditions in DIV16 mouse hippocampal neurons. The postsynaptic marker PSD95 (Fig. 3A) puncta size (Fig. 3B) and number per length dendrite (Fig. 3C) was unchanged, but PSD95 signal was significantly weaker in Brd2 KO compared to WT (Fig. 3D), indicating a weakening of the postsynapse in the absence of Brd2.

We then performed two different types of Ca^{2+} imaging experiments, in spontaneous and evoked conditions, to gauge neuron calcium signaling capabilities. We transduced DIV3 mouse primary hippocampal neurons with a GCaMP6f AAV under a CaMKII promoter and imaged cultures at DIV15 in both approaches. We then used a combination of a custom Cellprofiler pipeline, Fiji macro and peak calling R script (for code see Appendix) to analyze Ca^{2+} signals.

First, we imaged neurons in ACSF containing TTX and lacking Mg^{2+} . TTX suppresses action potentials, while the absence of Mg^{2+} removes the Mg^{2+} block of NMDA receptors, allowing calcium influx. This allowed us to observe single, spontaneous, synaptic vesicle fusion events in the form of transient increases in GCaMP6s fluorescence in dendritic spines. WT and KO example videos are shown in Figure 4A (scan the QR code with your smartphone camera to view the video). The arrow indicates a single synapse in each condition. The corresponding fluorescence intensity over time at this synapse is shown in Figure 4B. Figure 4C shows five frames of one synaptic calcium transient event (1 frame = 550 ms) at the indicated synapses from WT or KO neurons, and a corresponding video (Fig. 4D). While average event fluorescence intensity (Fig. 4E) and frequency (Fig. 4F) were unchanged, KO event duration was significantly shorter (Fig. 4G). Figure 4H shows an example overlay of WT and KO events with different durations.

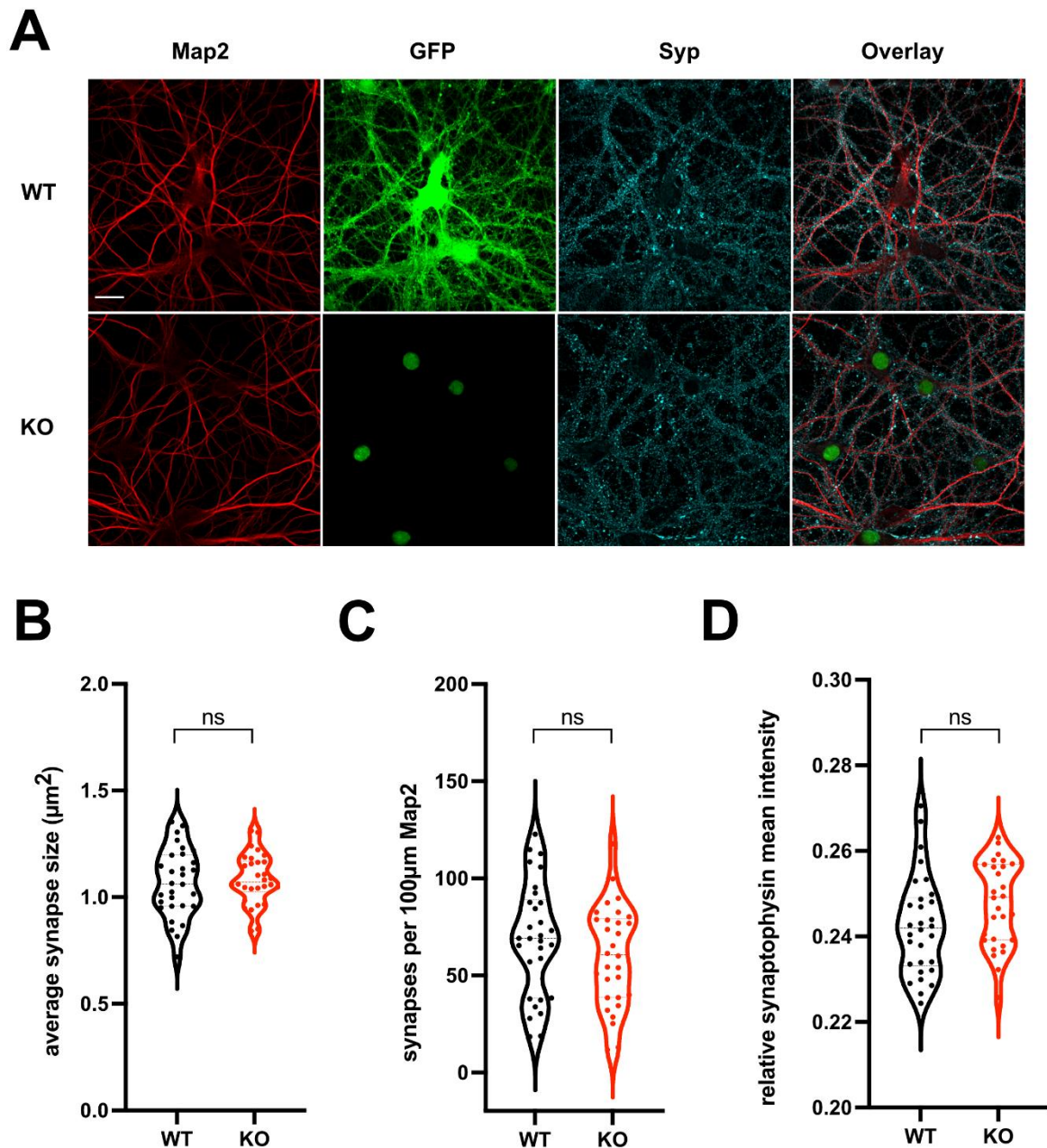


Figure 2: A: Representative pictures from ICC performed with Brd2 KO and WT primary hippocampal neurons. Cells were stained with antibodies for Map2 and Syp. GFP reporter signal is introduced by the viral constructs that were applied. Nuclear GFP signal indicated Brd2 KO neurons. Scale bar: 20 μm . **B:** A comparison of synapse size between conditions based on Syp signal. **C:** A comparison of synapse number between conditions based on Syp and Map2 signal. **D:** A comparison of mean intensity of Syp signal. (n = 30; pictures were taken from 6 coverslips generated from 3 separate cultures; significance determined by Student's t-test).

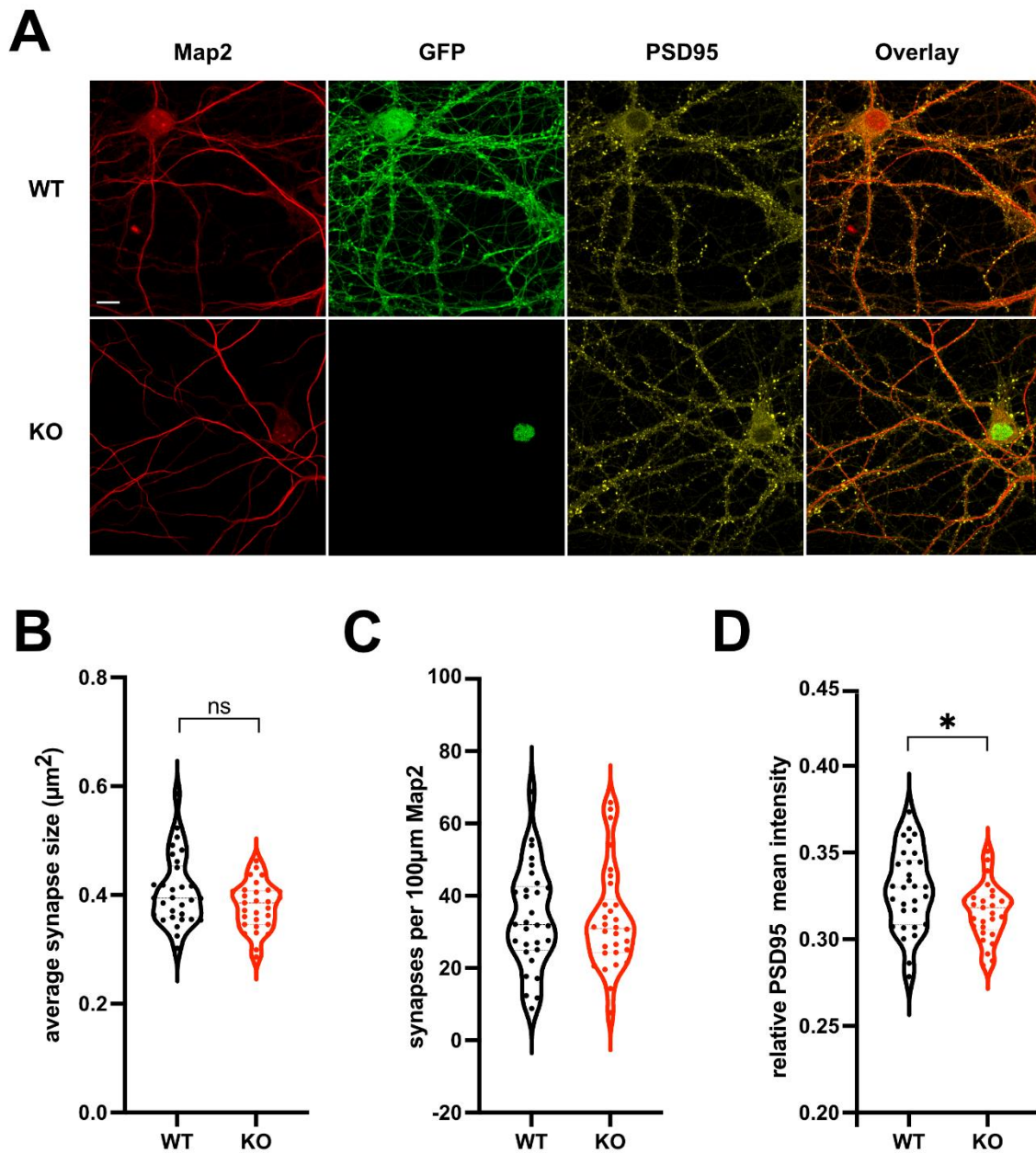


Figure 3: **A:** Representative pictures from ICC performed with Brd2 KO and WT primary hippocampal neurons. Cells were stained with antibodies for Map2 and PSD95. GFP reporter signal is introduced by the viral constructs that were applied. Nuclear GFP signal indicated Brd2 KO neurons. Scale bar: 10 μm **B:** A comparison of post synapse size between conditions based on PSD95 signal. **C:** A comparison of post synapse number between conditions based on PSD95 and Map2 signal. **D:** A comparison of mean intensity of PSD95 signal ($n = 30$; pictures were taken from 6 coverslips generated from 3 separate cultures; significance determined by Students t-test).

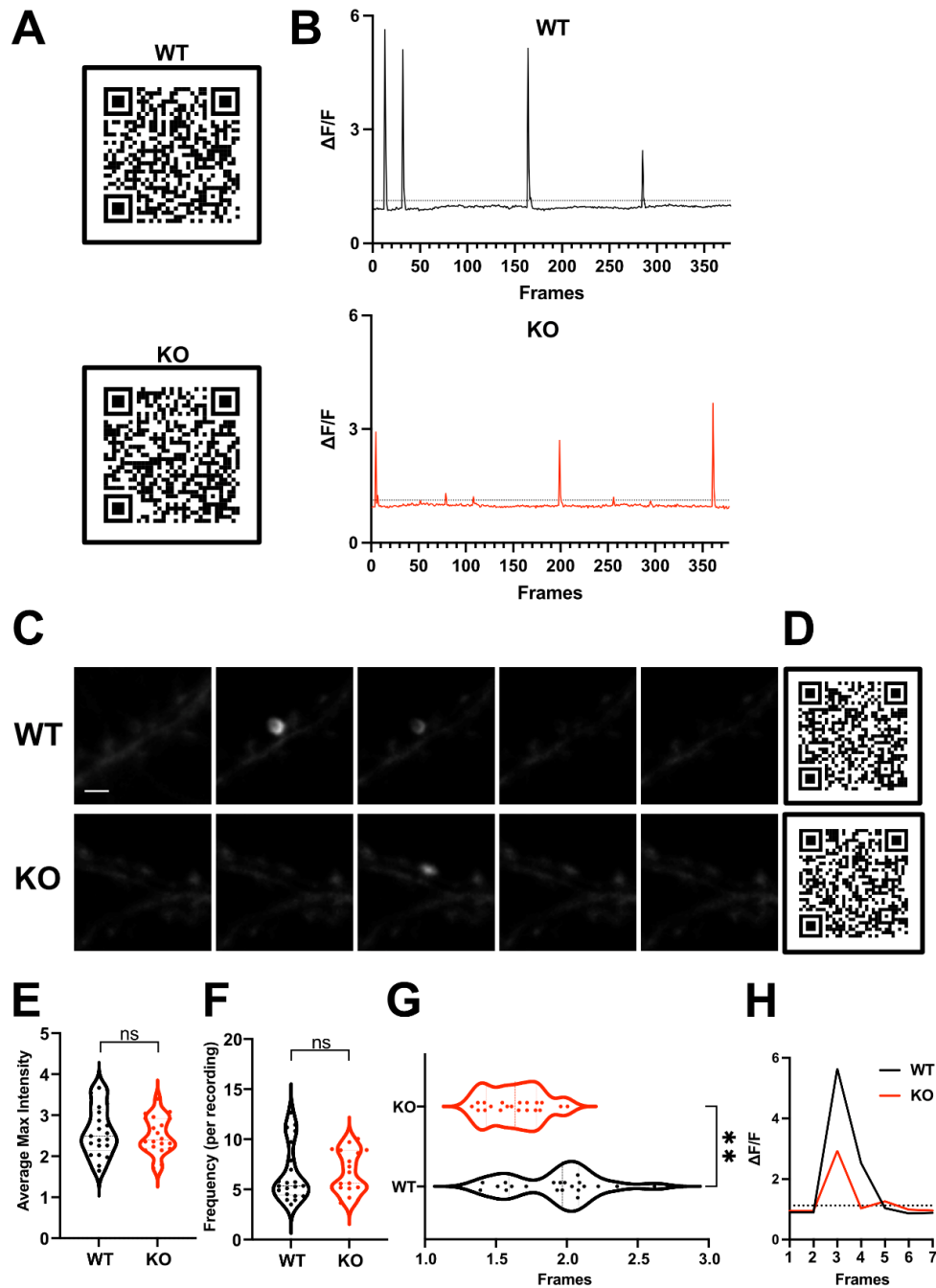


Figure 4: **A:** Two example videos of single spine recordings from either WT or Brd2 KO primary hippocampal neurons transfected with AAV8 GCaMP6f. The QR code can be scanned with the camera of a mobile phone and leads to a video of the recording. Fluorescence signal represents calcium; the green arrow indicates a single mushroom spine. **B:** Traces depicting the changes in normalized fluorescence intensity of the spine indicated in videos in **A** over the course of the recording for either the WT or Brd2 KO condition. The dotted line represents the cut-off above which signal was considered a peak instead of background noise in downstream analysis. **C:** Five isolated frames from each condition before, during and after a synaptic event. Scale bar: 2 μ m. **D:** A short example video of a single spine event for both conditions. **E:** A graph of the average maximum intensity of spine events between conditions. **F:** A graph depicting the average event frequency between conditions. **G:** A graph depicting the average event duration between conditions. **H:** An example trace of two peak events, one for each condition (n= 20; recordings were taken from 5 coverslips from 2 separate cultures; single dots represent the averaged values of all measurements collected in one recording; significance determined by Student's t-test).

We then examined evoked calcium responses to depolarization with bath applied 45 mM KCl. A baseline fluorescence in 5 mM KCl ACSF control conditions was first acquired for 55 frames, followed by application of a final concentration of 45 mM KCl ACSF to depolarize neurons. Figure 5A shows WT and Brd2 KO example videos over the course of the entire experiment (3 min. 30 sec.), and Figure 5B shows the response in WT and KO neurons after the addition of KCl at frame 55(1frame = 550ms). We observed a potential delay in the onset of calcium signal in Brd2 KO neurons, which we could not precisely quantify due to the frame rate of acquisition. Figure 5C shows average fluorescence change ($\Delta F/F$) of WT and KO cultures. A significant difference in amplitude or response was observed, (Fig. 5D). Normalization of the fluorescence decay to maximum amplitude (Fig. 5E) also revealed an increase in decay time in Brd2 KO neurons compared to WT (Fig. 5F).

The increased Tau of calcium signal decay we observed might be expected with an upregulation of Ryr1, which is responsible for the release of Ca^{2+} from the ER after the initial calcium influx from the plasma membrane. However, the weaker KCl response (Fig. 5C) and shorter Ca^{2+} signal duration in individual synapses in Brd2 KO neurons (Fig. 4G,H) is contradictory to the expected phenotype caused by Ryr1 upregulation alone.. We therefore hypothesized that there must be an additional Ca^{2+} master regulator that is changed in Brd2 KO neurons.

We consulted the sequencing again, and found TRPC6, the channel protein responsible for replenishing Ca^{2+} stores in the ER of hippocampal neurons (Zhang et al. 2016) significantly downregulated, which we could validate via qPCR (Fig. 6A). We then co-stained DIV16 WT and Brd2 KO cultures with primary antibodies for the synaptic marker Syp and for TRPC6 itself (Fig. 6B). Using a custom Cellprofiler pipeline we measured TRPC6 signal intensity in Syp puncta (Fig. 6C). We found a significant decrease of TRPC6 in the synapses of Brd2 KO neurons (Fig. 6D). We concluded that the lack of TRPC6 leads to a deficit of Ca^{2+} in the ER of KO neurons causing the cells to attempt a compensation via an increase in Ca^{2+} expulsion. However, our data indicates that this attempt at compensation is insufficient to restore normal calcium signaling.

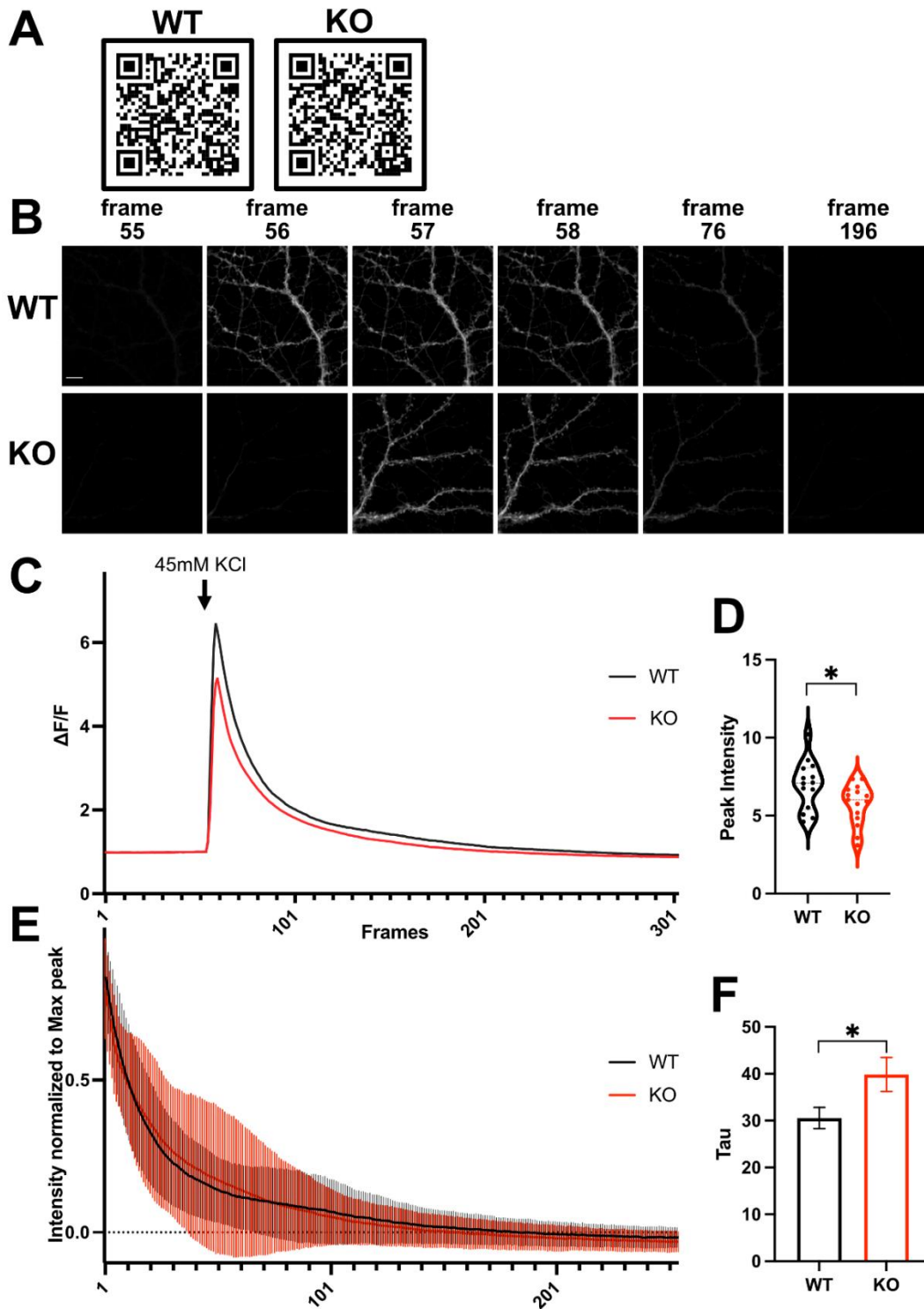


Figure 5: **A:** Two example videos of a Brd2 KO and WT culture transduced with AAV8 GCaMP6f being stimulated with 45mM KCl. The QR code can be scanned with the camera of a mobile phone and leads to a video of the recording. **B:** Six isolated frames from the respective videos depicting the exact moment before stimulation (frame 55) at stimulation (frame 56) and different timepoints after the stimulation (one frame is roughly equal to 0.55 seconds. Scale bar 10 μ m.) **C:** Averaged traces for both conditions of all recordings. **D:** A graph depicting the normalized maximum peak intensity post stimulus between Brd2 KO and WT (significance determined by Student's t-test). **E:** A graph depicting average signal decay post peak for both conditions. **F:** A graph of the calculated signal decay constant Tau for both Brd2 KO and WT ($n = 15$ for Brd2 KO and 14 for WT; recordings were taken from 5 coverslips from 2 separate cultures; error bars indicate SD).

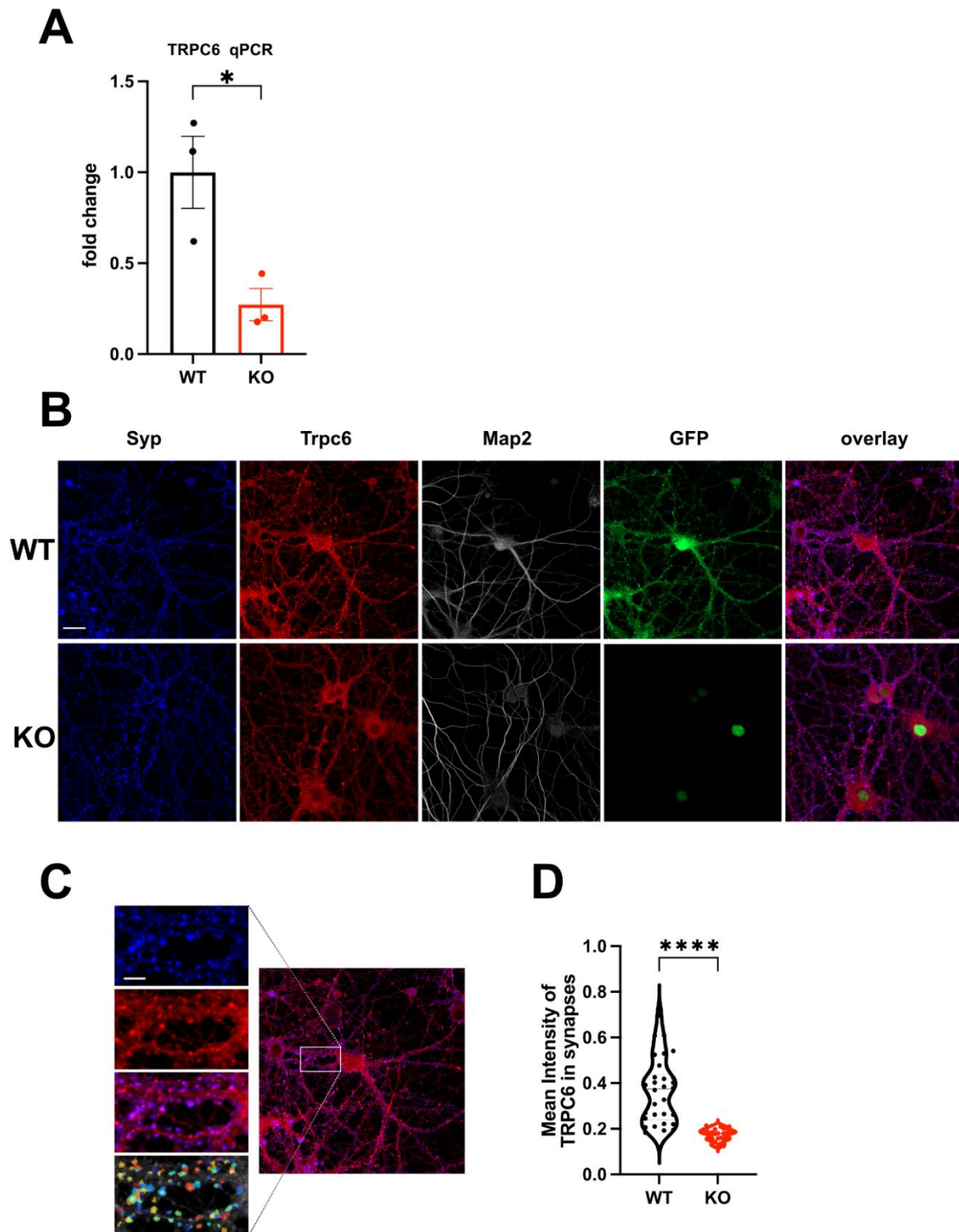


Figure 6: **A:** A qPCR performed for TRPC6 with cDNA generated from Brd2 WT or KO primary hippocampal cell cultures (significances determined by Student's t-test). **B:** Representative images from ICC of cultures stained for Map2, Syp and TRPC6 for both Brd2 KO and WT conditions. Scale bar: 20 μ m. **C:** A depiction of the analysis approach for determining TRPC6 signal strength in synaptic puncta with CellProfiler. Syp signal was thresholded and used to identify synaptic puncta. TRPC6 signal was then measured in these areas. Scale bar: 5 μ m. **D:** A graph of the mean TRPC6 intensity measured in synaptic puncta ($n = 30$; each dot represents the average value of a single image; pictures were taken from 6 coverslips generated from 3 separate cultures; significance determined by Student's t-test).

3.3 Chapter 3 – Behavior of Brd2 cKO and OE mice

Since Brd2 is a known developmental gene, we first performed qPCR with tissue from B6J WT mice (Janvier) of different ages, to determine whether Brd2 is still expressed in the later stages of life and could therefore play a role in neuronal function postnatally (Fig. 1 A). Unsurprisingly Brd2 expression in the hippocampus was at its highest level one week after birth (P7), when mice go through several neuronal developmental phases as pups. From young adult (3 month) to geriatric age (24 month) Brd2 mRNA levels were consistent at about 40-50% of the P7 expression level, indicating that the protein remains relevant for physiological function of adult hippocampal neurons. Western blots performed with 10 µg protein from sub-cellular fractions from three-month-old B6J mice showed a strong enrichment of Brd2 in the soluble nuclear and chromatin bound fractions (Fig. 1B), as expected for a chromatin associated protein.

To study the function of Brd2 in mice postnatally, we crossed mice that had LoxP recombination sites upstream of the second and downstream of the third Brd2 exon, with mice carrying Cre recombinase under the CaMKII promoter (Fig. 1C). When the CaMKII promoter becomes active between P15 and P21 (Mayford et al. 1996) the recombinase cuts the two exons out, leading to a frameshift in the ORF of Brd2 mRNAs which in turn should lead to degradation, preventing translation into further protein. Figure 1D shows PCRs of DNA from a fl/+, +/+ and homozygous fl/fl animal beside each other. A PCR for the Cre recombinase gene is shown below. Unlike constitutive homozygous Brd2 knockout mice, which die by embryonic day 11.5 (Shang et al. 2009), our Brd2 conditional knockouts (cKO) survived to adulthood and showed no outward signs of deformities.

Next, we compared Brd2 mRNA levels between the cerebellum and CA1 region of the hippocampus in 3-month-old Brd2 fl/fl cre- and cre+ animals by qPCR (Fig. 1E). Brd2 expression was much more reduced in the cKOs CA1 compared to control, than it was in the cerebellum. Since CaMKII expression is much stronger in mouse forebrain and hippocampus compared to other brain regions (Mayford et al. 1996) we concluded that our Brd2 cKO was forebrain and hippocampus specific as intended. A difference in Brd2 protein expression was also observable in Western blots from the nuclear fraction CA1 of 3-month-old cKO animals compared to their WT littermates, convincing us that

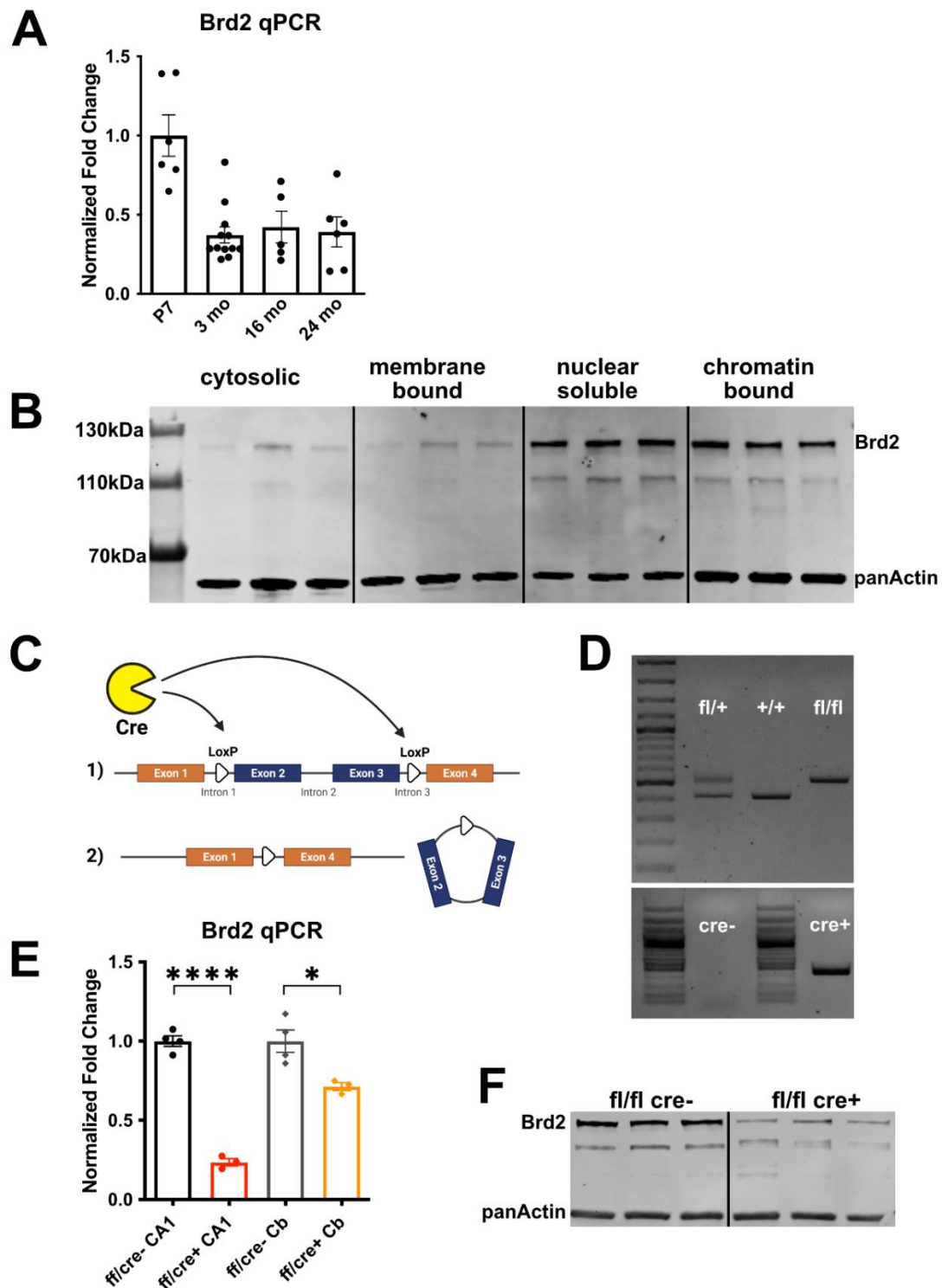


Figure 1: **A:** A Brd2 qPCR performed with cDNA generated from hippocampal tissue of B6J WT mice (Janvier) acquired at different ages. **B:** A western blot performed with protein subfractions extracted from hippocampal tissue of 3 month old WT mice using Brd2 and pan Actin antibodies. **C:** A depiction of the concept by which Brd2 cKO was achieved. **D:** A genotyping performed for the 5' LoxP site of Brd2 or the cre gene. **E:** A graph showing qPCRs performed with cDNA generated from the cerebellum or the CA1 hippocampal region of 3 month old Brd2 fl/fl cre+ and cre- mice using primers spanning the 5' intron-exon boundary junction of Brd2's exon 2 (significance between cre+ and cre- conditions determined by Student's t-test.) **F:** Western blot performed with nuclear protein extract from the CA1 region of three month old Brd2 fl/fl cre+ and cre- mice using Brd2 and pan Actin antibodies.

the cKO in adult mice was successful (Fig. 1F). Since the second visual band did not correspond to the size of any of Brd2 reported isoforms, we considered it an artifact.

Brd2 cKO animals had no gross abnormalities in the affected regions, indicated by coronal sections from 3-month-old WT and cKO mice stained for the neuronal markers Map2 and NeuN (Fig. 2A and B). Since we could tie the decrease of acetylation levels of one of Brd2's binding sites (H4K12) to a decline in cognitive performance in mice (Peleg et al. Fischer Science 2010 PMID: 20448184), we were specifically interested in studying the learning and memory performance of our Brd2 cKO mice. To ensure that no potential anxiety phenotype would interfere with our memory tests, we first performed two control experiments.

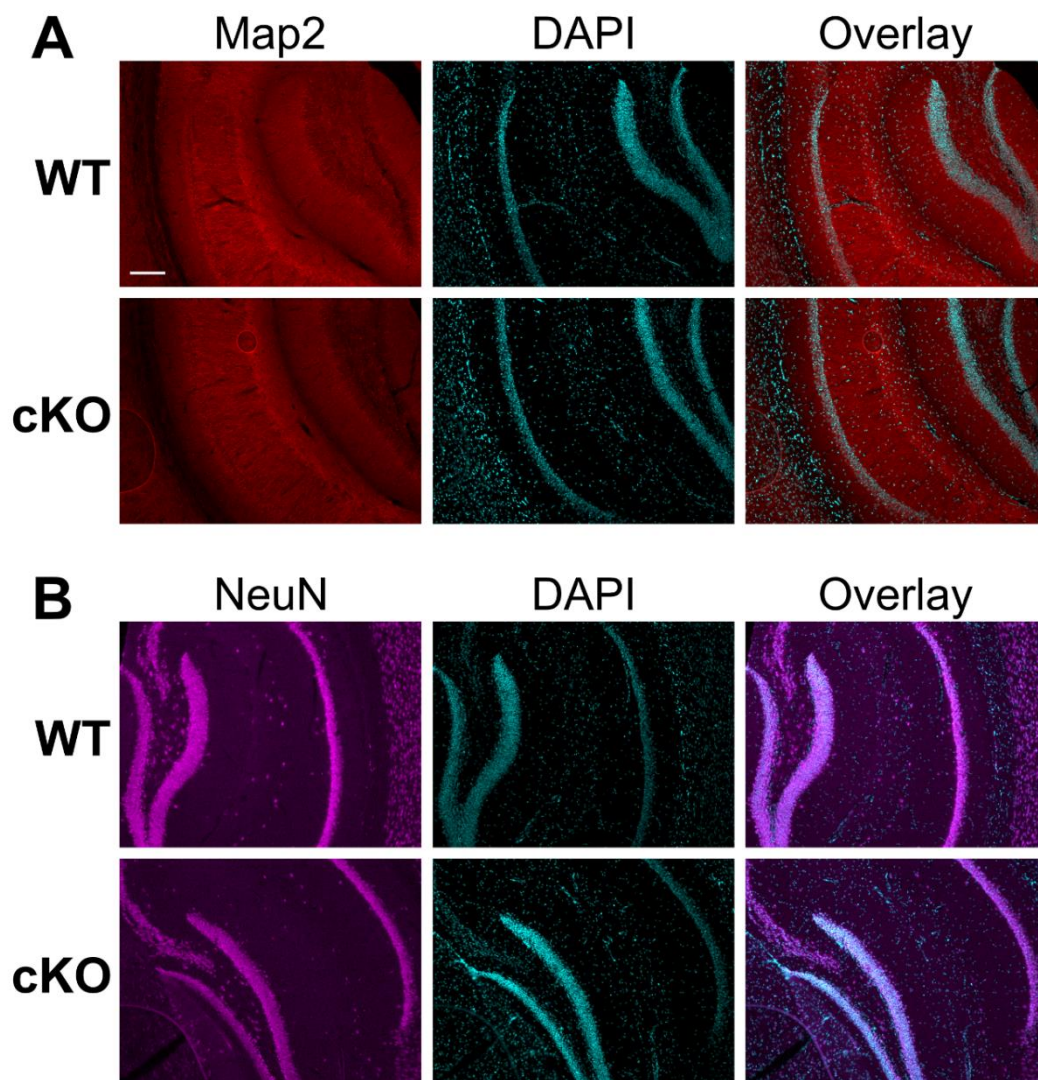


Figure 3: A: IHC images of coronal sections from three month old Brd2 cKO mice or their WT littermates stained for Map2 and DAPI. **B:** IHC images of coronal sections from three month old Brd2 cKO mice or their WT littermates stained for NeuN and DAPI.

The open field (OF) test is a classical test for locomotion, exploratory behavior and, to a degree, anxiety in rodents. Animals are placed in the middle of a square box that is positioned in a well-lit room. The movements of the mouse are then recorded via video (Fig 3A). Since rodents naturally avoid direct light and open spaces, the time the animals spend in the central area can be compared to the time they spend in the areas close to the walls, to give an indicator of their anxiety levels and readiness to explore their surroundings. We found no difference between exploratory behavior in WT and Brd2 cKO mice in this test (Fig 3B). There was a trend in the cKOs for faster movement speed, which could be taken as an indicator for mildly increased anxiety, however this difference was not significant (Fig 3C). We concluded that the Brd2 cKO animals' locomotion was not limited by the lack of Brd2 in the hippocampus.

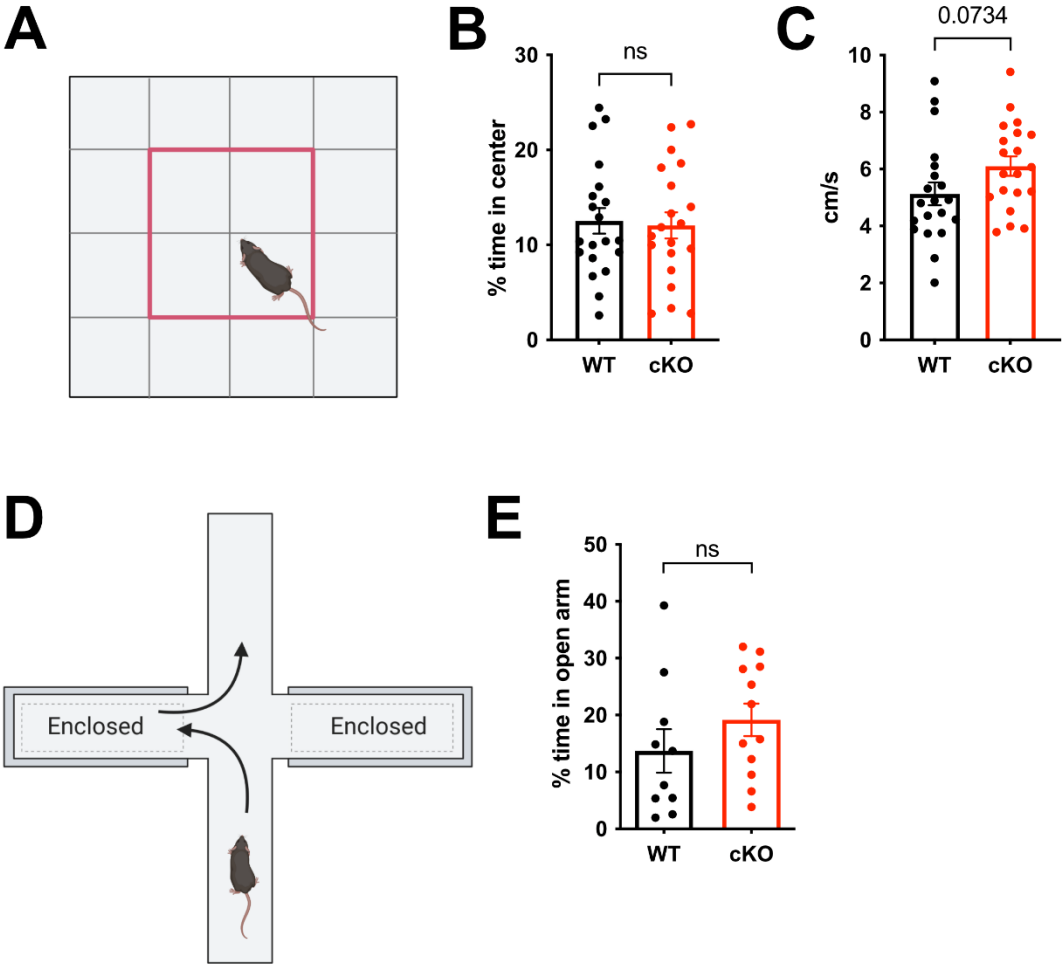


Figure 3: **A:** A depiction of an Open Field test paradigm (Created with [BioRender.com](https://www.biorender.com)). **B:** A graph showing the percentage of time Brd2 cKO or WT mice spend in the center of the open field arena. **C:** A graph of the average movement speed of mice in both groups during the open field test (n = 20 for both groups). **D:** A depiction of an elevated plus maze paradigm (Created with [BioRender.com](https://www.biorender.com)). **E:** A graph showing the percentage of time Brd2 cKO or WT mice spend in the open arms of the elevated plus maze (significance determined by Student's t-test).

To fully exclude an anxiety driven phenotype, after observing the trend in Figure 3C, we performed the Elevated Plus Maze (EPM) test. In this behavior test mice are placed on a plus shaped platform in a well-lit room. The platform has two arms without walls (open) and two arms surrounded by walls (enclosed). Since mice instinctively avoid bright light and open spaces, they spend most of the time in the maze in the closed arms. More time spent in the enclosed arms is a strong indicator for anxiety, while more time spent in the open arms is an indicator for the lack thereof (Fig. 3D). We found no significant difference in the percentage of total time spent in the open arms between Brd2 cKO and WT littermates (Fig. 3E) and therefore concluded that Brd2 cKO mice show no increase or decrease in anxiety levels.

After having validated the absence of phenotypes that might interfere with the reliability of memory tasks, we proceeded with different behavioral paradigms to evaluate the Brd2 cKO animals' memory performance.

We first performed a novel object recognition (NOR) test with mice that were previously used in the OF test. In this three-day test animals are placed into an open field arena on day one to get familiarized with the surroundings. Since our animals already had that experience during the OF test, we directly proceeded to day two, the habituation phase. Here, two similar objects (in our case two black plastic cubes) are placed in the arena together with the mouse who is then given time to explore. Since mice are naturally curious, they will investigate the objects. The time the animal investigates each object was recorded. We then placed the animals back in their home cage and replaced one of the objects with a new one. After a waiting period (5 min.) the animals were again placed in the arena and recorded (Fig. 4A). This tests the animal's object recognition and short-term memory (STM) based on the time they spend exploring the new object. The next day, 24h later, we also replaced the second object before placing the mice in the arena once more. Again, the time spent with each object was recorded. This allows for the evaluation of the animal's long-term memory (LTM). A mouse with intact memory formation should show a preference for the new object, since it remembers having already investigated the old one. Both groups showed a significant preference for the new object on day two, indicating that the absence of Brd2 in CaMKII positive neurons has no detrimental effects on LTM as such (Fig 4B). In STM the Brd2 cKOs showed significantly more interest in the new object when compared to

habituation, which the control did not. However, they did not perform statistically significantly better than their WT littermates (Fig 4B).

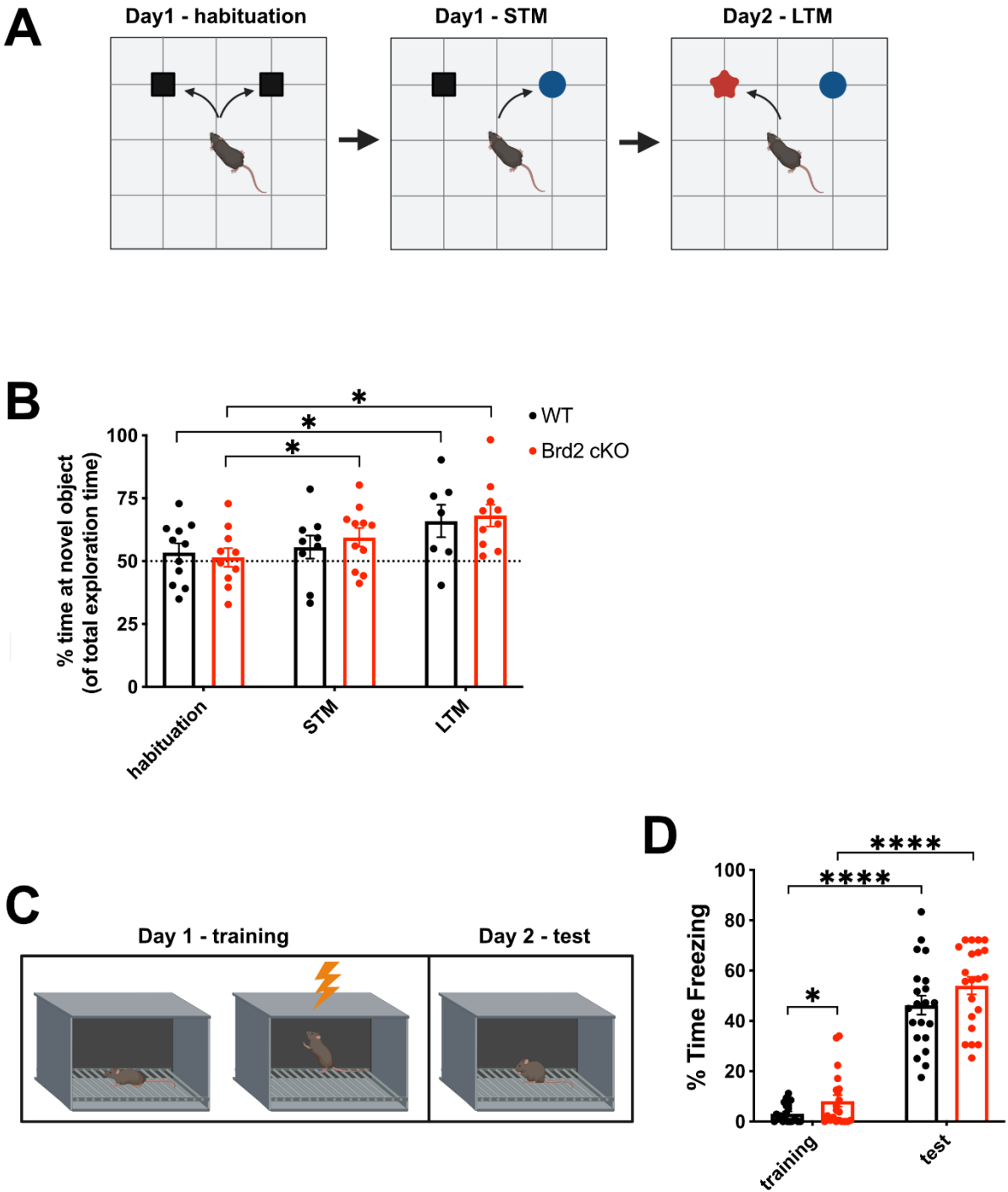


Figure 4 A: A depiction of the Novel Object Recognition paradigm (Created with BioRender.com). **B:** A graph showing the results of a Novel Object Recognition test performed with Brd2 cKO mice and cre-WT littermates (significances were determined using a one way ANOVA followed by post hoc Dunnet's test). Mice that did not explore the objects were removed from the analysis.) **C:** A depiction of a Fear Conditioning paradigm. **D:** Graph showing the freezing behavior during Fear Conditioning of both WT and Brd2 cKO mice (significances were determined using a one way ANOVA followed by post hoc Dunnet's test).

Next, we tested associative fear memory via fear conditioning (FC) (Fig. 4C). In this test mice are placed in an enclosed box with a metal grid on the floor. The animals are free to explore this new environment for 3 min. at the end of which they receive a 0.5 mA foot shock for 2 seconds. The animals are then placed back into their home cage. 24h later they are exposed to the same context again. A camera records the movement of the mice during both days. We then compared the amount of time the animals spend unmoving in so-called fear induced freezing behavior, as an indicator of the fear memory of the animals. Both groups froze for comparable amounts of time during testing, however some of the Brd2 cKO animals showed reduced movement during training, which led to a significant difference compared to the control (Fig. 4D). Overall, our data suggest that the fear memory of Brd2 cKO mice remains unchanged. We then performed the Morris Water Maze (MWM) navigation task (Fig. 5A) with our Brd2 cKO animals and their WT littermates. The MWM is a relatively challenging task, designed to test spatial learning and navigation in rodents by placing them in a round pool of opaque water. A platform is placed in one position close to the water's surface, invisible to the mouse. The animal is then given one minute to find the platform after being placed in the pool, using visual cues placed on the sides of the pool, while being recorded on video. This is repeated four times, from different starting positions in the pool, per training day. Upon end of the training session the animal is put back into its home cage. After several days of training the animals learn where the platform or „escape“ is located, which they are motivated to find since they are removed from the unpleasant experience of the pool earlier, if they locate the escape faster. We tracked the animals' learning by how fast they reached the platform during training sessions. Figure 5B shows the learning curves of our two groups A and B. The time scales are different, since the final test day is determined by the animals reaching a learning plateau when the latency to reach the platform stays stable at a certain level for several days in a row. The next day a Probe Test (PT) is performed instead of training. This consists of removing the platform from the pool, placing the mouse in the pool facing the wall and then recording its movement for one minute. An animal that has learned the position of the platform and not just developed a strategy to find it faster (e.g. swimming in a circle) will spend most of the time in the pool around the area in which the platform was located before. By dividing the area of the pool into quadrants and calculating the percentage of time the animal spent either in the target quadrant (TQ)- the quadrant formally containing the platform, or the other quadrants (OQ), one is able

to test if the animal formed a memory of where the escape was located. While the cre-WT animals showed a clear preference for the target, the Brd2 cKO mice did not distinguish between the quadrants, indicating that they had not formed a memory of the platform's position (Fig 5D). The swimming speeds on the first day of training and on PT day were comparable between the groups (Fig 5E), excluding swimming speed as a possible confounding factor.

We concluded that while Brd2 cKO mice do not display severe cognition deficits in simple associative memory tasks, the absence of Brd2 in CaMKII positive neurons postnatally seems to interfere with memory consolidation or recall in more complex memory tasks like the MWM. The learning curves of Brd2 cKOs are similar to those of WT controls (Fig 5B), indicating cKO animals remembered that the platform existed and had formed strategies to reach the platform faster than in the beginning of the experiment. The fact that they did not show a preference for the TQ, however, suggests that they have no clear memory where the platform was located or were unable to recall where it should be relatively to the clues.

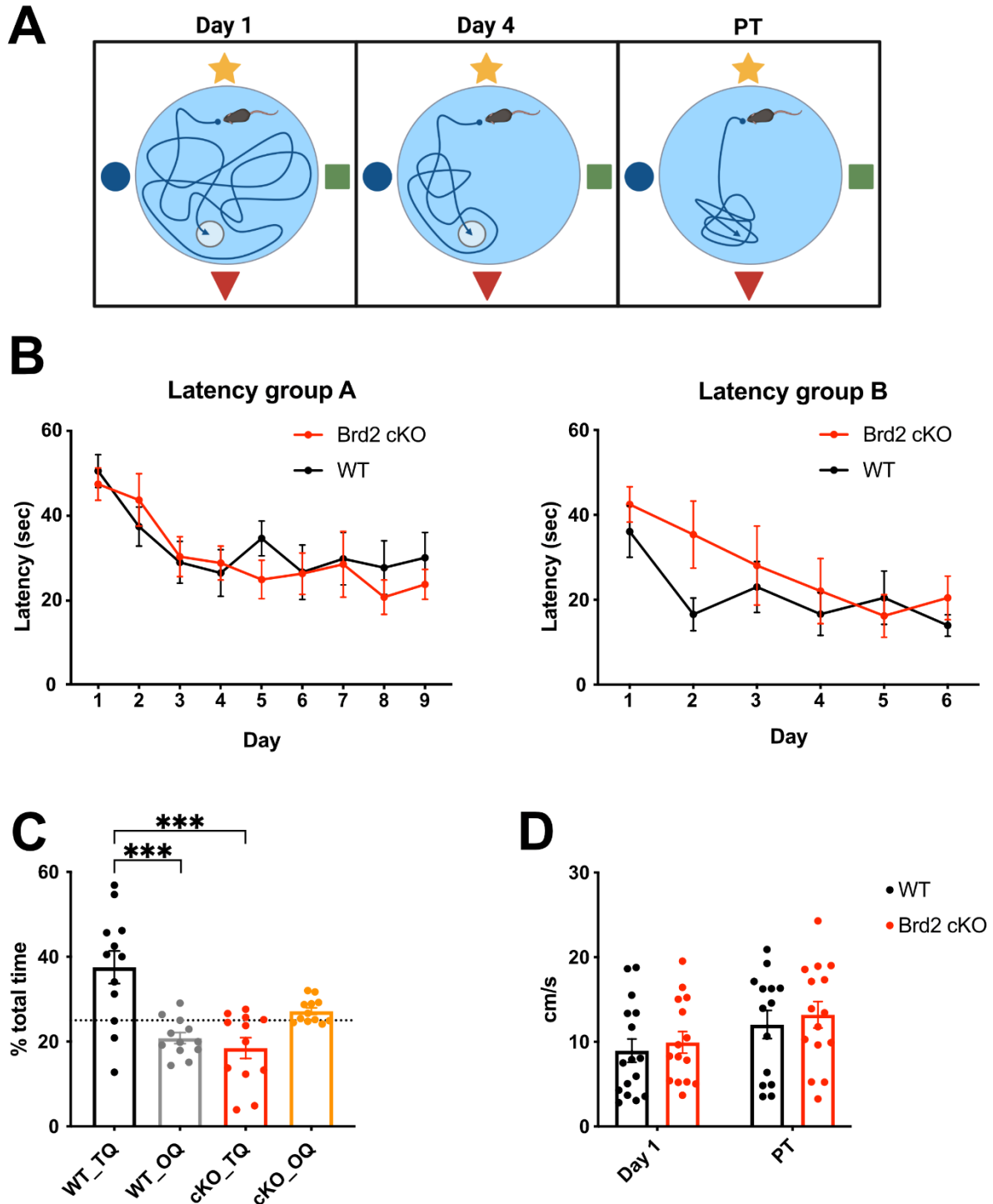


Figure 5: **A:** A depiction of the progression of a Morris Water Maze test. (Created with BioRender.com). **B:** Two graphs showing the escape latency of two separate groups of mice during Morris Water Maze training, performed by two different experimenters. **C:** A graph plotting the percentage of time WT and Brd2 cKO mice spend in the target quadrant during the probe test. The values collected from both test groups were pooled. **D:** A graph showing the swimming speed of mice during the first day of training and the probe test. (significances between conditions were determined by Students t-test).

BET Chromatin readers such as Brd2 are not all enzymatically active and therefore do not all have direct influence on gene expression. However, due to their role in scaffolding and recruitment of other transcriptionally active or chromatin remodeling proteins, a lower, or higher, availability of Brd2 in the cell's nucleus could influence related gene expression and function (LeRoy et al. 2008, Cheung et al. 2017).

To test this hypothesis, we cloned Brd2 fused to a polypeptide myc tag into an AAV 1/2 hybrid vector (Fig. 6A). We then produced virus from this plasmid, and stereotactically injected it into the lateral ventricle of ten-week-old B6J mice, ventral to the hippocampus. Our control group consisted of mice injected with the same virus carrying EGFP instead of Brd2-myc.

We aimed to reach three to ten-fold over-expression in our target tissue to avoid cytotoxicity by overburdening the cell with foreign protein. A qPCR performed with cDNA generated from tissue dissected two weeks after application of the AAV showed an over-expression (OE) of about five-fold on average in the dentate gyrus, the part of the hippocampus closest to the ventricle (Fig. 6B). We further verified over-expression of Brd2-myc at the protein level by staining hippocampal coronal sections of injected mice with myc (Fig. 6C).

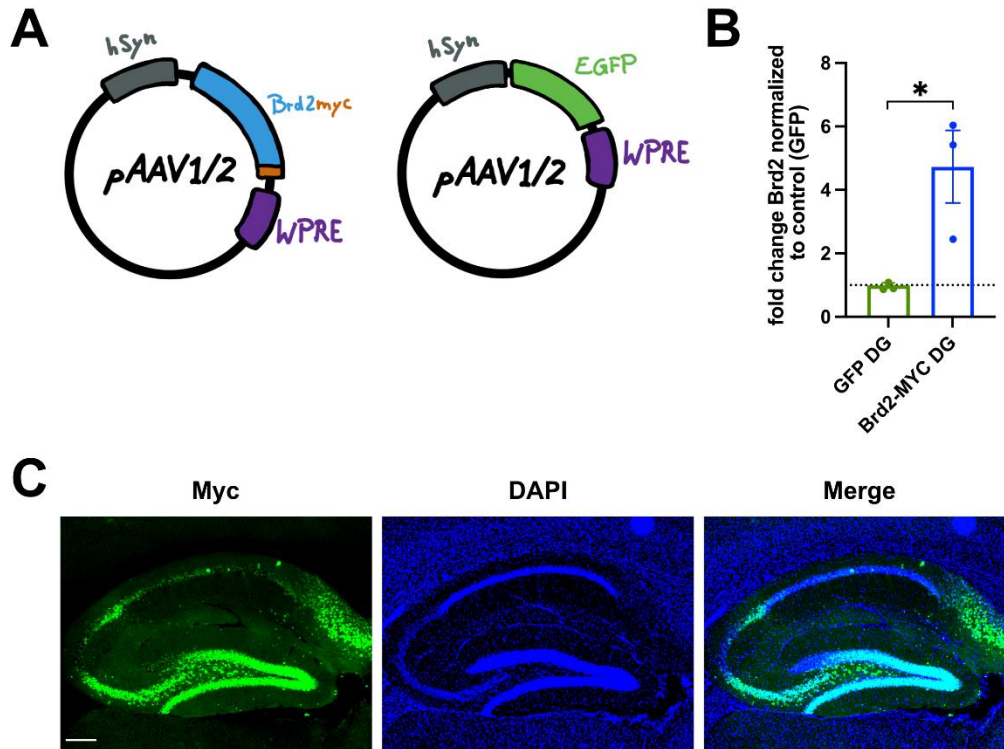


Figure 6: **A:** Simplified plasmid maps of the pAAV1/2 Brd2myc overexpression construct and its GFP counterpart. **B:** A qPCR performed for Brd2 with cDNA isolated from the dentate gyrus (DG) of mice either intracranially injected with AAV1/2 Brd2myc or the GFP control virus (significance determined by Student's t-test). **C:** An IHC image of a hippocampal coronal section stained with DAPI and a myc antibody to visualize Brd2myc overexpression in the brain of injected mice. Scale bar: 500 μ m. (Experiment was performed by Hendrik Urbanke for his Master's thesis, 2013).

We then proceeded to perform the same behavioral experiments that had shown differences in the performance of Brd2 cKO and WT mice, with our Brd2-myc and GFP animals. Exposure to the open field paradigm revealed no difference in anxiety levels or explorative behavior between Brd2-myc and GFP groups (Fig. 7A). We did not observe any gross behavioral or motor skill differences between Brd2-myc and GFP mice, reflected in similar movement speed of both groups (Fig. 7B). In novel object recognition both groups showed short term and long-term learning, however the Brd2-myc group performed significantly better in the STM task than the control (Fig. 7C). This was similar to what we observed in the Brd2 cKO (Fig. 4B) indicating that not only the absence but also the over abundance of Brd2 influences object memory.

Fear conditioning experiments performed with the Brd2-myc and GFP injected animals revealed two differences between the Brd2 cKO mice and the Brd2 over-expression cohort. In contrast to our cKO results, Brd2-myc animals did not show higher initial levels of freezing on the training day, but did display significant more freezing behavior on the testing day (Fig. 7D) suggesting that a higher amount of Brd2 in hippocampal neurons leads to an enhancement of fear memory formation or recall.

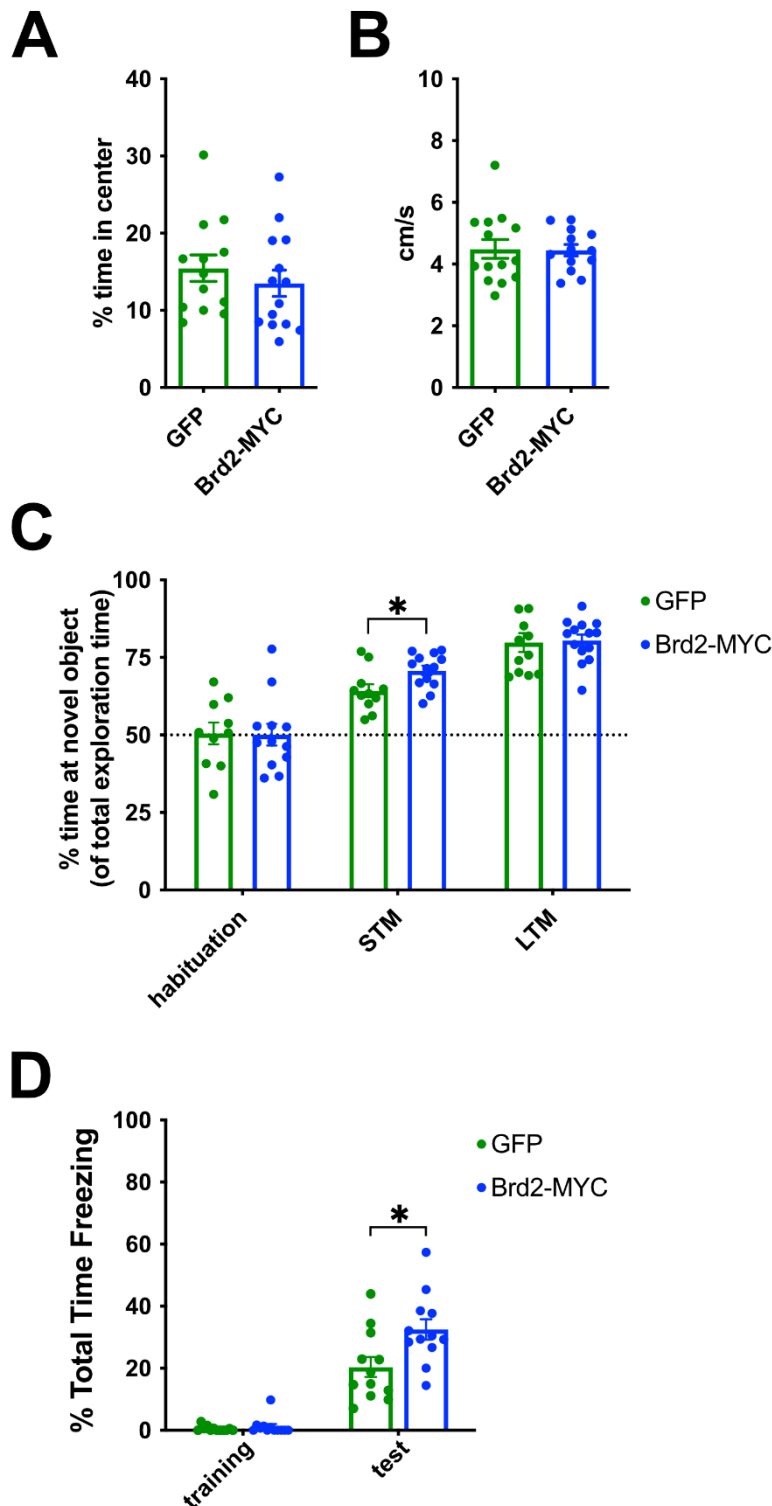


Figure 7: A: A graph showing the percentage of time Brd2 overexpressing (OE) and GFP mice spend in the center of an Open Field arena. **B:** A graph of the movement speed of the respective groups in the Open Field. **C:** A graph of the Novel Object Recognition (NOR) data collected from Brd2 OE and GFP control mice (significances between conditions were determined by Student's t-test). **D:** A graph depicting freezing behavior of Brd4 OE and GFP control mice during Fear Conditioning (FC) (significances were determined using a one-way ANOVA followed by post hoc Dunnet's test. Experiment was performed by Hendrik Urbanke for his Master's thesis, 2013).

Brd2-myc mice performed comparable to GFP control mice during the training days in the Morris water maze (Fig. 8A), but they showed no preference for the target quadrant in the Probe test, where GFP control mice did (Fig. 8B). There was no difference in swimming speed between Brd2-myc and GFP mice that could indicate a motor deficit as a confounding factor (Fig. 8C). This result indicates, that over-expression as well as removal of Brd2 from hippocampal neurons negatively influences performance in complex, spatial memory tasks. This suggests an underlying equilibrium of Brd2 is required for adequate memory formation. Taking all the behavioral data into account, we concluded, that the lack of, as well as the over-abundance of, Brd2 in hippocampus neurons both have a slight beneficial affect on short term memory but an overall detrimental effect on associative long term memory formation or recall required for

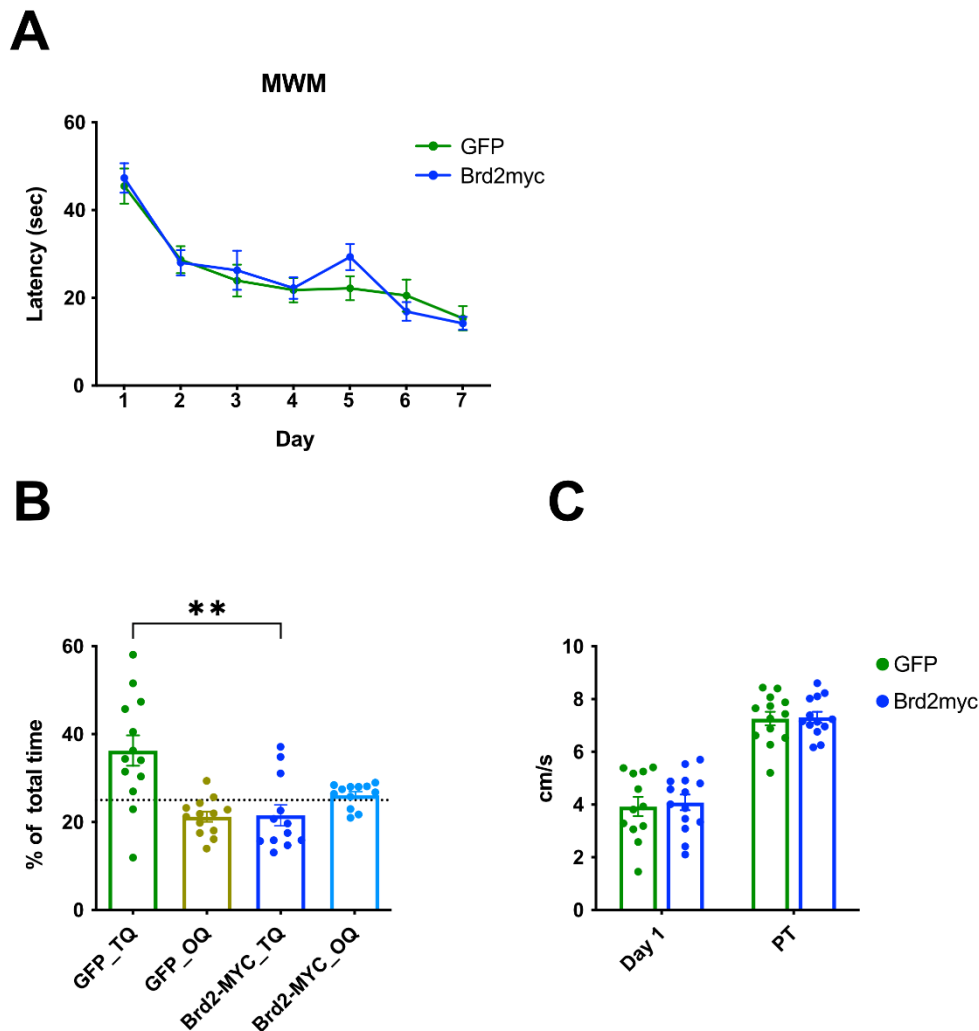


Figure 8: **A:** A graph showing the escape latency of Brd2 OE and GFP mice during the Morris water maze (MWM). **B:** A graph plotting the percentage of time Brd2 OE and GFP mice spend in the target quadrant during the probe test. **C:** A graph showing the swimming speed of mice during the first day of training and the probe test (significances were determined using a one-way ANOVA followed by post hoc Dunnet's test. Experiment was performed by Hendrik Urbanke for his Master's thesis, 2013).

complex tasks. Interestingly, the intensity of the fear response in Brd2-myc over-expression mice showed an enhancement.

3.4 Chapter 4 – Brd2 OE in primary hippocampal cell culture

Having observed a deficit in learning and memory in Brd2 over-expressing mice similar to the Brd2 conditional knock out, we decided to return to cell culture to investigate the effects of Brd2 over-expression in an isolated system, with the purpose of obtaining a deeper understanding of the role of Brd2 in hippocampal neurons.

First, we adjusted the viral concentration of our Brd2 over-expression AAV (see Chapter 3.3 Fig. 6) for use in cultures. An initial test showed that even low volumes (0.5 μ l on 100.000 cells) of concentrated virus led to expression levels of around 320-fold, far above what we deemed feasible for our study (Fig. 1A). After adjusting the virus dilution, we reached our desired levels of over-expression of approximately 6-fold (Fig. 1B), comparable to what we used for behavior experiments (Chapter 3 Fig. 6B).

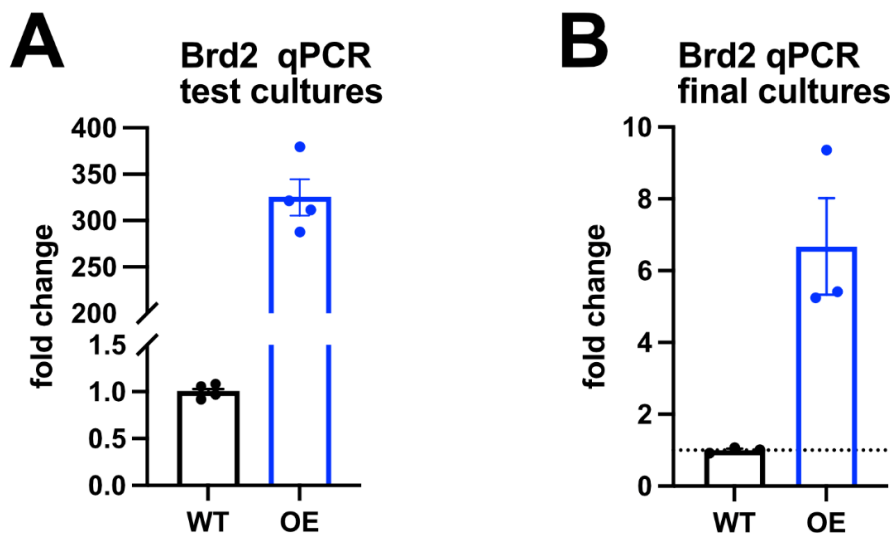


Figure 1: **A:** A qPCR performed with primers spanning the 5' intron exon boundary junction of Brd2's exon 2 from cDNA synthesized from Brd2 fl/fl primary hippocampal neurons transduced with concentrated AAV1/2 Brd2myc or AAV8 GFP. **B:** A qPCR performed with primers spanning the 5' intron exon boundary junction of Brd2's exon 2 from cDNA synthesized from Brd2 fl/fl primary hippocampal neurons transduced with 85-fold diluted AAV1/2 Brd2myc or AAV8 GFP.

We then performed ICC and calcium imaging experiments as described in chapter 2 with primary hippocampal neurons generated from Brd2 flox/flox E17.5 embryos. At DIV3 these cultures were transduced with an AAVs expressing GFP, GFP-cre or Brd2-

myc under the CamKII promoter, to generate wild-type (WT), Knockout (KO) and over-expression (OE) cultures, respectively.

Immunostainings performed to test the synaptic strength of Brd2 OE neurons provided surprising results. While, as mentioned before, we found no difference in the size or strength of pre-synapses in Brd2 cKO compared to WT, determined by anti-Synaptophysin signal (see Chapter 2 Results), stainings for Synaptophysin (Syn) in primary OE hippocampal neurons (Fig. 2A) revealed several indicators of a dramatic effect of Brd2 over-abundance on enhancing synaptic strength.

Pre-synapses of primary hippocampal neurons that over-expressed Brd2 were not only significantly larger than those of cKO and control neurons (Fig. 2B), they were also more abundant in number per length of the dendritic marker Map2 (Fig. 2C). Additionally, the strength of Synaptophysin signal was significantly increased in Brd2 OE synapses (Fig. 2D) indicating that the overall strength of pre-synapses in Brd2 OE neurons is significantly higher than in WT or KO.

ICC stainings for postsynaptic density protein 95 (PSD95) in Brd2 OE primary hippocampal neurons revealed an increased amount of PSD95 not only at synapses on dendrites, but surprisingly also in the soma (Fig. 3). The PSD95 signal in Brd2 OE neurons was so high, we were unable to use the same Cellprofiler based approach we designed for the analysis of WT and KO stainings of PSD95, due to the high somatic and dendritic signal. Comparing the ICCs of Brd2 KO to OE by eye, however, we concluded that the over-abundance of Brd2 influences the strength of synapses more dramatically than its absence.

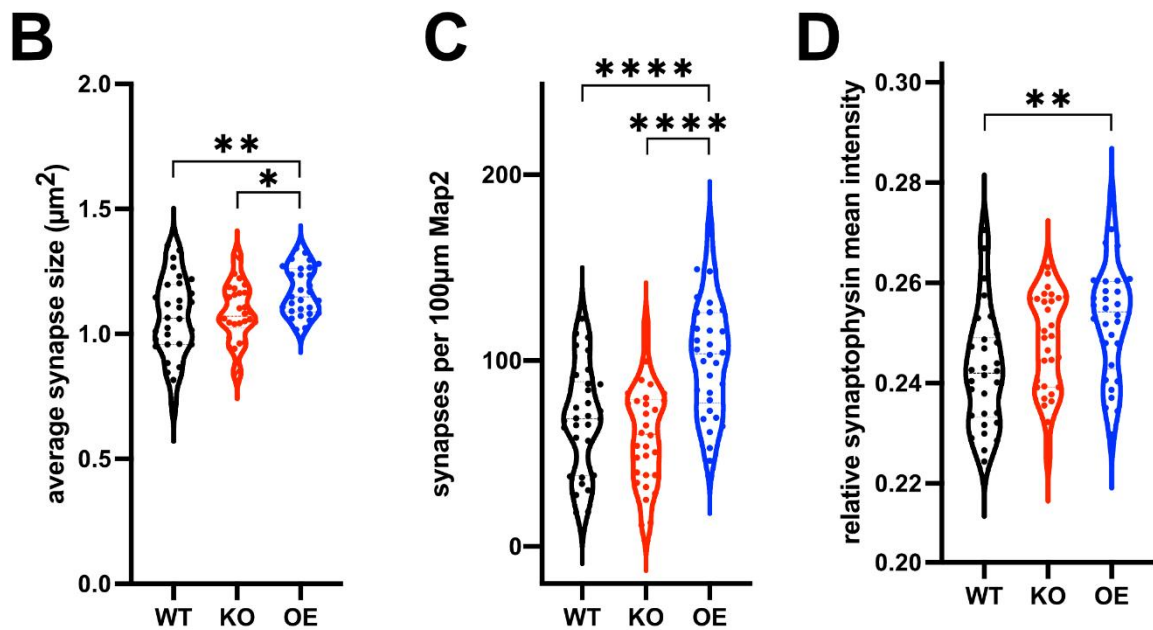
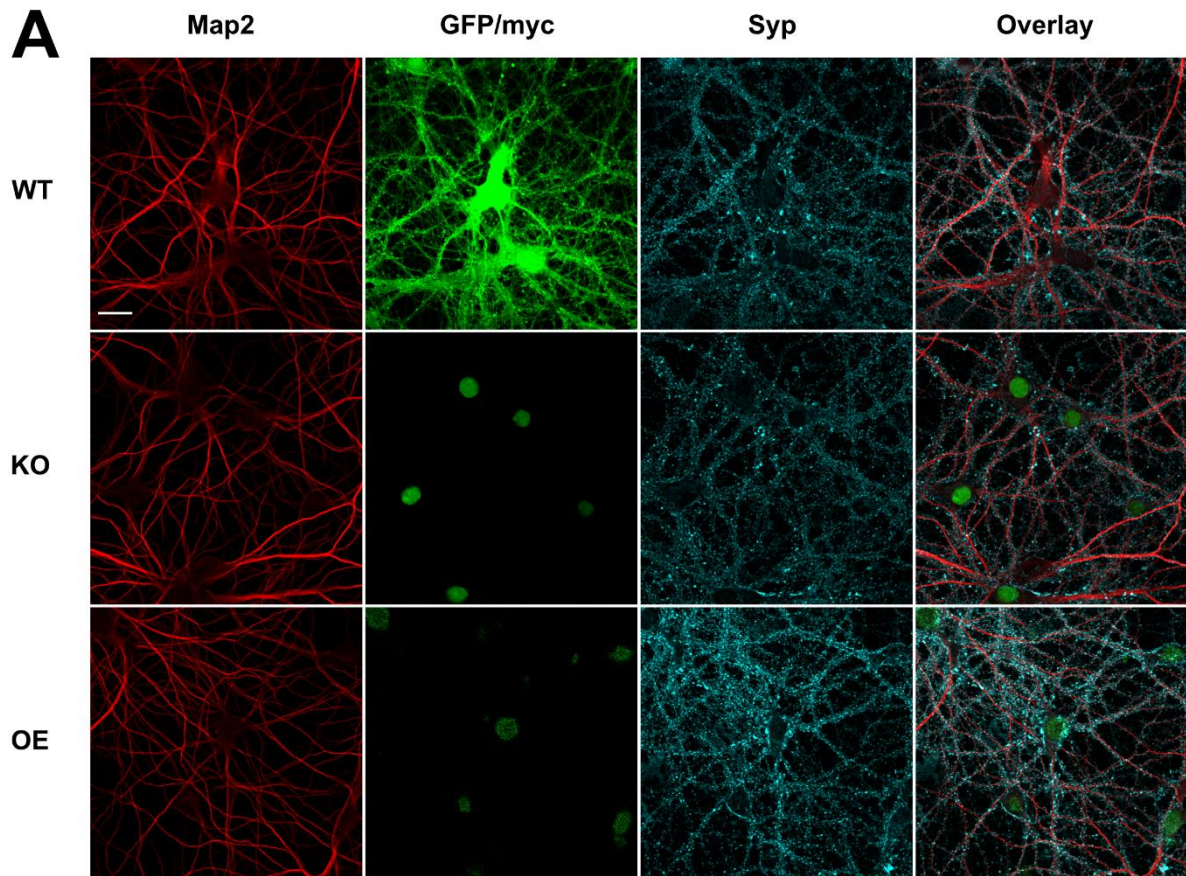


Figure 2: **A:** Representative pictures from ICC performed with Brd2 KO, OE and WT primary hippocampal neurons. Cells were stained with antibodies for Map2, Syp and in case of OE, myc. Scale bar: 20 µm. **B:** A comparison of synapse size between conditions based on Syp signal. **C:** A comparison of synapse number between conditions based on Syp and Map2 signal. **D:** A comparison of mean intensity of Syp signal. (Pictures were taken from 6 coverslips generated from 3 separate cultures; significances determined by one-way ANOVA followed by post hoc Dunnet's test).

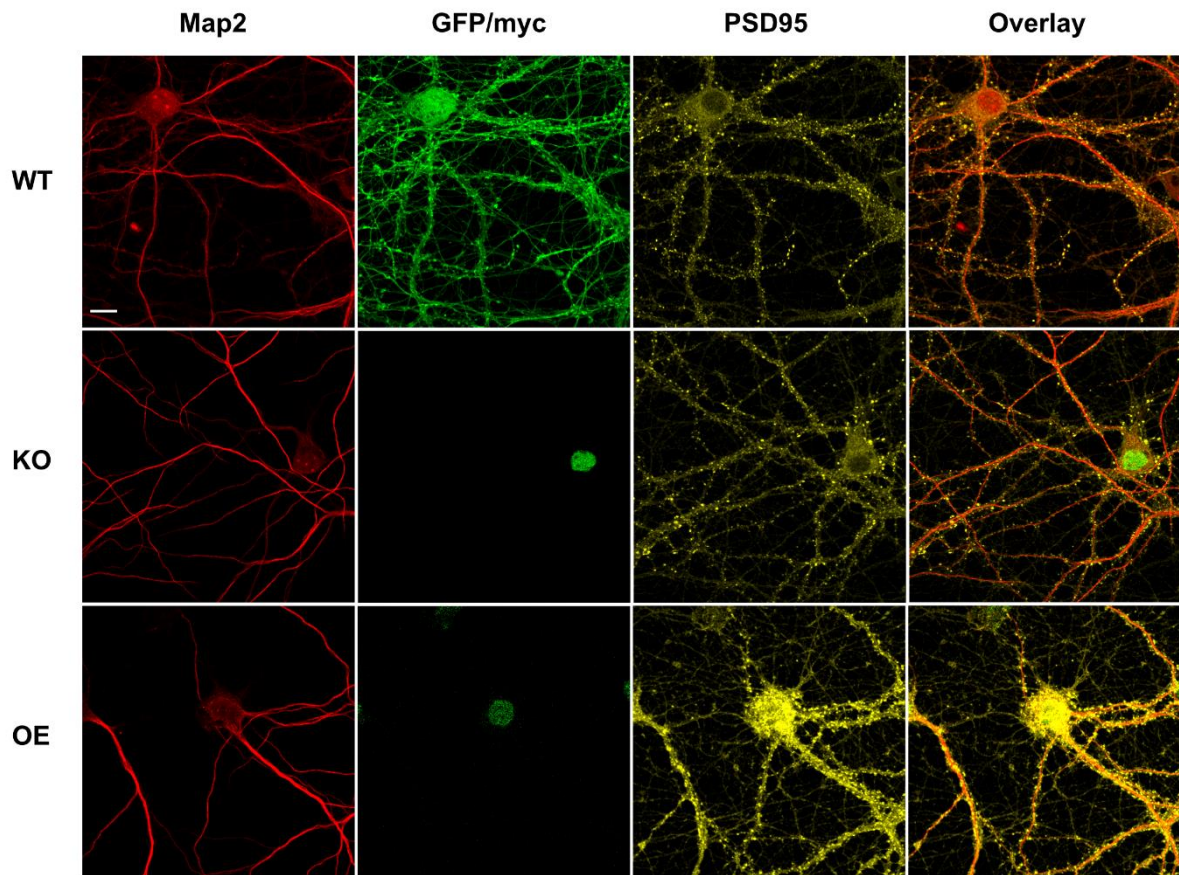
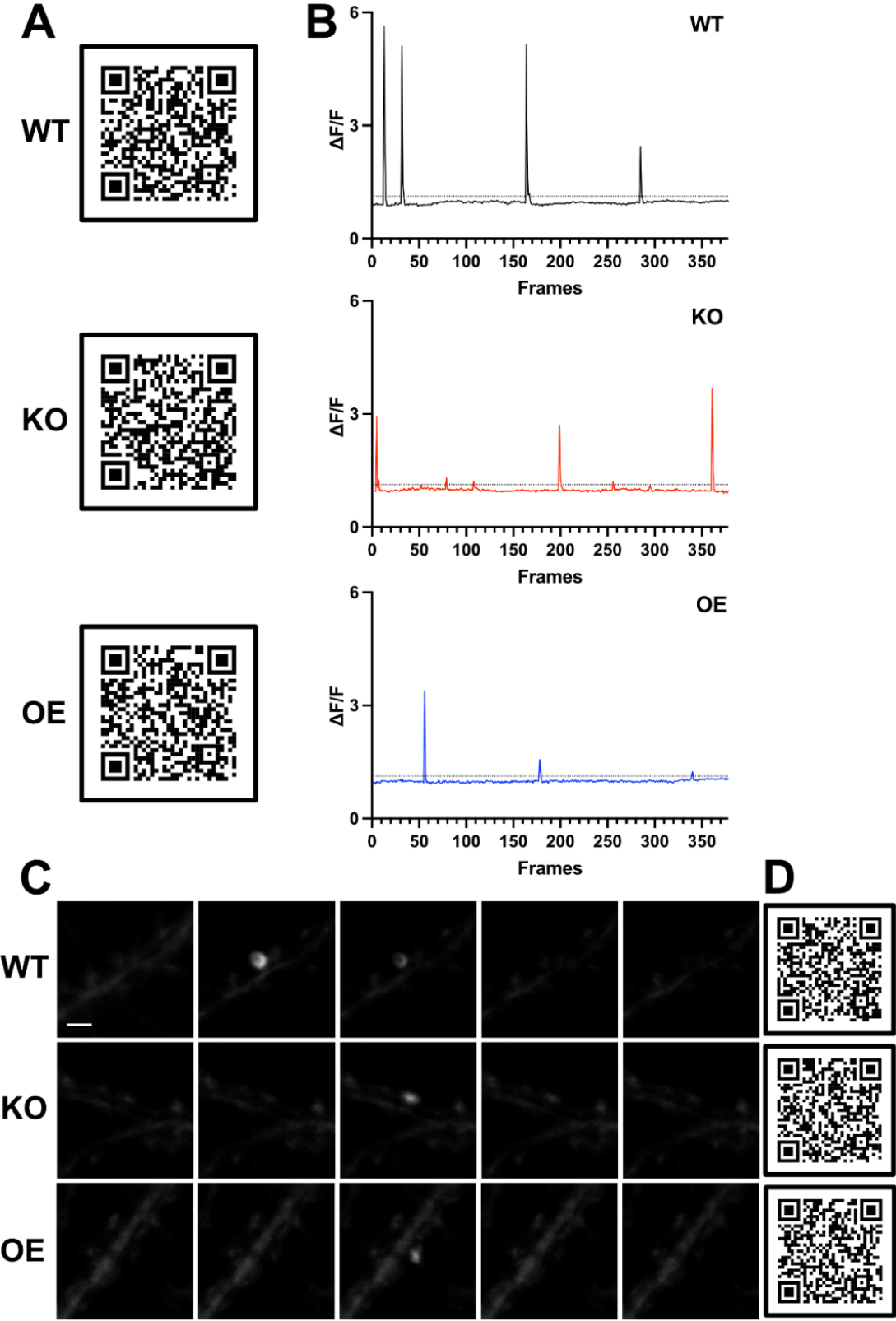


Figure 3: Representative pictures from ICC performed with Brd2 KO and WT primary hippocampal neurons. Cells were stained with antibodies for Map2, PSD95 and in case of OE, myc. Scale bar: 10 μm .

Since synaptic strength and calcium signaling of excitatory CaMKII positive neurons are directly linked (Malenka et al. 1988; Thanawala & Regehr 2013), we then investigated, if this apparent enhancement in synaptic strength could cause or influence the affected neurons calcium signaling. As mentioned previously (see Chapter 2 results) we performed calcium imaging using either ACSF containing TTX and no Mg^{2+} , or ACSF with addition of 45 mM KCl, to acquire videos of calcium transients in dendritic spines caused by single synaptic vesicle fusion events, or the calcium response upon stimulation with 45 mM KCl, respectively. Figure 4A shows example videos of the three conditions with arrows pointing at a single synapse. Figure 4B shows the change in fluorescence over time at the indicated synapse. Figure 4C depicts five frames of a single calcium transient event at each indicated synapse, with corresponding video (Fig. 4D). Although our ICC data suggests a strengthening of Brd2 OE synapses, the analysis of spontaneous calcium transients in dendritic spines revealed neither a difference in amount of calcium (Fig. 4E) nor frequency of events (Fig. 4F). The event duration, possibly reflecting the amount of calcium released from

internal stores was similarly reduced as in the Brd2 KO condition (Fig. 4G). Figure 4H shows examples of one event from each condition.



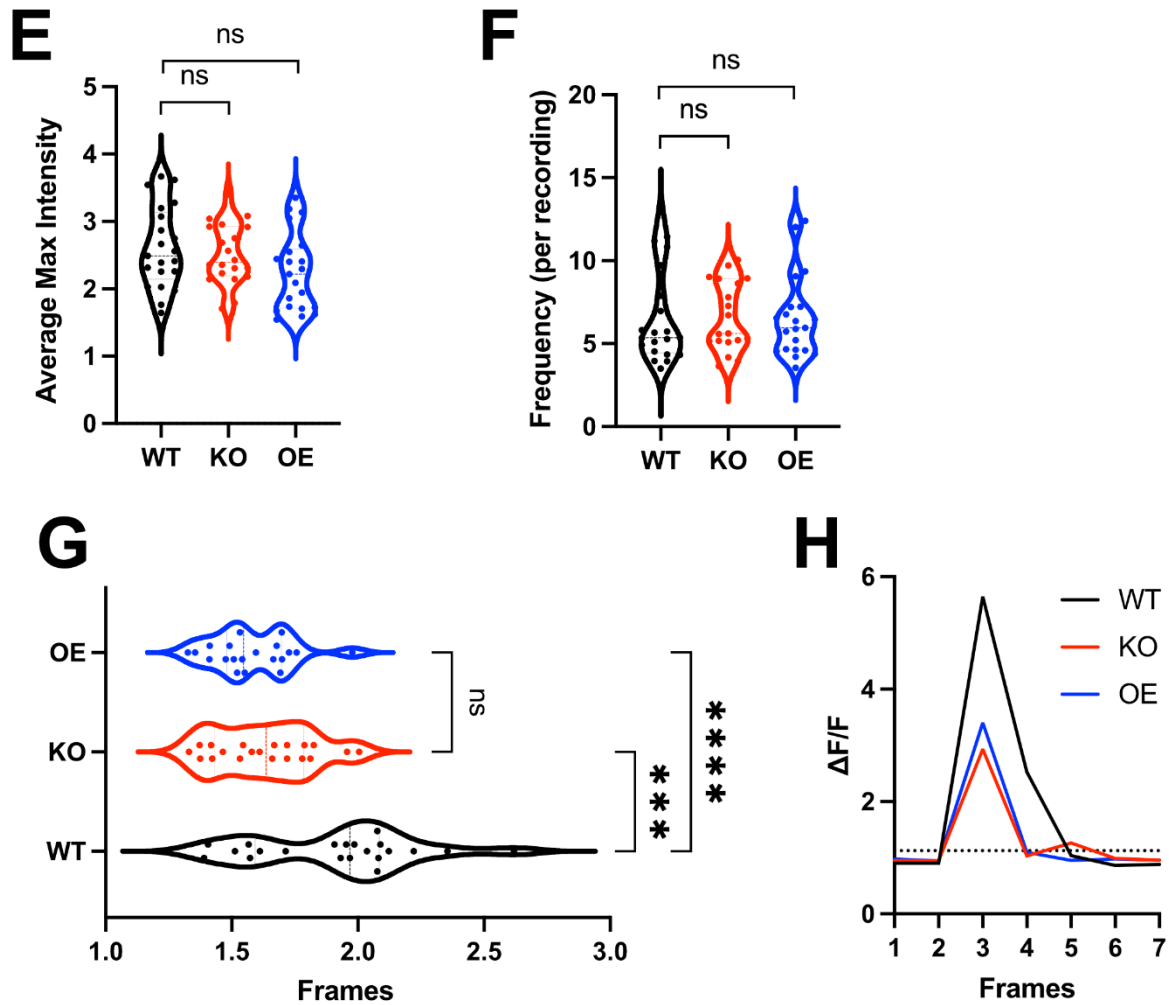
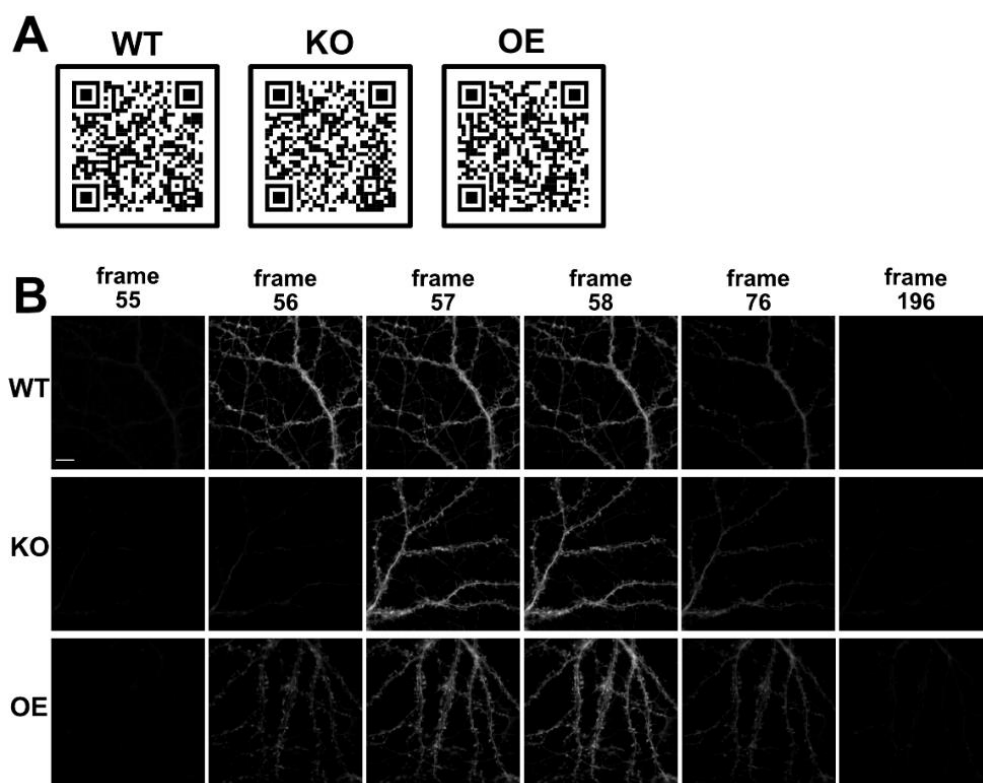


Figure 4: **A:** Example videos of single spine recordings from either Brd2 KO, OE or WT primary hippocampal neurons transduced with AAV8 GCaMP6f (the QR code can be scanned with the camera of a mobile phone and leads to a video of the recording; fluorescence signal represents calcium; the green arrow indicates a single mushroom spine). **B:** Traces depicting the changes in fluorescence intensity of the spine indicated in (**A**) over the course of the recording for each condition. The dotted line represents the cut-off above which signal was considered a peak instead of background noise in downstream analysis. **C:** Five isolated frames from each condition before, during and after a synaptic event. Scale bar: 2 μ m. **D:** A short example video of a single spine event for each condition. **E:** A graph of the average maximum intensity of spine events between conditions. **F:** A graph depicting the average event frequency between conditions. **G:** A graph depicting the average event duration between conditions. **H:** An example trace of three peak events, one for each condition. (Recordings were taken from 5 coverslips from 2 separate cultures; single dots represent the averaged values of all measurements collected in one recording; significances determined by ANOVA followed by post hoc Dunnet's test).

As mentioned above, in addition we performed KCl stimulation experiments with the same cells. Figure 5A shows example videos of the recordings and Figure 5B shows single frames before (frame 55), during (frame 56) and after stimulation. As with Brd2 KO neurons the calcium response appeared slightly delayed in Brd2 OE neurons compared to WT, but we did not quantify this effect due to the low frame rate of acquisition. The peak intensity of calcium response in Brd2 OE neurons after stimulation was in between the Brd2 KO and the WT response with no significant difference to either of them (Fig 5D). However, the calcium signal of stimulated OE neurons decayed faster than WT or Brd2 KO conditions (Fig. 5E). The Tau of the decay was significantly different between conditions (Fig. 5F). Since we hypothesized that some of the calcium signaling deficits in Brd2 KO neurons are caused by a down-regulation of TRPC6, a calcium channel required to refill internal calcium storage in the ER, we investigated if a deregulation was also evident in Brd2 OE neurons. As before we performed a qPCR to determine TRPC6 mRNA levels as well as co-immunostainings for TRPC6 and Syp, in which we analyzed TRPC6 signal intensity in synapses using a custom CellProfiler pipeline. The qPCR revealed reduced TRPC6 expression in OE neurons, comparable to what we observed in Brd2 KO cells (Fig. 6A). This effect was also evident in TRPC6 stainings (Fig. 6B). The analysis showed TRPC6 levels reduced in synapses, similar to what we found in the Brd2 KO cultures



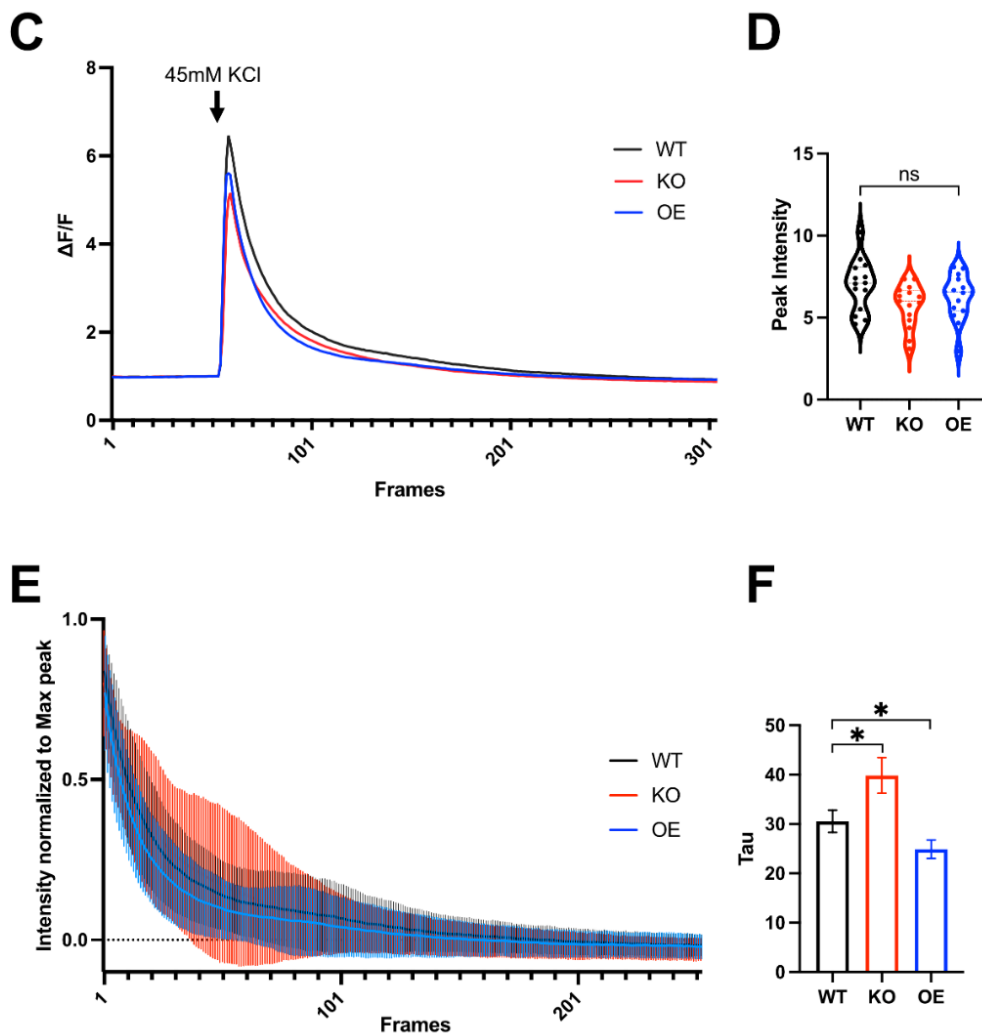


Figure 5: **A:** Three example videos of Brd2 KO, OE and WT cultures transduced with AAV8 GCaMP6f being stimulated with 45mM KCl. The QR code can be scanned with the camera of a mobile phone and leads to a video of the recording. **B:** Six isolated frames from the respective videos depicting the exact moment before stimulation (frame 55), at stimulation (frame 56), and different timepoints after the stimulation. (One frame roughly equals 0.55 seconds. Scale bar: 10 μ m). **C:** Averaged traces for each condition of all recordings. **D:** A graph depicting the normalized maximum peak intensity post stimulus between conditions (significances determined by ANOVA followed by post hoc Dunnet's test). **E:** A graph depicting average signal decay post peak for all conditions. **F:** A graph of the calculated signal decay constant Tau for Brd2 KO, OE and WT (n = 15 for KO and OE, 14 for WT; recordings were taken from 5 coverslips from 2 separate cultures; error bars indicate SD).

(Fig. 6C). This data, together with the reduction in calcium transient duration (Fig. 4G,H), further supports our hypothesis, that Brd2 abundance directly or indirectly influences TRPC6 expression and that TRPC6 expression could be linked to the availability of calcium from the ER of neurons. The data from calcium imaging (Fig. 4) as well as the TRPC6 stainings (Fig. 6) and the ICC of synaptic markers (Fig. 2 & 3) point towards a nuanced, non-binary relation between Brd2 levels and expression of affected genes, i.e. we found TRPC6 mRNA (Fig. 6A) and protein (Fig. 6B) deregulated

similarly in KO and OE (Fig. 4H). To further validate this idea, we examined how the candidate genes generated from the KO sequencing data behaved in relation to Brd2 overabundance.

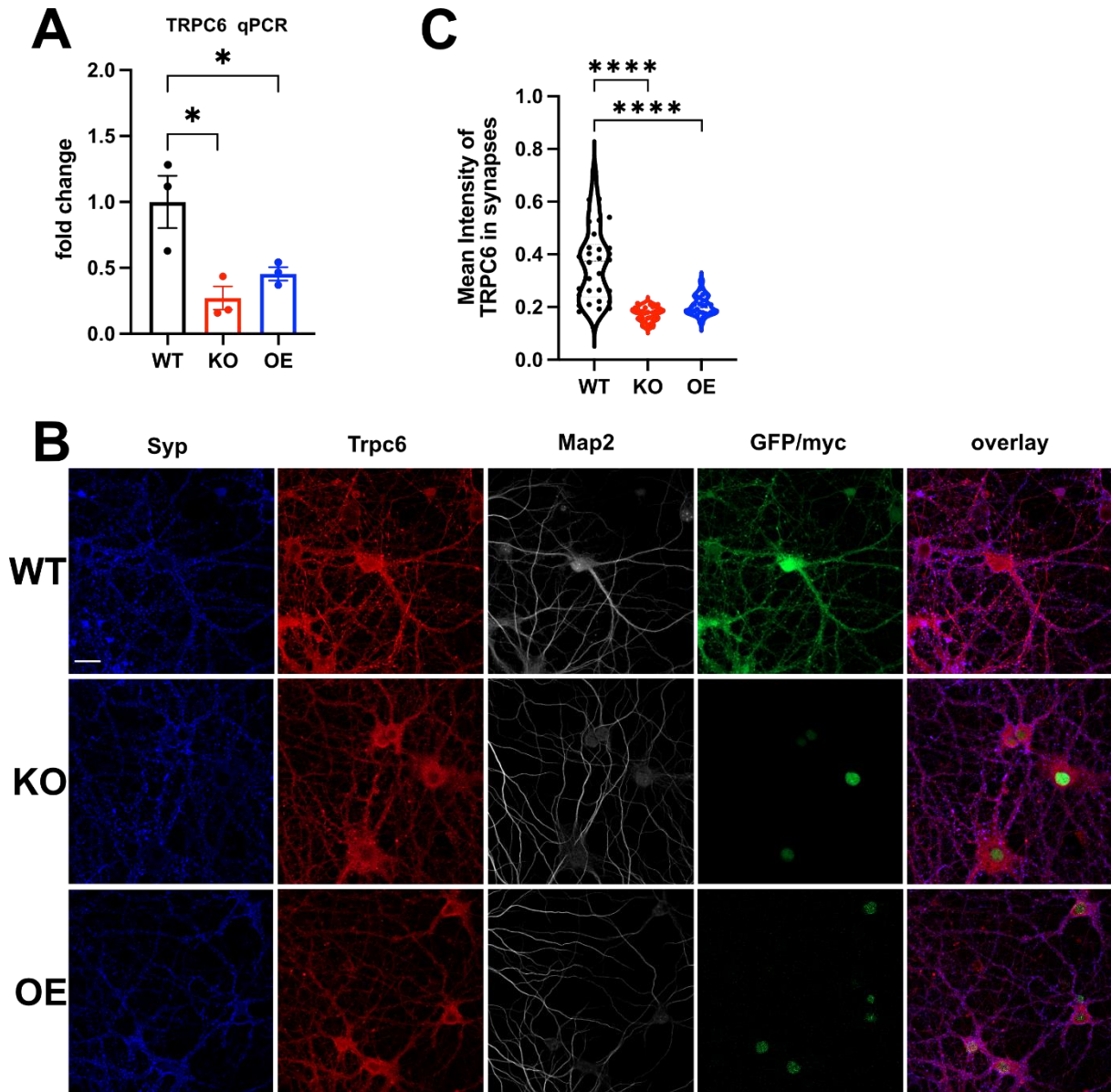


Figure 6: **A:** A qPCR performed for TRPC6 with cDNA generated from Brd2 KO, OE or WT primary hippocampal cell cultures (significances determined by ANOVA followed by post hoc Dunnet's test). **B:** Representative images from ICC of Brd2 KO, OE and WT cultures stained for Map2, Syp, TRPC6 and in the case of OE, myc. Scale bar: 20 μ m. **C:** A graph of the mean TRPC6 intensity measured in synaptic puncta. (Each dot represents the average value of a single image; pictures were taken from 6 coverslips generated from 3 separate cultures; significances determined by ANOVA followed by post hoc Dunnet's test).

Figure 7 shows expression levels of qPCRs normalized to WT samples. While the pattern of similar gene behavior between Brd2 KO and OE held true for the neuronal immediate early genes we tested (Fig. 7A - C), mRNAs for the calcium release related channel Ryr1 (Fig. 7D) and the GluA1 transporting protein Myo5b (Fig. 7E) were not deregulated when compared to the WT control. This indicates a distinct difference in the effect of Brd2 absence versus overabundance that might explain the similarities in some phenotypes and the differences in others. Interestingly we found the ECM protein Aggrecan down-regulated to similar levels in KO and OE conditions (Fig. 7F).

Aggrecan is a proteoglycan that is a critical component of perineuronal nets (PNNs) surrounding neurons. Together with other linker proteins, Aggrecan serves as a scaffold surrounding the cells (Matthews et al. Hockfield 2002). It is well established that the density of PNNs, ECM structures that stabilize synapses and neurites in the CNS, have a direct influence on synaptic plasticity as a consequence on learning and memory (Sorg et al. Miquel 2016). A too dense and therefore rigid PNN surrounding a synapse can impair its formation and strengthening, while a sufficient amount of PNNs seems to be necessary to support adult mushroom spines (Bosiacki et al. 2019). We theorized that a lack of aggrecan and resulting damage to PNNs could be linked to some of our synaptic or even behavioral phenotypes and decided to investigate this possibility. To establish if and how the PNN density surrounding the synapses of our cultured neurons was altered, we stained with plant lectin *Wisteria floribunda* agglutinin (WFA), which binds Aggrecan and is commonly used to label it (Ueno et al. 2018) in conjugation with a fluorophore. We co-stained for VGlut1 to allow analysis of PNN density in the vicinity of excitatory synapses imaged by STED microscopy. Figure 8A shows a scheme of the staining process and the analysis. Contrary to what we expected based on the mRNA data (Fig 7F), we found the PNN density surrounding Brd2 OE synapses not significantly decreased but rather increased, while the Brd2 KO showed the expected significant reduction (Fig. 8B). It is however possible that the level of Aggrecan mRNA was higher at an earlier time point, leading to an increased translation of the Aggrecan protein and PNN density, before we took our samples on DIV16 at which point the mRNA could have been down-regulated via a feed-back loop due to the protein's overabundance. Independent of the direction of the deregulation, it has been shown that PNNs makeup and density do influence synaptic composition and abundance at least in cultured neurons (Gottschling et al. 2019), which could explain the phenotypes we saw in our Syp and PSD95 staining (Fig. 2 & 3) and possibly

why both conditions, cKO and OE perform worse than the WT in complex spatial learning tasks (Chapter 3, Results Fig. 5 & 8).

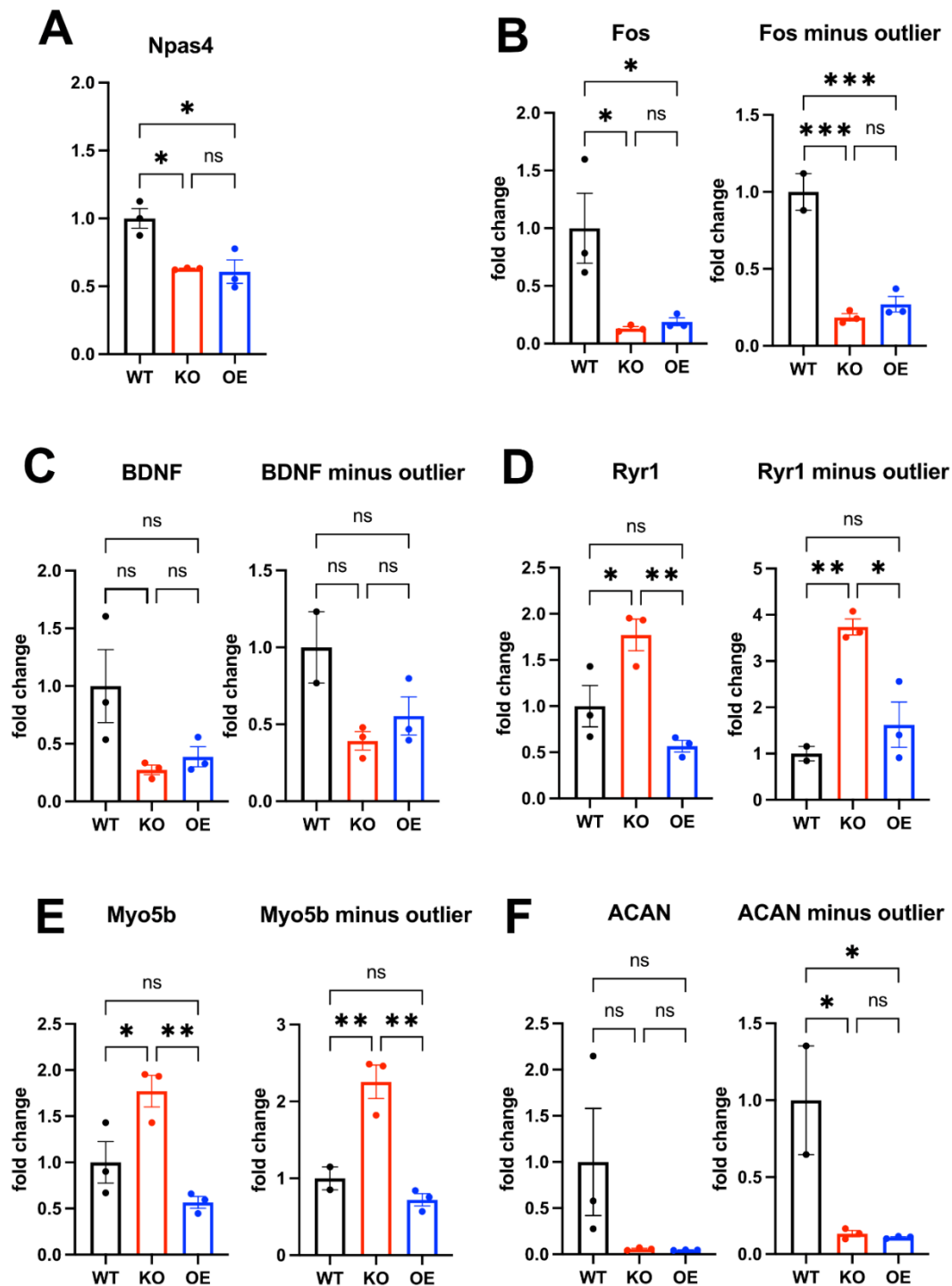


Figure 7: Graphs of qPCR data generated from RNA of primary hippocampal Brd2 KO, OE and WT neurons using primers for **A:** Npas4 **B:** Fos **C:** BDNF **D:** Ryr1 **E:** Myo5b **F:** Aggrecan (significances determined by ANOVA followed by post hoc Dunnet's test).

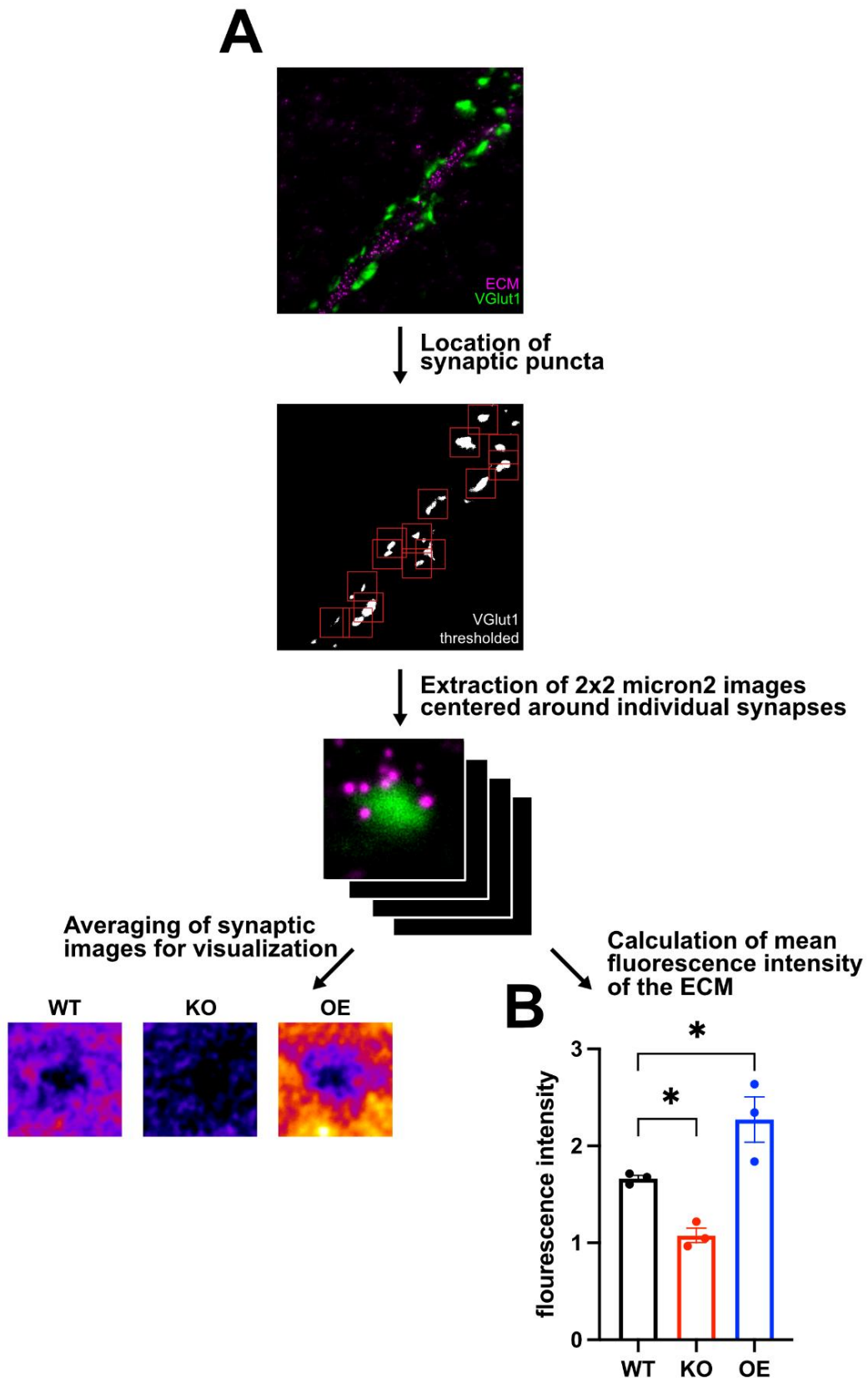


Figure 8: A: Depiction of the workflow for perineuronal net (PNN) immunostaining and analysis. **B:** A graph depicting the fluorescence intensity of aggrecan signal (n=3 cultures; each dot represents the average of 10 images taken from 2-3 coverslips; significance was determined by one-way ANOVA followed by a post hoc Dunnet's test).

We therefore decided to investigate if our candidate genes could in theory be involved in the learning phenotypes we observed in mice. Since our conditional knockout in mice was specific to excitatory neurons in the hippocampus, we decided to extract nuclei from the CA1 region, the part of the hippocampus most tied to spatial learning (McHugh et al. 1996). For this, the tissue was fixed with paraformaldehyde before the cells were broken open by sonication. Neuronal nuclei were then stained with fluorophore-bound NEUN antibody and sorted via Flow Cytometry by size and fluorescence (Sakib et al. 2021).

Unfortunately, the only tissue available was Brd2 KO and WT (OE tissue was unavailable) deep frozen for some time and the RNA extraction proved challenging due to unforeseen problems with the quality of Trizol required for extracting RNA from cell nuclei in solution. This led to a much smaller amount of RNA than usual which limited us to only a few qPCR experiments. We used a Picochip approach with a Bioanalyzer and found the RNA quality suboptimal but sufficient for our experiments, with RNA integrity numbers of 6.6 to 7.8. We used 8 µg RNA transcribed into cDNA. We then performed qPCRs. While sample quality was suboptimal, and variability between samples quite high, the results still showed that in NEUN positive CA1 neurons of Brd2 cKO mice, of the candidate genes we tested, neither the immediate early genes (Fig. 9 A, B), nor calcium or GluA1 related genes (Fig. 9 C-E) are deregulated. This might in theory be due to compensatory effects by surrounding cells in vivo that are not present in our cultures, differences in age and stage of samples from which we took cells, or different timepoints in the onset of KO in vitro and in vivo. It is however apparent, that the expression levels of Aggrecan in cell culture (Fig. 7F) and in nuclei extracted from tissue seem to be down-regulated to similar levels (Fig. 9F). The difference between WT and cKO was not significant due to the high variability in the WT introduced by one high sample (Fig. 9F). If this sample is removed the difference is significant in an unpaired T-test (Fig. 9G).

These data suggest that it is at least possible that a potential reason for the spatial learning deficits we observed in Brd2 cKO and Brd2 OE animals could be PNN-related, i.e. due to an either too dense, or not dense enough ECM surrounding neurons and especially synapses. This claim is however highly speculative and would need further investigation to be considered a theory.

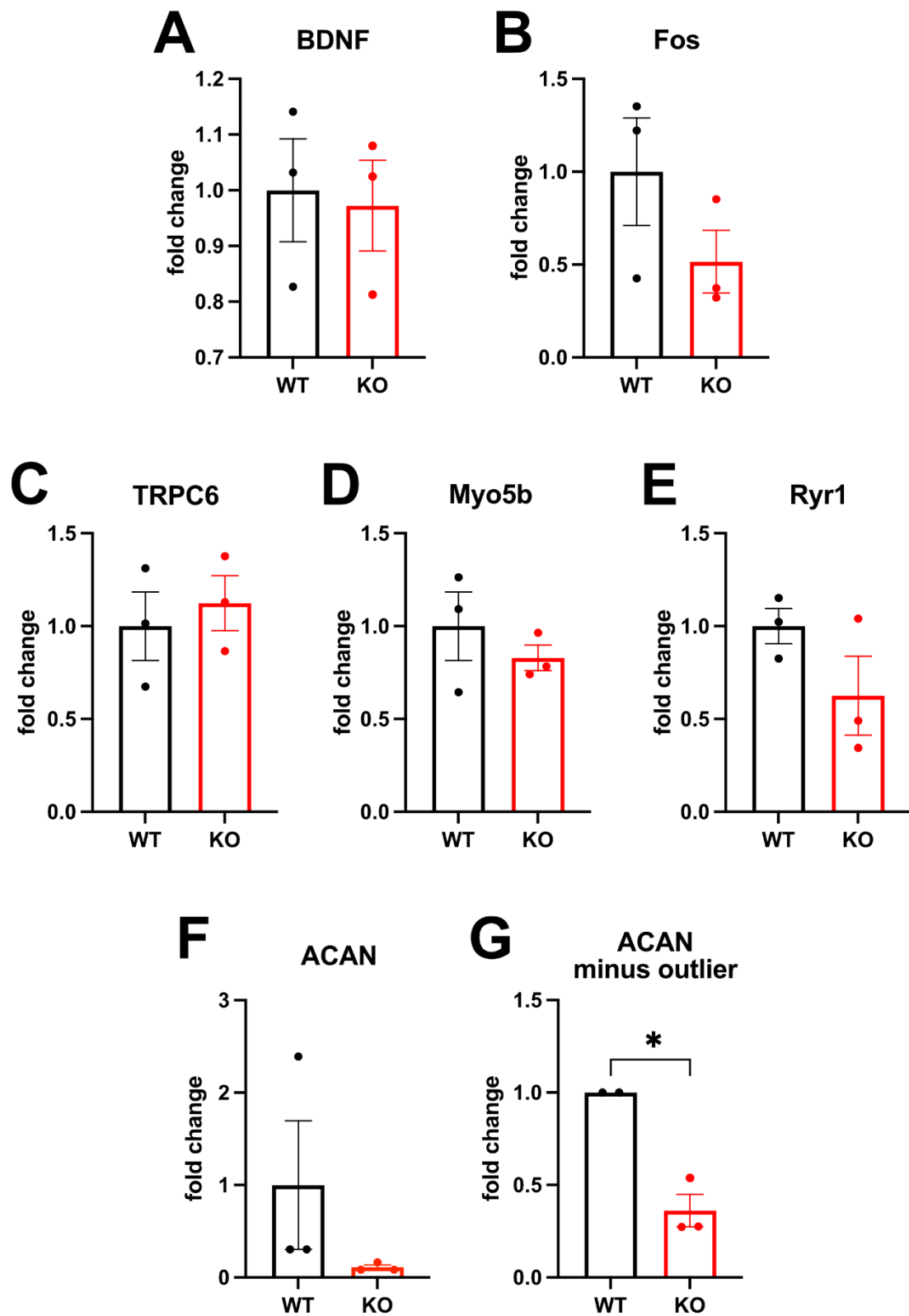


Figure 9: Graphs of qPCR data generated from RNA of CA1 hippocampal regions of Brd2 cKO and WT neurons using primers for **A:** BDNF **B:** Fos **C:** TRPC6 **D:** Myo5b **E:** Ryr1 **F, G:** Aggrecan (significances determined by Student's t-test).

3.5 Chapter 5 – Brd4 cKO and OE

Like Brd2, Brd4 is a known developmental gene (Houzelstein et al. 2002; Shang et al. 2009). We therefore choose an approach similar to Brd2 cKO for our initial studies. A qPCR performed with RNA isolated from the hippocampus of B6J mice (Janvier) from different age groups revealed that in contrast to Brd2 (Chapter 3 Fig. 1A), the expression of Brd4 remains constant over different ages (Fig. 1A). A western blot performed with 10 µg of sub-cellular protein fractions from the CA1 region of the hippocampus of three-month-old B6J mice showed a strong enrichment of Brd4 in the chromatin bound fraction (Fig. 1B). Contrary to what we observed in a similar experiment for Brd2, Brd4 was only weakly present in the nuclear soluble fraction, possibly indicating a higher level of chromatin interaction by Brd4 compared to Brd2 in three-month-old mice (or an unknown function of Brd2 that it performs when not bound to the putative target residue on Histone 4).

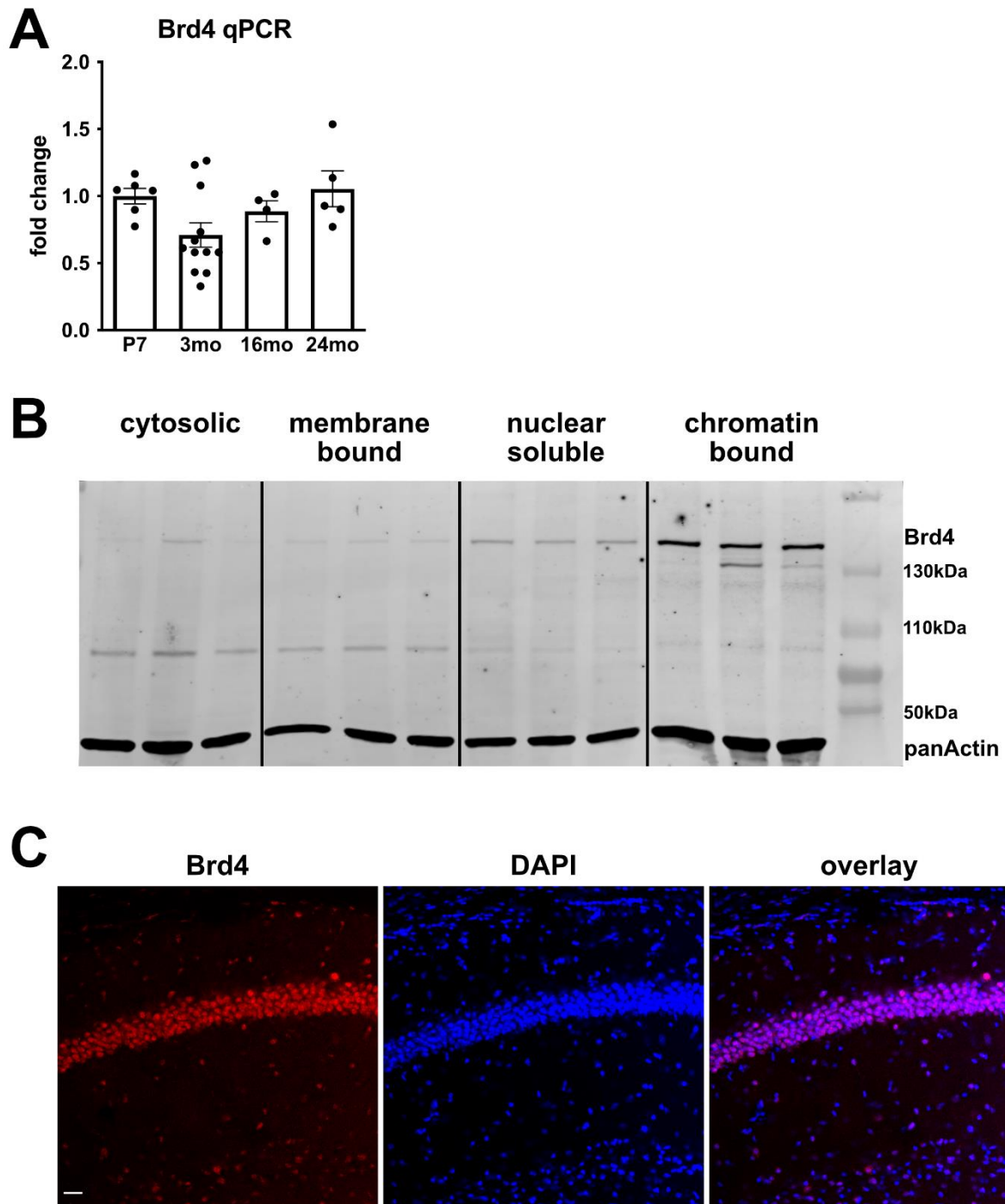


Figure 1: **A:** A Brd4 qPCR performed with cDNA generated from hippocampal tissue of B6J WT mice (Janvier) acquired at different ages. **B:** A western blot performed with protein subfractions extracted from hippocampal tissue of 3 month old WT mice using Brd4 and pan Actin antibodies. **C:** A coronal section of hippocampus immunostained with a Brd4 antibody and DAPI. Scale bar: 25 μ m.

In contrast to Brd2 we were able to acquire an antibody against Brd4 that was suitable for immunostaining of tissue slices. An immunostaining of a coronal section of the hippocampus is shown in Figure 1C. The area depicted is from the CA1 region. Brd4 signal is clearly visible in the nuclei of the stained pyramidal layer neurons, as evident by the overlay with DAPI. This nuclear localization is as expected for a chromatin associated protein.

As with Brd2, we intended to study the effect of Brd4 absence in hippocampal neurons. Since prenatal homozygous deletion/inactivation of Brd4 leads to unviable embryos (Houzelstein et al. 2002) we generated a postnatal Brd4 conditional knockout (cKO) by mating mice carrying LoxP recombination sites flanking the third and fourth exon of Brd4, with mice that carried cre recombinase under the CaMKII promoter. After the CaMKII promoter becomes active between P15 and P21 (Wang et al. 2013) cre recombines the two exons out of the genome leading to a frameshift and subsequent production of nonsense mRNA from the Brd4 gene (Fig. 2A) which is then degraded. Figure 2B shows PCRs conducted with primers surrounding the LoxP insertion site on intron 2 of the Brd4 gene. From left to right the photo shows amplicons from a WT mouse with two unaltered introns (+/+), a homozygous animal (fl/fl) and a heterozygous example (fl/+) where the ca. 100bp size difference consisting of the LoxP site and the rest of the insertion cassette on one allele, and the WT version on the other, is clearly visible. The gel on the right shows PCR results from cre- and cre+ mice, using primers that amplify cre.

Since the Brd4 LoxP mice were delivered on a B6N background we crossed the animals for ten generations with B6J mice, our usual experimental background and the background of our CaMKII cre line, to ensure minimal variability in future behavioral and sequencing experiments due to inherent genetic differences in these lines. Matings of the resulting backcrossed parental lines B6J Brd4 fl/+ cre- with B6J Brd4 fl/+ cre+ to create B6J Brd4 fl/fl cre- and cre+ animals intended for breeding of behavior cohorts, resulted in almost no Brd4 fl/fl cre+ offspring. Six matings only yielded three cre+ pups, according to our genotyping. Since the litters usually had 5 to 7 animals, we would have expected at least ten cre+ Brd4 fl/fl pups following Mendel's law of segregation. Tissue samples for genotyping were only taken at postnatal day 21 when the pups were removed from their mother's cage to a new one. Mice that died before that time were not registered. However, upon request we were informed that every

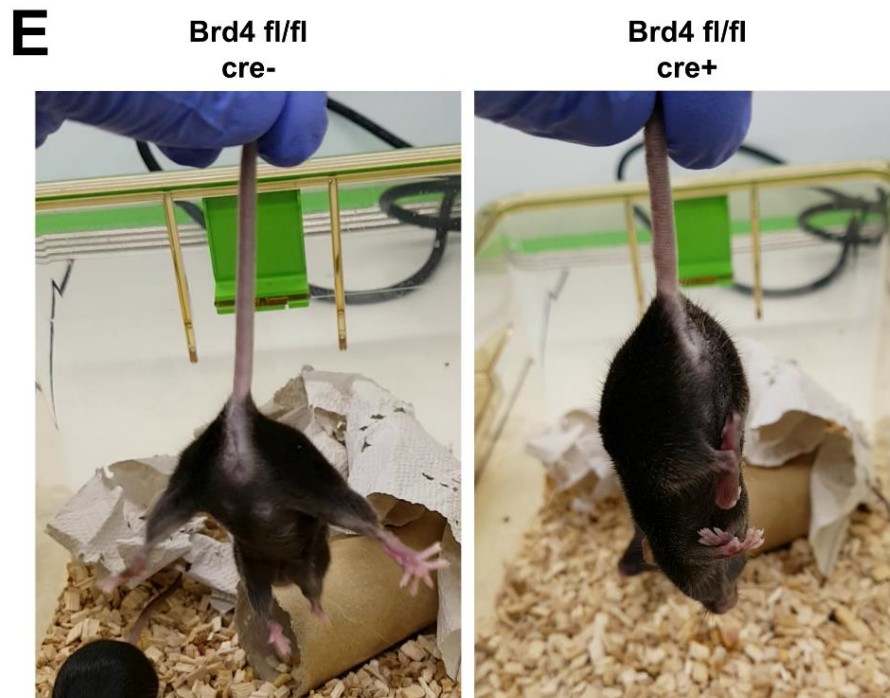
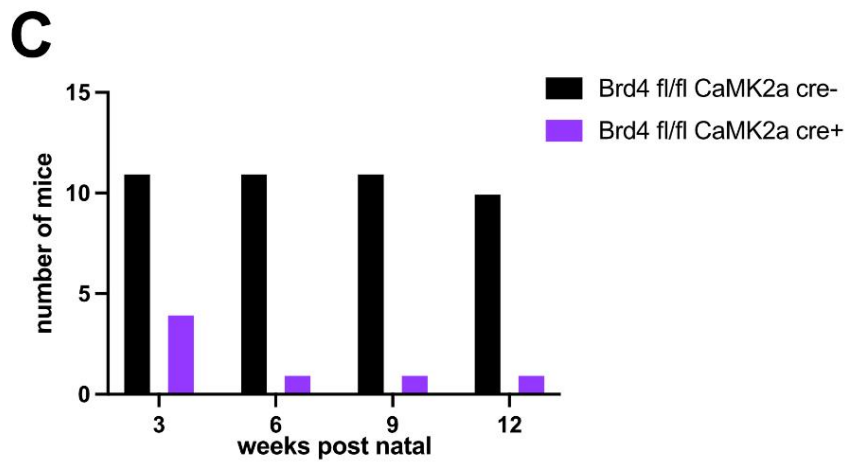
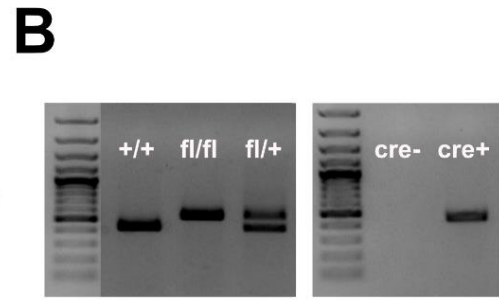
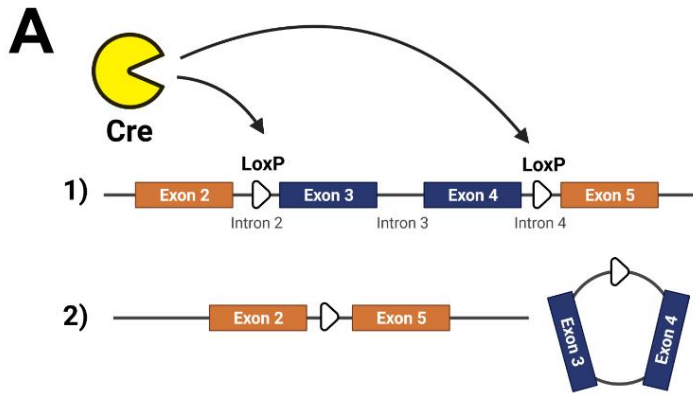
litter had contained one or several pups that died shortly before postnatal week three. A plot of the number of living homozygous Brd4 fl/fl animals with or without the cre gene is shown in Figure 2C. Of the initial three animals that reached three weeks of age and were therefore genotyped, two died between week three and week six. The only animal that survived until three months of age, a female, showed strong behavioral abnormalities and signs of neurological damage. Figure 2D shows a video of the animal in a group cage with its two cre- littermates. It is evident that the animal shows apathetic behavior while not displaying any outward signs of pain such as squinted eyes and nose or upright fur in the neck region. We performed a simple reflex test by lifting the mouse by its tail and lowering it back to the cage. Healthy mice should spread their limbs, anticipating contact with the surface, while claspings or even cramping of the hind legs is an indicator of neurological damage to one or several brain regions including the cortex (Lalonde and Strazielle 2011). Figure 2E shows two pictures taken from this test performed with a cre- littermate (left) and the cre+ mouse (right). The control animal shows expected behavior, indicating no neuronal damage, while the cre+ animal shows not only so called „bat like posture“, but also cramping of the hind paws. For a better impression, Figure 2F provides short video clips of the test with both mice.

Other studies already reported a detrimental effect on cell growth and health in living mice with heterozygous Brd4 deletion (Houzelstein et al. 2002). We theorized that if the CaMKII driven expression of Cre and the subsequent removal of Brd4 from CaMKII expressing excitatory neurons was the reason for the phenotype we observed, we should be able to reproduce these results in neuronal cell cultures. For this purpose we mated two Brd4 fl/+ cre- mice, genotyped the pups after dissection while the hippocampi were kept on ice in Hibernate medium (Thermo Fischer) and cultured the primary neurons from Brd4 fl/fl and Brd4 +/+ tissues. The resulting cells were either transduced with an AAV2 carrying a GFP-cre fusion construct under a CaMKII promoter or exposed to a medium swap with the same volume used for applying the virus, on DIV3. We did not use a GFP carrying virus as a control, since the Neurite Outgrowth Staining Kit (Thermo Fisher) we used for evaluation of cell health uses a fluorescence-based readout the same wavelength as GFP. The fluorescence generated by the nuclear GFP-cre signal did not interfere with this assay.

On DIV10 we used the aforementioned kit to determine cell health and viability based on metabolic rate via ELISA. The Neurite Outgrowth Staining Kit allows evaluation of metabolic rate, and overall cell health, by converting a non-fluorescent substrate into green fluorescent dye upon metabolization. The intensity of the fluorescence (normalized to an empty control well just containing the substrate) can then be compared between samples. We found that the introduction of the cre virus to Brd4 fl/fl primary hippocampal neurons caused a significant reduction in fluorescence and therefore cell health to about 50% of the control value (Fig 2G).

Taking into account that these cultures were not pure neuronal cultures but also probably contained a large amount of glia (see Results Chapter 1), the effect on neurons alone was probably even more pronounced than evident by this method, which does not differentiate between cell types. To control for possible detrimental effects caused by the introduction of the AAV itself, we compared its effect on two Brd4 +/+ wells transduced in parallel to the untransfected Brd4 fl/fl cells and found no difference in fluorescence intensity between groups (Fig. 2H).

We concluded that our Brd4 KO, in line with former publications, seems to have a severe impact on cell health in culture as well as in animals. The data suggests knockout of Brd4 two to three weeks postnatally in mice is almost certainly lethal before affected animals reach six weeks of age. The sole surviving Brd4 fl/fl CaMKII cre+ mouse showed signs of severe neurological damage and behavioral abnormality and was, with high probability, an outlier that survived due to some alteration in either cre activity or susceptibility of its loxP sites. We stopped all further matings of Brd4 fl/fl to Brd4 fl/fl CaMKII cre mice since our interest was in generating a viable Brd4 cKO suitable for behavioral tests.



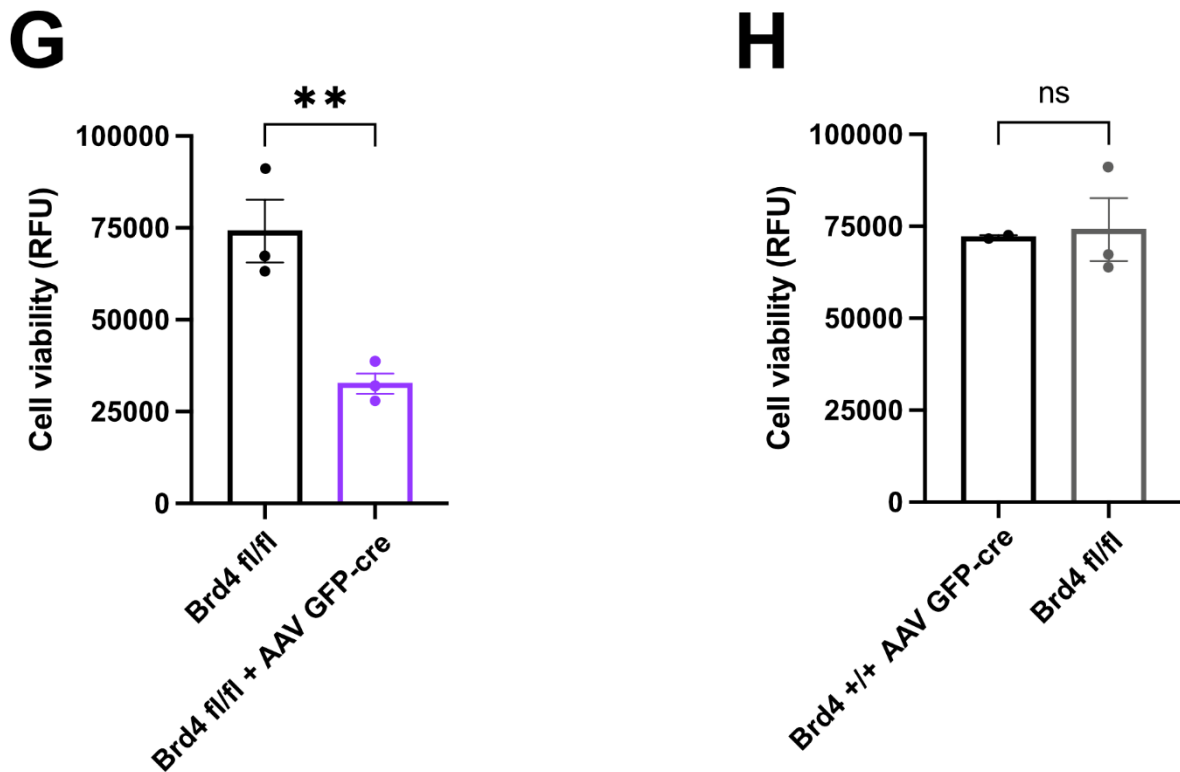


Figure 2: **A:** A depiction of the concept by which Brd4 cKO was achieved. (Created with BioRender.com). **B:** A genotyping performed for the 5' LoxP site of Brd4 or the cre gene. **C:** A graph showing the survival of Brd4 fl/fl cre- and cre+ mice. Number of surviving mice was recorded every three weeks following weaning. **D:** A video showing the only surviving Brd4 fl/fl cre+ mouse together with two Brd4 fl/fl cre- littermates. The Brd4 fl/fl cre+ mouse shows atypical behavior by not exploring its environment. **E:** Example pictures taken during a reflex test of Brd4 fl/fl cre+ and cre- littermates. **F:** Videos taken during the reflex test. **G:** Cell viability of DIV10 Brd4 fl/fl primary hippocampal neurons with or without AAV GFP-cre, measured with a neurite outgrowth kit. **H:** Cell viability of DIV10 Brd4 fl/fl or Brd4 +/+ neurons transduced with AAV GFP-cre. Significance determined by Student's t-test).

We theorized that a later onset of Brd4 deletion - at a time point at which the developmental aspect of Brd4's functions is less critical - might have a less severe impact. We identified an approach using a driver line carrying an ERT-cre fusion protein under the CaMKII promoter as a possible solution. ERT-cre is a fusion protein consisting of the cre recombinase molecule fused with a mutated version of the human estrogen receptor (ER) that, due to an introduced point mutation, does not bind endogenous estrogen but only to exogenous synthetic estrogens such as Tamoxifen (therefore ERT). The fusion protein, unlike cre by itself, is located in the cytoplasm upon translation. Only when the ERT binds synthetic estrogen, cre is released, and can relocate to the nucleus and perform recombination upon recognizing loxP sites (Fig 3A). We decided to apply Tamoxifen orally via gavage (Fig. 3B) since Tamoxifen is only soluble in oil (here sunflower oil) and injections with oil are much more painful and stressful for the animals than a gavage with the same solution. Since mouse brains

go through several important developmental changes in the first few postnatal weeks (Chen et al. 2017) we induced at eight weeks, close to the adult stage at which we would usually perform behavioral experiments. Breeding Brd4 fl/fl ERT-cre animals with their cre negative counterparts, did not result in increased pup mortality. We tested an initial batch of ten mice that were Brd4 fl/fl and either ERT-cre⁺ or ERT-cre⁻. To ensure Tamoxifen as such was not driving any observed effects, both groups received three gavages containing 100 mg Tamoxifen over the course of five days, with one day in-between applications at an age of eight weeks.

We documented the weight of the mice to ensure the procedure, drug or the KO did not negatively affect their health. Figure 3C shows the documented data. One of the ERT-cre⁺ animals died two weeks after induction. However, since the weight of all animals stabilized and increased after the week of gavage, we concluded that the death was unrelated to the Brd4 KO or the drug. Two weeks after receiving the last dosage, animals were sacrificed and their brains were dissected for the hippocampal subregion CA1, CA3 and DG. We isolated DNA and RNA from the CA1, and performed a genomic PCR to ensure recombination and knockout of Brd4 had indeed happened. We used a forward primer upstream of the first loxP site and a reverse primer downstream from the second (Fig. 3D). A picture of the resulting gel electrophoresis is shown in Figure 3E. The red arrows indicate shortened amplicons which are a result of the removal of exons 3 & 4 in ERT-cre⁺ animals, and the full-length bands show a reduction of intensity in these cases. However, the intensity of both bands seems to indicate that a good portion of the Brd4 gene was not recombined, even when taking into account that not all cells in the CA1 express CaMKII. A qPCR of the same samples supported this assumption (Fig. 3F). Overall, a significant reduction of Brd4 mRNA, about 25%, was reached in Brd4 fl/fl ERT-cre animals three weeks after induction. Compared to Brd2 (see Chapter 2 results figure 1E) we considered this change relatively minor and decided to increase the Tamoxifen dosage of the next batch of animals. Unfortunately, the onset of SARS COVID-19 led to a month long shut-down of our animal facility, followed by block of all matings not needed for maintenance of lines for several month after. We were therefore not able to further pursue this do to time constraints.

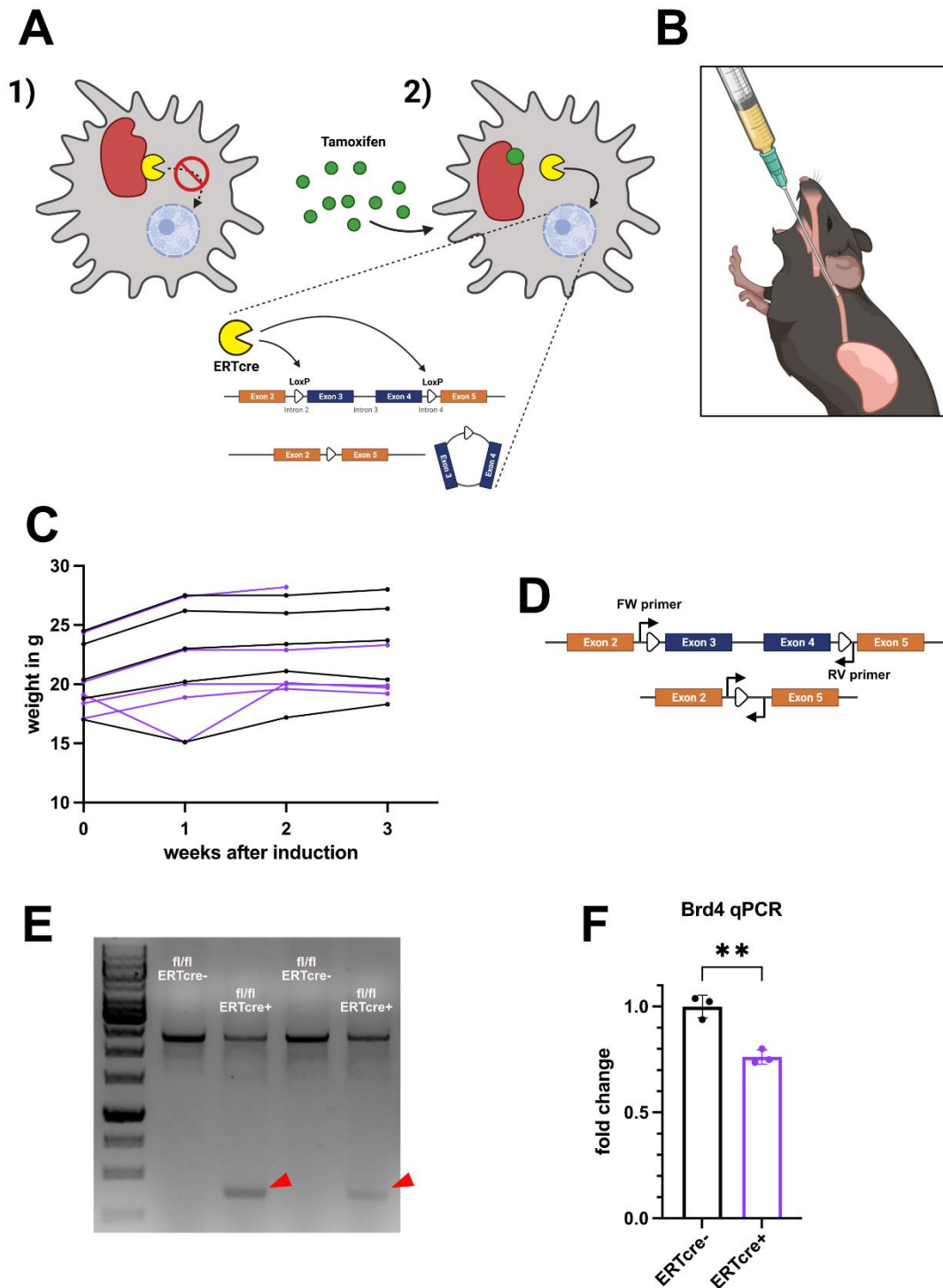


Figure 3: **A:** A depiction of the tamoxifen-inducible Brd4 cKO using a CaMKII: ERTcre driver line. (Created with [BioRender.com](https://www.biorender.com)). **B:** A depiction of tamoxifen application via oral gavage. (Created with [BioRender.com](https://www.biorender.com)). **C:** Body weight of Brd4 fl/fl ERTcre+ and Brd4 fl/fl ERTcre- mice during and after the application of tamoxifen. **D:** A depiction of the position of primers used to test for recombination via PCR. (Created with [BioRender.com](https://www.biorender.com)). **E:** A PCR using primers as depicted in D with DNA isolated from the CA1 region of tamoxifen-treated Brd4 fl/fl ERTcre- and Brd4 fl/fl ERTcre+ mice. Red arrows indicate shorter PCR product due to recombination. **F:** A graph showing a qPCR performed with cDNA generated from the CA1 hippocampal region of 3 month old Brd4 fl/fl cre+ and cre- mice using primers spanning the 5' intron-exon boundary junction of Brd4's exon 3 (significance between cre+ and cre- conditions determined by Student's t-test).

In parallel we prepared over-expression constructs of Brd4 for future experiments. Since the coding region of Brd4 is roughly 4.2kb in size and commercial companies did refuse to clone mouse Brd4 due to its numerous low complexity regions, we had to find an approach that would allow for an insert of this size and still produce viable virus, allow introduction of a tag for future pulldown or staining experiments, and avoid introducing deletions and therefore frame-shifts in the low complexity regions. We were able to overcome these challenges by combining plasmids provided by the Garcio-Domínguez lab (RSV-FLAG-Brd4) and the Kaang lab (pAAV-CW3SL-EGFP) with an oligo cloning approach. Figure 4A shows a simplified map of the CW3SL backbone which is optimized for the expression of large inserts in neurons (Choi et al. 2014). By removing the EGFP coding region via restriction digest and inserting an oligo carrying specific digestion sites, we were able to clone the flag-Brd4 construct from the RSV into the CW3SL backbone (Fig. 4B). We then proceeded to produce virus from both the EGFP and the flag-Brd4 pAAVs. Even though the insert size of CW3SL-flag-Brd4 was 900bp over what is considered a suitable size for AAV packaging, we were able to produce usable virus with this approach. Figure 4C shows a qPCR of our initial test with different viral dilutions (three samples each). The 1:500 dilution resulted in a three-fold increase. If we take into account that the cultures used for this experiment were not purely neuronal, nor are all neurons in culture CaMKII positive, it is reasonable to assume that the effect is masked to a degree. Overall, this gives us a useful tool for future experiments in the form of the only brain-specific Brd4 AAV we are aware of.

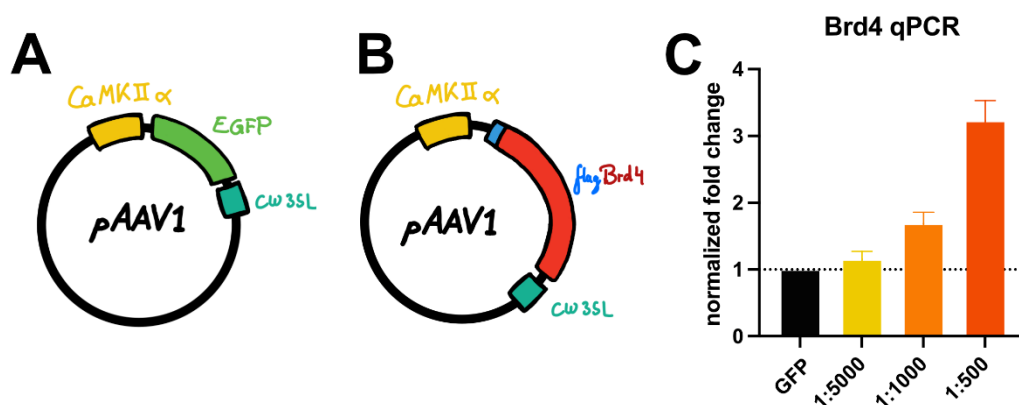


Figure 4: **A:** A simplified map of the pAAV1 CW3SL EGFP plasmid used for cloning Flag-Brd4. **B:** A simplified map of the pAAV1 CW3SL Flag-Brd4 plasmid used for virus production. **C:** A qPCR performed for Brd4 from primary hippocampal neurons transduced with different amounts of Flag-Brd4 virus or GFP control virus (n=3 wells; error bars indicate SD).

In conclusion, although lacking definitive final data, we conclude that Brd4 is more essential for brain development and possibly brain function in mice than Brd2, at least in the three-week period after birth, to the point that its absence is lethal to the animal.

This goes in line with other studies performed in mouse heart. Here the animals also showed a much more severe phenotype upon conditional knockout of Brd4 compared to Brd2 (<http://hdl.handle.net/11858/00-1735-0000-002E-E63B-F>).

3.6 Chapter 6 – Miscellaneous

This chapter contains several scientific observations I made during the course of my Ph.D. studies, which I, based on the data collected, consider non-artifacts and potentially relevant for further studies or helpful to other scientists observing the same phenomena or phenomena explainable by my observations. I will give a short overview of the observation, present the related data I collected and give a brief hypothesis of the possible indication as well as a brief overview of potential ways to study the observed effect. These subchapters therefore have no clear separated structure of intro, material and methods, results and discussion.

3.6.1 TRPC6 forms condensed structures on the neurites of cultured primary hippocampal neurons

TRPC6 antibody stainings in primary hippocampal neurons show a general signal throughout the whole cell as well as areas of punctate high intensity (Fig. 1A, blue arrows). Initially we assumed these puncta were synapses which might display a higher density of TRPC6 for faster refilling of neuronal internal calcium storages needed for signal transduction upon stimulation. However, upon enhancing the images and overlaying the TRPC6 signal with synaptophysin (Syp) signal, we determined that regions of high TRPC6 intensity occur in synaptic areas as expected (Fig. 1B green arrows) as well as independent of synapses (Fig. 1B white arrows). While all synapses show some TRPC6 signal, as is expected for a protein that is essential for refilling internal, neuronal calcium stores, not every synapse overlays with high intensity TRPC6 signal.

It seems unlikely that these regions, which we labeled TRPC6-hubs for simplicity, are staining artifacts. The representative staining in Figure 1A shows that the number of hubs declines together with the overall signal, in the absence or overabundance of

Brd2, which goes in line with the respective mRNA levels (Chapter 3 results Fig. 6A). To test this hypothesis, we created two CellProfiler pipelines to quantify our Brd2 OE and KO data, which performed the following steps:

For the TRPC6 channel:

1. Isolate the desired channel from other channels in the same image.
2. Threshold signal to 40% of the maximum intensity to remove all non-hub signal.
3. Measure the area (in pixels) occupied by the thresholded TRPC6 signal.
4. List and export the results to a spreadsheet.

For the Map2 channel:

1. Isolate the desired channel from other channels in the same image.
5. Enhance tubelike structure in the image to select the neurites and exclude the soma.
6. Transform the image into a mask since further processing requires a black/white image.
7. Shrink all neurites in the image to the width of one pixel (skeletonize).
8. Measure the area (in pixels) occupied by the skeletonized image, which equals total neurite length since all objects are one pixel in width.
9. List and export the results to a spreadsheet.

We then proceeded to calculate the area occupied by TRPC6 hubs in μm^2 based on the length and width of one pixel ($0.312 \times 0.312 \mu\text{m}$) and compared it to the length of neurites in the respective image, based on the length of Map2 that was calculated using pixel length. We then divided the area covered by TRPC6 hubs by $100\mu\text{m}$ of

Map2 to get a value representing hubs relative to neurons present in the image for all conditions. All pipelines and analysis files can be found in the Appendix section.

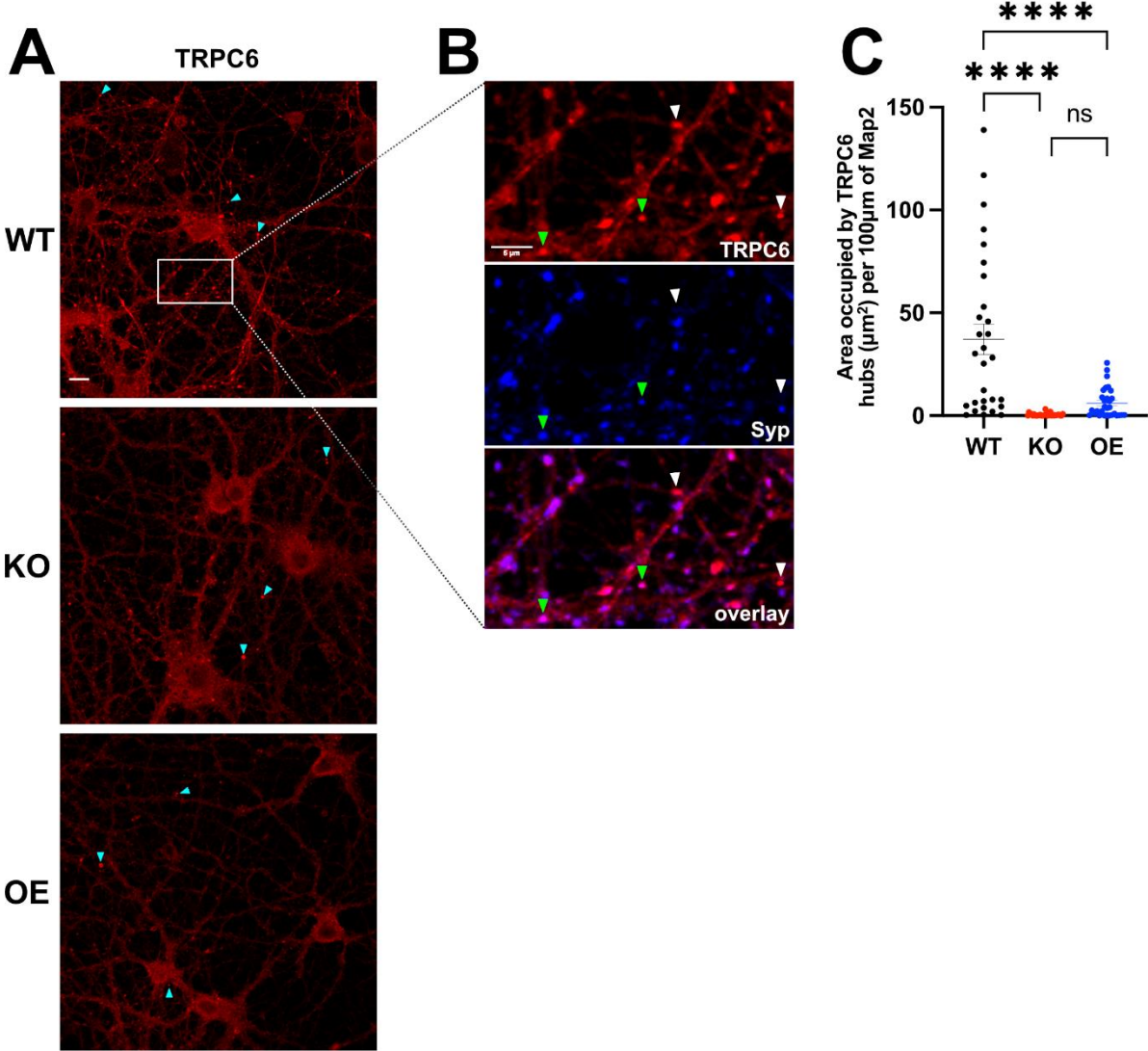


Figure 1: A: Representative images of ICC stainings for TRPC6 from Brd2 KO, OE and WT primary hippocampal cultures. Blue arrows indicate TRPC6 hubs. Scale bar: 10 μm . **B:** Zoom of the indicated region in A. Syp signal marking synapses is in blue. Green arrows indicate areas where TRPC6 hubs and Syp overlap. White arrows indicate TRPC6 hubs without Syp signal. Scale bar: 5 μm . **C:** A graph depicting the area occupied by TRPC6 hubs normalized to MAP2 signal between conditions (significance determined by one-way ANOVA with post hoc Dunnet’s test).

We plotted the resulting values and performed a one-way ANOVA with multiple comparison. The result is shown in Figure 1C. As expected, based on visual inspection, the analysis shows a clear, significant, decrease of TRPC6 hubs in samples with overall reduced abundance of TRPC6 mRNA and protein. This indicates that the occurrence of hubs and overall abundance of TRPC6 are linked and that hubs are not artifacts but more likely, at least in primary cultured cells, fulfill a physiological function. TRPC6 fulfills an important role in the replenishing of Ca^{2+} ions required for adequate signaling (see Chapter 3 results Fig. 4 & 5).

Since neurons (and all other cells) require calcium for several physiological functions it is expected, that TRPC6 signal may be found all over the cell.

It stands to reason, that a high density of TRPC6 indicates regions that a neuron uses to refill its internal stores in areas where higher than average amounts of Ca^{2+} is required. Such regions would include but not be restricted to synapses. Naturally, one would expect either a bigger endoplasmic reticulum (ER) in these hub regions, or a higher throughput of Ca^{2+} ions which in turn would make faster replenishment necessary. Based on these hypotheses it is also a valid assumption that the post-synapse, as the synaptic region that performs secondary calcium signaling should show stronger TRPC6 density than the pre-synapse.

To test these assumptions the following experiments would need to be performed:

1. Manipulation of TRPC6 levels via siRNAs to validate reduction of hubs with the overall signal, i.e. if TRPC6 is directly affected and not indirectly as is the case in this study.
2. ICC co-stainings for Syp, PSD95 and TRPC6 imaged with STED microscopy to determine co-localization and intensity of TRPC6 with the respective pre- and postsynaptic markers.
3. Co-staining of TRPC6 with markers for the ER (e.g. Calnexin), imaged with STED microscopy to check if ER signal intensity and localization correlate with TRPC6 hubs.
4. Co-staining of STIM2, Orai2 and TRPC6. These proteins together form the so-called "Store-Operated Calcium Channel Complex (SOC)" required for calcium

replenishing in neurons. In regions of high TRPC6 intensity STIM2 and Orai2 should either be:

- A. Increased, in which case a co-staining with ER markers should also reveal an increased ER signal in close vicinity, if the throughput and required amount of calcium in this region is increased.
- B. Increased, in which case a co-staining with ER markers should reveal no increased ER signal in close vicinity, if only the calcium throughput in this region is increased.
- C. Unchanged, in which case a co-staining with ER markers should also reveal an increased ER signal in close vicinity, if only the required amount of calcium in this region is increased but not at a higher frequency.

To establish if the hubs persist in vivo and therefore potentially prove their importance and biological function, the stainings should be repeated with mouse brain slices. In an optimal case with two groups of animals one of which had TRPC6 knocked down via stereotactic injection of siRNAs or siRNA expressing AAVs.

3.6.2 JQ1 could be a general stimulant independent of its BET-inhibiting properties

In our paper published in 2017 (Benito et al 2017) we could show that the BET inhibitor JQ1 has an enhancing effect on the performance of mice in certain memory tasks (Benito et al. fig. 1 d, h) as well as LTP (Benito et al. fig. 1 i). These differences were accompanied by transcriptional changes in the hippocampus beneficial to the performance of neurons in memory tasks specifically (e.g. ion channel activity, exocytosis of neurotransmitters) but also to overall cell health and activity (e.g. DNA repair, RNA export) (Benito et al. fig. 3). At the time of the study, inhibition of histone binding by BET proteins, the published targets of JQ1 (Filippakopoulos et al. 2010), seemed the most likely mode of action by which these effects were triggered.

The benefits of JQ1 seem universally applicable to other tissues (<http://hdl.handle.net/11858/00-1735-0000-002E-E63B-F>; Gillette et al. 2015). Our Brd2 and Brd4 cKO data in the brain, and data other labs collected from the KO of Brd2 and Brd4 in other mouse organs such as the hear (<http://hdl.handle.net/11858/00->

1735-0000-002E-E63B-F) suggest that the observed effects might be independent of BRD protein inhibition, or at least suggest additional mechanisms at play.

A pilot experiment we performed with Brd2 cKO mice that received an IP JQ1 injection right after fear conditioning (FC) training seems to support this hypothesis. The experiment was performed as described above (see Chapter 4) with two alterations. Three groups of mice, consisting of equal amounts of male and female animals (except the cKO vehicle-injected group, with four males and six females) were trained for three minutes on the first day and injected IP with a JQ1 solution (50 mg kg⁻¹) before being returned to the home cage. The next day animals were exposed to the context for five instead of three minutes (Fig. 2A). This was to replicate the conditions of the 2017 paper (Benito et al. 2017) where we observed that enhanced freezing behavior in JQ1 injected animals is more prominent in the later minutes of the exposure.

In FC experiments we performed beforehand, we could show that on test day, male Brd2 cKO mice show similar freezing behavior to their WT littermates (Fig 2B adjusted from Chapter 3 results Fig. 4D). This behavior was reproduced by mice injected with vehicle solution, as expected. Brd2 cKO animals injected with JQ1, however, showed significantly more freezing behavior than WT vehicle-injected (vh) animals and a strong trend toward increased freezing when compared to cKO vehicle-injected (vh) animals (Fig. 2C). This result was comparable to our former observations concerning the enhancement of learning behavior when JQ1 was given during the consolidation phase of memory formation. The data suggest that a cognitive enhancement under JQ1 influence is not only most likely independent of Brd2 function, but that the absence of Brd2 also has no influence on it.

Since JQ1 has a higher affinity to Brd4 compared to Brd2 and Brd3 (Filippakopoulos et al. 2010), Brd4 seems the most likely candidate to be affected by JQ1. However, the absence of Brd4 has a detrimental effect on mouse brains and hearts, while JQ1 has a positive one. It therefore seems unlikely that the effects of JQ1 on cognition are caused by inhibition of Brd4. While it is hypothetically possible that Brd4 performs yet unknown functions when not chromatin bound, we found no evidence in this direction in the literature.

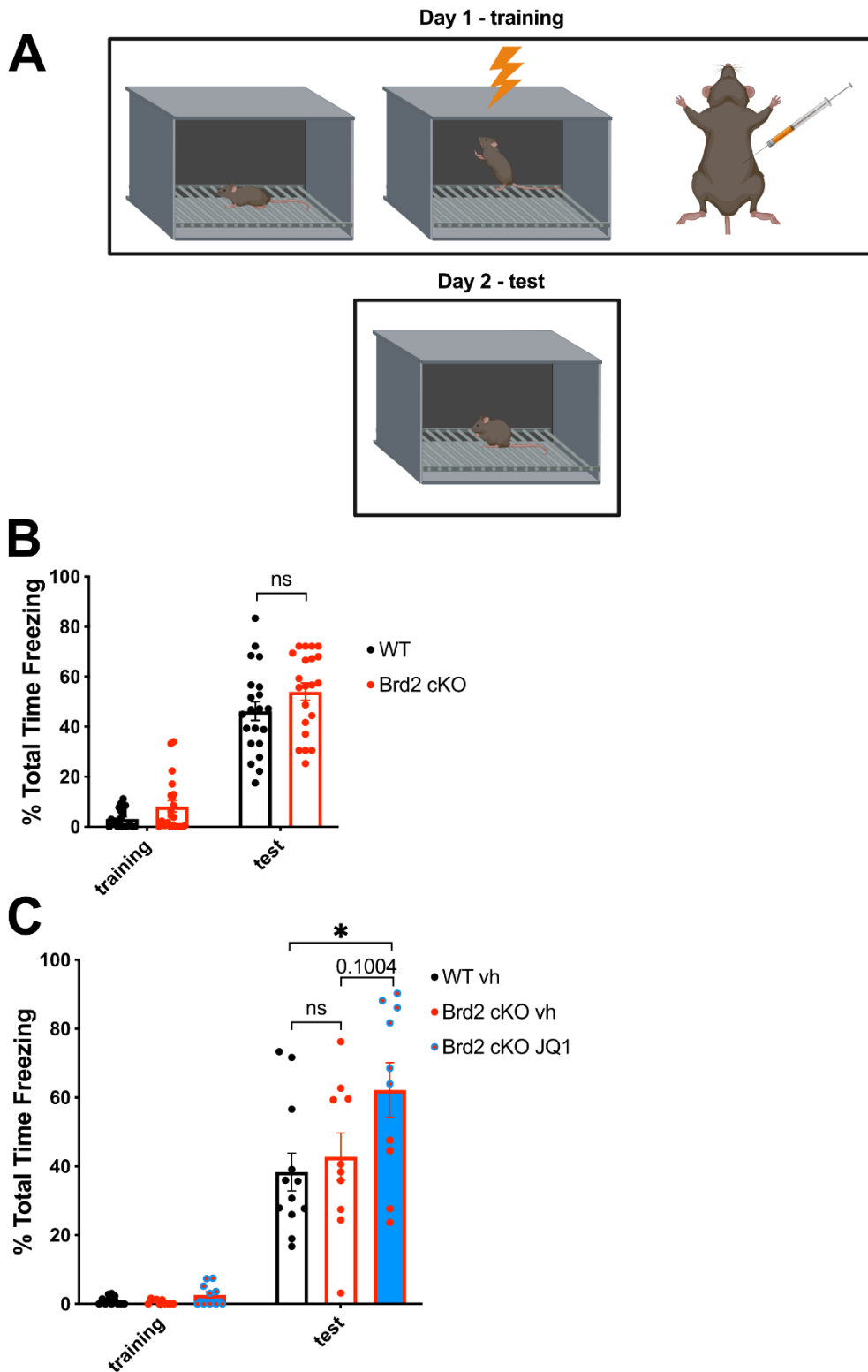


Figure 2: **A:** A depiction of the Fear Conditioning paradigm combined with JQ1 injections. Animals received injections directly after training before being returned to their home cage. (Created with BioRender.com) **B:** Graph showing no difference in the freezing behavior during Fear Conditioning of WT and Brd2 cKO mice (significance was determined using a Student's t-test). **C:** Graph showing fear conditioning for Brd2 KO mice injected with JQ1 or vehicle, compared to WT mice injected with vehicle (significances were determined using a one-way ANOVA followed by post hoc Dunnet's test).

A recent publication performed on immortalized cell lines showed that blocking or removing Brd4 from its chromatin binding sites does not diminish promoter-enhancer interactions in which it is involved, at least in cases of short-term inhibition like in our experiments. The same publication points out that transcriptional deregulations take place nonetheless (Crump et al 2021), which further supports the above statement. In general, JQ1 is widely shown to positively affect disease models (Li et al. 2019; Jiang et al. 2020) however this contrasts with the detrimental effects observed in BET KO and KD models (Houzelstein et al. 2002; Shang et al. 2009).

The following questions arise:

1. Are the beneficial effects of JQ1 on learning and memory exclusively based on its influence on epigenetic mechanisms?
2. Are the transcriptional effects of JQ1 caused exclusively by inhibition of BET proteins?

These questions could be addressed by these respective experiments:

1. Removal of the pyramidal cell body layer of a hippocampal slice to isolate the Schaffer collateral from their respective cell bodies. Repeat the stimulation experiments in the CA1 dendritic region under JQ1 influence as conducted in Benito et al. 2017 to determine if an LTP enhancement takes effect in absence of the soma, proving an independent mechanism from chromatin modification.
2. The existence of degradation approaches for associated proteins (Crump et al. 2021) allows one to test whether stereotactic injection with AT1 and iBET to degrade putative BET targets of JQ1 paired with IP injections of JQ1 would produce comparable behavioral and transcriptional phenotypes. Alternatively, one could down-regulate all BETs via stereotactic injection of BET siRNAs or generation of viable triple cKOs and combine these approaches with JQ1 injection and the respective cognition and sequencing experiments.

In general, we find it questionable, that a drug that targets such a highly structurally and functionally conserved domain as the bromodomain, which is also present in many other chromatin associated proteins (Josling et al. 2012; Fujisawa et al. 2017), exclusively inhibits the tested targets. First evidence of off-target mechanisms has

already been reported (Weilong et al. 2015) and recent publications suggest potential negative off-target effects of JQ1 in certain cancers (Wang et al. 2020).

In conclusion, while JQ1 is not used in clinical approaches itself due to its short half-life, several drugs based on its overall structure and function are tested for clinical applications (Wasiak et al. 2020; Gilham et al. 2021).

Even if exclusively specific to the bromodomains of BETs or one BET alone, a drug that inhibits a protein or protein family with such a broad spectrum of interaction partners, which in turn influence transcription on several levels themselves, seems unlikely to be suitable for long term consumption without significant uncontrollable side effects.

4. DISCUSSION

While a full investigation of all aspects of BET function in the hippocampus or the brain as a whole would have gone beyond the scope of this thesis, several novel and relevant observations about the connection of these chromatin readers to memory formation could be made. The collective data clearly shows that Brd4 removal from CaMKII positive neurons, even at an advanced level of brain development, is almost certainly deadly to mice. While mice with a similar knockout strategy of Brd2 do survive to adulthood, they display clear signs of memory formation deficits at this point (Chapter 3, Fig. 5). Data collected by colleagues from the University Medicine Göttingen working with the same BET knockout lines driven by a heart specific promoter (α MHC) did not find any phenotype for Brd2 cKO in the heart muscle, however they observed similar results for Brd4 cKO in myocardial cells. Brd4 fl/fl cre⁺ offspring were not viable after postnatal onset of the cre driving promoter. After switching to a tamoxifen induced cre line, they observed no phenotypes in induced Brd2 cKO mice, but found a severe deformation of the heart muscle leading to a basal concentric hypertrophy in Brd4 cKO animals (<http://hdl.handle.net/11858/00-1735-0000-002E-E63B-F>). This would suggest, that in the heart, Brd2 plays a less severe role in adult animals, suggesting that any phenotype we observed in the brain, a post mitotic tissue which is similar to the heart in this respect, might be more related to Brd2's role as a development and cell cycle regulator than to its function in the adult brain. This hypothesis is supported by the collected qPCR data which shows a reduction of Brd2 expression to about 40-50% post P7, while Brd4 expression throughout the brain remains on a similar level during adulthood and old age (see Results Chapter 3 Fig. 1A, Chapter 5 Fig. 1A).

From a general perspective it seems likely, that Brd4 is overall the most relevant BET chromatin reader due to the high number of diverse pathways research has found it involved in. It is possible that this is a misconception due to a researcher's bias towards this particular BET family member based on its prominent role in cancer (French 2010) and the fact that it was discovered early in BET research that the fusion of Brd4 and its neighboring gene NUTM1 causes a severe form of epithelial cancer, the so-called NUT carcinoma. Even taking this into account however, Brd4 is the largest of the BETs and possesses regions close to its N-terminus, which it does not share with other family members. These regions contain active sites that allow it to phosphorylate Pol II

(Ballachanda et al. 2012) and acetylate the histone mark H3K122, which is essential for nucleosome eviction and the opening of chromatin to allow for transcriptional onset. This makes Brd4 the only BET member with proven enzymatic activity to date, again underlining its overall importance. While homozygous Brd2 full body KO in mice is deadly at embryonic day 13.5 due to the non-closure of the neural tube (Shang et al. 2009), Brd4 KO embryos do not even develop to that age, showing severe deformities already in the blastocyst stage (Houzelstein et al. 2002). Additionally, Brd4 is the BET with the most proven direct or indirect interaction partners on the protein level (about 1300 documented interaction partners as of 24.08.2021) according to thebiogrid.org.

While BETs to this date are mostly being studied in connection to cancer or overall developmental effects, our brain-derived data in combination with previous studies strongly indicate an overall essential role in normal tissue development and postnatal function of Brd4. Further experiments with inducible KO lines, which would allow for a later and therefore potentially less lethal KO onset, in the brain should be performed to finalize these findings. Extrapolating from existing data, a full Brd4 KO in CaMKII positive neurons would most certainly lead to severe disturbances in transcriptional regulation with the result of cognitive deficits or even macroscopic physiological changes in affected tissue. A hypothetical phenotype could be a reduction in the thickness of the pyramidal layer of the Cornu Ammonis (CA) regions of the hippocampus caused by the diminished survival rate of newly differentiated neurons in the dentate gyrus (DG) (Fig. 1). This scenario seems most likely based on our cell culture data (Results Chapter 5 Fig. 2G) which shows a clear reduction in the metabolic rate of Brd4 fl/fl cre+ neurons which can directly be linked to their overall well-being and survival. Since pyramidal cells represent most of the excitable neurons in the forebrain of mice and humans, and pyramidal cells in the hippocampus derive from neuronal precursor cells in the DG, where they are still generated postnatally, removal of Brd4 would probably lead to an overall reduction of pyramidal neurons.

The hippocampus (Fig. 1) is the brain area involved in the creation and consolidation of spatial memories. It has also been shown to play a major role in the consolidation of memories that are not created in the hippocampus itself (Nagayoshi et al. 2017) and can therefore be considered the central linchpin of memory formation in the brain overall. Disturbances in its function would most likely have a severe impact on the cognitive performance of affected individuals. A reduced number of excitatory neurons

could diminish the overall potentiation capabilities of the hippocampus, interfering with its ability to facilitate the creation of new memories.

Beside the developmental aspect in itself, the removal of Brd4 from already

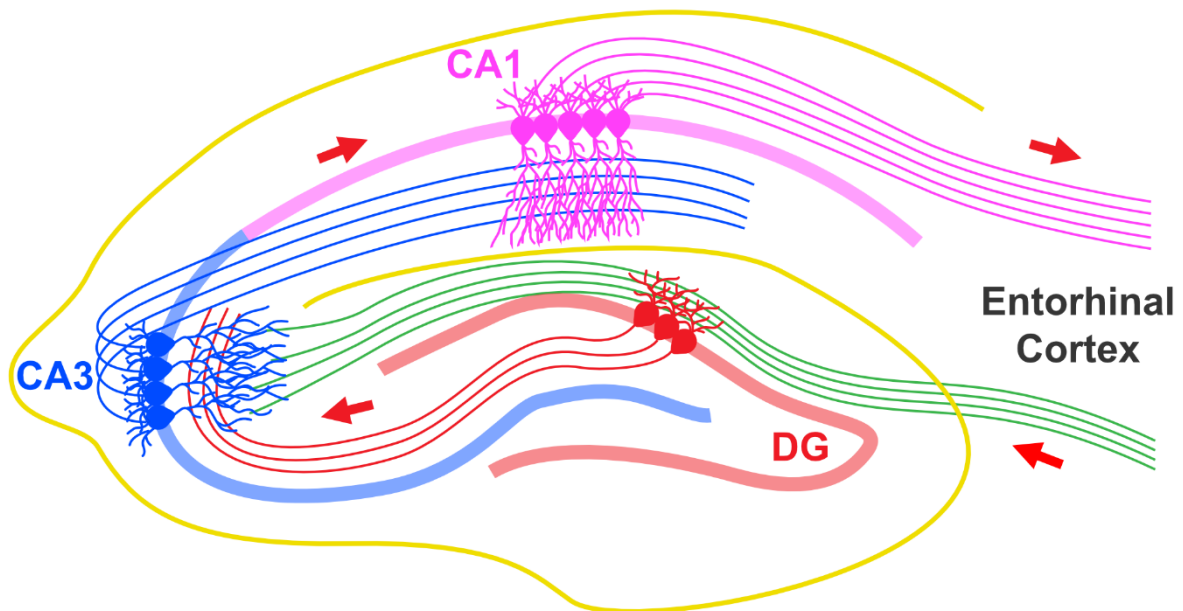


Figure 1: Circuit diagram of the hippocampus showing the connects from the dentate gyrus (DG) to CA3, and from the CA3 to CA1 region.

established, mature excitatory neurons could potentially cause an impairment of LTP formation on the transcriptional level. This seems likely since Brd4 has been shown to be involved in the activation of the BDNF gene (Sartor et al. 2015) and phosphorylation of c-Fos (Zhou et al. 2020). Accumulation of phosphorylated and therefore stabilized c-Fos is an important transcriptional activator in LTP and learning events of different brain areas (Robison and Nester 2011; Gandolfi et al. 2017).

However even with the assumption that Brd4 is the protein overall involved in more pathways and more essential to cell survival in developmental phases, the collected data strongly suggests that Brd2 fulfills an important role in the postnatal brains of mice. While BETs have been shown to form heterodimers (Garcia-Gutierrez et al. 2012) it is also reported that Brd2 and Brd4 fulfill important roles in transcriptional regulation independent of each other (Hsu et al. 2017; Cheung et al. 2017). We did not find Brd4 mRNA upregulated in the RNA sequencing of Brd2 KO cell culture samples. This indicates no compensatory effect of one BET taking over functions of another and

further supports the assumption that BET chromatin readers function independently from each other.

Taking these points into account it seems likely that the phenotypes observed in cell culture are caused by the absence of Brd2 itself. Since we were able to link transcriptional changes to corresponding physiological phenotypes, such as the weakening of the post synapse as a result of reduced calcium signaling during synaptic events (Results Chapter 2 Fig. 3D and Fig. 4G), it appears evident that BET and neuronal function are linked. This is further supported by the overall clustering of the transcriptionally deregulated genes in the Brd2 KO cultures. Affected mRNAs were strongly over-represented in biological process GO terms related to calcium signaling and synaptic transmission (Results Chapter 2 Fig. 1C) and the localization of deregulated gene products was predominantly associated with synaptic locations (Results Chapter 2 Fig. 1D).

While we lack sequencing of the overexpressed (OE) samples, we could show in qPCR that the overabundance of Brd2 does not have the opposite effect on the transcriptional levels of observed candidate genes, but rather mirrors the effect of the Brd2 KO in some cases (Results Chapter 4 Fig. 7A, B, C, F), but not in all (Results Chapter 4 Fig. 7D, E). This resulted in functionally similar physiological phenotypes concerning Ca^{2+} imaging for synaptic calcium response (Results Chapter 3 Fig. 4G) but internal calcium responses post whole cell stimulation with KCl was, contrary to the Brd2 KO condition, accelerated in Brd2 OE (Results Chapter 4 Fig. 5E, F). Both conditions showed a clear reduction in the expression of TRPC6 on mRNA and protein levels (Results Chapter 4 Fig. 6). However, Brd2 OE neurons did not compensate with transcriptional increase of Ryr1 and Myo5b mRNAs (Results Chapter 4 Fig. 7D, E). This is surprising since it seems a reasonable assumption that in a neuron affected by an artificially lowered abundance of TRPC6 - the channel required to refill internal calcium stores in neurons (Zhang et al. 2016) - compensatory transcriptional programs would counteract the lowered secondary calcium response capabilities of the cell by increasing sensitivity to stimuli via increased GluA1 localization to the PSD (Lise et al. 2006) or increased calcium expulsion volume (Johanning et al. 2015).

Lowered TRPC6 levels could explain the observed phenotype in synaptic Ca^{2+} imaging as well as the weaker post-synaptic protein signal in Brd2 KO and Brd2 OE primary hippocampal neurons. Interestingly, immunostainings for Syp in Brd2 OE cells clearly

show an increase in signal strength and synaptic size (Results Chapter 4 Fig. 2). An even more extreme phenotype can be observed in PSD95 stainings of the same neurons, in which PSD95 not only occurs in higher abundance but also in atypical localization at the soma and the dendritic membrane outside of synaptic areas in Brd2 OE neurons (Results Chapter 4 Fig. 3). This would indicate that high Brd2 expression has a transcriptionally activating effect on processes involved in the strengthening of the PSD or at least related protein expression or retention thereof independent of calcium related pathways. Naturally, this is not necessarily beneficial to the neurons overall function and could hint at a disturbance of the weighting of synaptic signals such that weak stimuli might still trigger a strengthening of the synapse making the sorting of signals required to form differentiated memories in an actual organism challenging.

It is also important to note that aggrecan, the major scaffolding protein of the perineuronal net (PNN) (Kiani et al. 2002) shows a down-regulation of mRNA levels in both Brd2 KO and OE (Results Chapter 4 Fig. 7F) but is more abundant on the protein level surrounding synapses in OE compared to the other two conditions (Results Chapter 4 Fig. 8). Both scenarios could have potentially detrimental effects on the synapse. A higher density PNN would hinder synaptic growth while a lower density PNN could fail to give a maturing synapse the required structural support to be retained (Bosiacki et al. 2019). Taking into account the apparent size increase in the presynapse, it seems possible that the strengthening of the PNN is a reaction to the increased structural ECM support Brd2 OE synapses would require. Since we only had immunostainings and RNA from DIV16 neurons available and applied our viruses at DIV3 in these experiments, it is possible, that the expression of aggrecan mRNA was strongly increased during an earlier phase of cell development in OE neurons to support the increased synaptic growth. Aggrecan expression could have been reduced by the time of our observation due to compensation of high protein levels cells had accumulated at this point. While dependent on many factors, mRNAs in living cells as a rule are not very stable and decay in only a few hours in human cells (<http://book.bionumbers.org/how-fast-do-rnas-and-proteins-degrade/>). It seems likely that this is comparable if not faster in mice with their - in comparison to humans - accelerated metabolisms. Since the maturation of synapses in primary hippocampal cultures is continuous but evident only by DIV16 in most cases (Banker & Goslin,

“Culturing Nerve Cells”, MIT press, 1991) the above-described scenario is feasible, pointing to a possible dependence of aggrecan levels on Brd2 overabundance.

Overall, the data strongly suggest that two or more different transcriptional programs govern the effects we observed and that they are independent of each other. It must be noted that with the data we have collected it is not easily apparent what is a direct and what is an indirect effect of Brd2 absence or overabundance, due to the high level of interconnection between transcription, chromatin state, chromatin readers and other chromatin related factors. When studying epigenetic master regulators with hundreds of interaction partner such as BETs one needs to keep in mind that they are not only dependent on the availability of their binding sites as such. They are also very likely directly or indirectly influenced and are influenced in turn by TF activation and abundance, HATs, HDACs, HMT, histone demethylases, Dnmts, the overall DNA methylation levels inherited by the cell, the epigenetic code overall and the abundance of their interaction partner proteins themselves. It also must be mentioned that this complexity can be extended to factors like post translational protein modifications that occur outside of the nucleus, which can have enhancing as well as repressing effects on transcription (Mattioli et al. 2021). In addition, factors inside the nucleus can prevent or enhance the translation of a transcribed mRNA, such as microRNAs targeting it (e.g. suppression via RNA interference) (Li et al. 2020) or methylation of an mRNA to stabilize it (and therefore make it available for translation for a longer time) (Li et al. 2020) (Fig. 2).

Most effects on transcription we observed in the form of changes of levels of isolated nuclear mRNA from Brd2 cKO animals did not equal what we found in cell culture samples (Results Chapter 4 Fig. 7 and 9). The neuronal ECM scaffolding protein aggrecan was the exception (Results Chapter 4 Fig. 7F and 9F). As mentioned in Results Chapter 4 this could have several possible reasons including different overall chromatin or transcriptional states between cultured versus in vivo hippocampal neurons, timepoints of KO onset and effects surrounding in cell culture compared to brain tissue. We saw no immediate apparent morphological changes in our low magnification microscopy images of Brd2 cKO hippocampal slices. However, the effects one could observe in case of a transcriptional aggrecan mRNA deregulation may only be apparent when at synapses. To test if aggrecan over abundance (in the case of Brd2 OE) or deficiency (in the case of Brd2 cKO) could be involved in the behavioral

phenotypes we observed, a simple experiment would be to co-stain hippocampal slices generated from the brains of Brd2 OE and KO mice for synaptic markers as well as aggrecan, and image them by STED microscopy at high resolution. Subsequently an analysis of synaptic size and intensity combined with ECM density in the vicinity of the synapse would answer the question if the phenotype observed in cell culture (Results Chapter 4, Figure 8) is also evident in the animal and could therefore be at least partially responsible for the learning deficits Brd2 OE and cKO mice display in the Morris water maze.

Naturally, this experimental approach assumes that deregulation of aggrecan

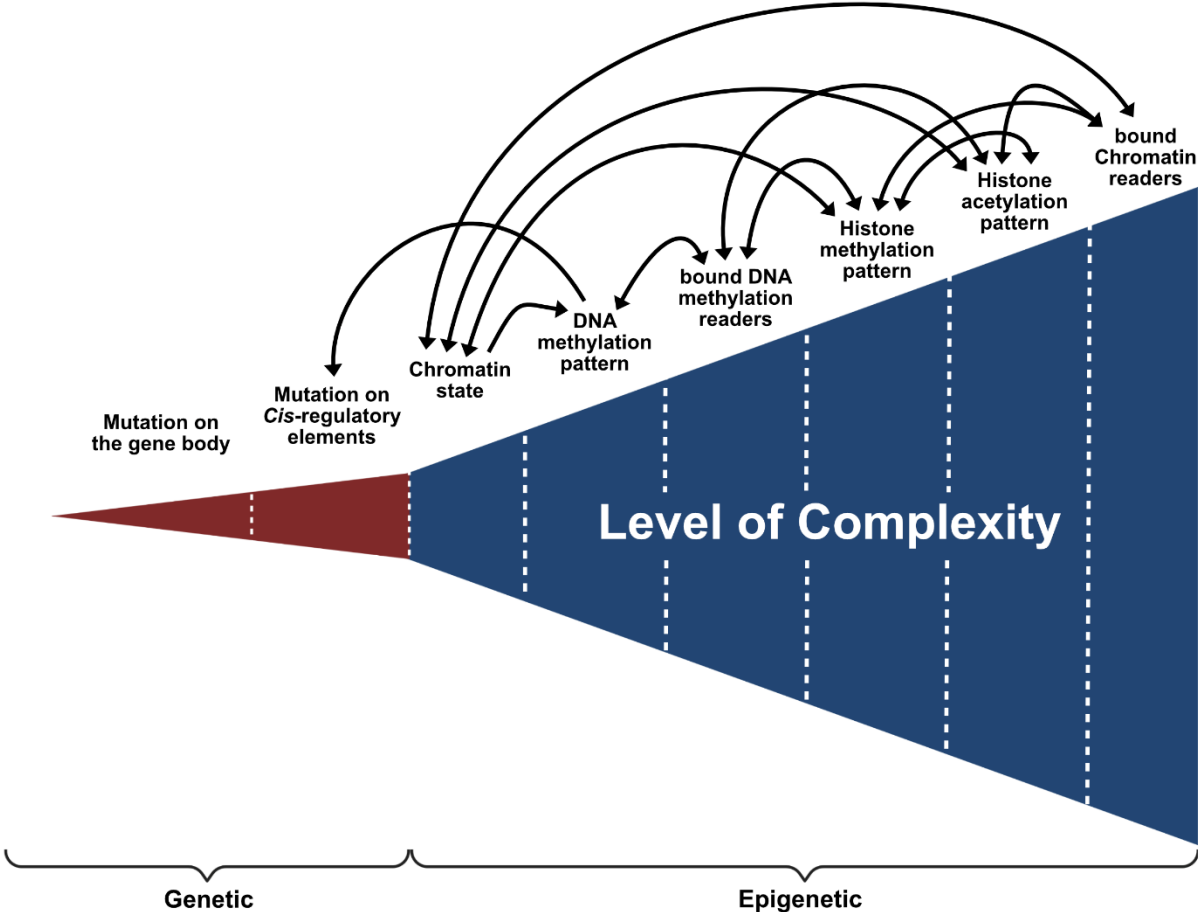


Figure 2: Depiction of the different enhancing or suppressing influences on gene transcription at the chromatin level. Arrows indicate examples of factors that directly influence each other. (Created with BioRender.com)

expression is in fact evident in OE animals which one would have to test beforehand via qPCR. If producing another Brd2 OE cohort, it seems advisable to also create an inducible Brd2 cKO line to allow later KO onset similar to OE. This could allow a better

understanding of whether the spatial memory deficit is due to Brd2 absence from around p15 onward and therefore most likely linked to postnatal brain development, or due to the absence of the BET during training of the task and thus either tied to its role in transcriptional regulation during memory formation and/or absence in newly generated neurons from the DG.

Without RNA sequencing data from Brd2 OE tissue and culture samples for direct comparison to KO and WT conditions it is challenging to cross-correlate underlying transcriptional deregulations and their possible connection to each other or to the chromatin reader in question. What can be stated with certainty concerning this data is, that a deregulation of Brd2 expression in this system has a clear detrimental effect on the overall physiological function of affected cells, at least in the aspects we experimentally observed. By the nature of Brd2 itself it cannot be excluded, that these phenotypes are more related to its overall function as a regulator of developmental and cell cycle processes. Additionally, one has to take into account that primary cell culture remains an artificial and isolated system and might not be representative of what happens in an animal itself, especially since the Brd2 KO or OE in animals takes place at a later time point when compared to cell culture in our experiments. On the other hand, our behavior data clearly shows that disturbing the finely regulated transcriptional programs that Brd2 has direct or indirect influence on, also has a detrimental effect on a mouse's performance in spatial memory tasks (Results Chapter 3 Fig. 5C and Fig. 8B). If the effects are based on developmental processes or an influence of Brd2 on transcription during training of the task is not easily answered. We found no gross apparent differences in brain structure (Results Chapter 3 Fig. 2A and B), making an exclusively developmental phenotype, at least at the macroscopic level, unlikely. This is also supported by the Brd2 over-expression via stereotactic AAV injection, which takes places in young adult animals at ten weeks of age. Here it also seems unlikely that the behavioral effect is based on changes in overall brain development since immunostainings again showed no gross morphological changes in brain structure (Results Chapter 3 Fig. 6C). If causes of the phenotype observed are indeed developmental in nature this could only be related to newly generated pyramidal neurons from the DG (see above).

To determine if one or both of our BETs of interest would localize to certain histone marks upon LTP formation I would propose another approach. Both Brd2 and Brd4

bind H4K12ac, a mark that is reduced in old mice and whose reinstatement correlates with improved performance in spatial tasks (Peleg et al. 2010). An experiment to verify if a) these BETs are recruited to H4K12ac in the case of LTP formation in a hippocampal context and b) determine which BET is more prevalent at this histone mark could give insight into their potential relevance for LTM. An approach would be to repeatedly stimulate primary hippocampal neurons in culture, or better a section of a brain slice, in a chemical or electrophysiological fashion, followed by fixation of proteins and DNA using paraformaldehyde or a similar chemical that ensures cross-linking of a BET-assembled protein complex with DNA. The resulting samples could then be processed for a chromatin immunoprecipitation (ChIP) of the respective BETs or H4K12ac itself to perform DNA sequencing (ChIPseq) or a similar analysis to detect associated molecules of interest. Since protein complexes recruiting TFs or Pol II usually do not associate with histones longer than a few seconds (Mueller et al. 2013), additionally to the stimulation paradigm a high amount of sample would be needed (estimated at least 200k nuclei/sample) to ensure enough BET is „caught“ in a chromatin binding state at the point of fixation.

Unfortunately, BET targeting antibodies we tested so far in pilot pull down experiments proved unsuited for this approach and the antibodies we found to give at least satisfactory results in western blots in terms of signal strength and specificity, often have their epitope in the area of the bromodomain, which in the case of binding to the mark and subsequent fixation should not be accessible to the antibody. One faces a similar problem when attempting to pull down an acetylated histone mark in order to identify its interaction partners as bound marks would be covered by the binding partners itself, again making it inaccessible to an antibody. To circumvent these limitations, one could transduce primary hippocampal neurons in culture or inject animals with a virus carrying a transgenic construct consisting of a bait (here the histone tail) with a nuclear localization sequence and a tag enabling an easy and effective pull down, such as an ALFA-tag (Götzke et al. 2019). However, a valid bait would still need to be proven to be acetylated *in vivo*. Even, if possible, the recruitment of BETs is, as with all chromatin readers, very dependent on other chromatin associated proteins and overall chromatin state. A baited approach in a stimulation paradigm could therefore not be considered representative and might not be feasible for this purpose.

Simultaneously, one could create a mouse line that carries two distinct small peptide tags fused to the N-terminus of Brd2 and Brd4 respectively via sequence insertion with a CRISPR/Cas9 approach. The N-Terminal regions of both Brd2 and Brd4 have a relative low complexity and are not involved in any of the protein's active sites (<https://www.rcsb.org/3d-view/5Z1R?preset=validationReport>). In tertiary structures the N-terminus is located at the periphery of both proteins, which would allow easy access for tag-specific antibodies and therefore pulldowns post fixation. While this would still not allow a measure of H4K12 acetylation in the context of BET association as such, one could at least use a digestion approach for lysine rich proteins such as histones and perform a targeted mass spectrometry for the H4K12 specific peptide resulting from the digest. A comparison to non-stimulated samples could provide a solid indication if one or both of the tagged BETs increase association with H4K12 (or another histone site of interest) in an LTP paradigm. Additionally, DNA sequencing (ChIPseq) with a portion of the same samples could allow a direct correlation to genes whose transcription is most likely suppressed or enhanced by BET proximity in the moment of fixation, especially if complemented by RNA sequencing of another portion of the same samples or samples collected at a slightly later time point to compensate for the likely scenario that the BET histone association would probably predate the changes in mRNA expression. Performing this experiment could give a clear overview of Brd2 and Brd4 recruitment and its link to transcription following LTP inducing stimulations.

In theory one could even consider performing untargeted mass spectrometry to identify members of the assembled complex predating the moment of transcription. However, one has to take into account that cross-linking tends to interfere with the digestion of proteins and untargeted mass spectrometry usually does not identify all peptides represented in a sample in the case of a low amount of input protein as expected in this scenario. This could of course potentially be counteracted if the hypothetical pull-down is very effective so that the digestive product used as input is highly enriched for the actual BET interaction partners and the BET itself and does not contain unspecific peptides. Still, this approach would require a sufficiently high amount of overall input which is not easily reached in a small tissue sample like a hippocampal slice where the target of the pulldown is also not highly abundant, assembled in the complex only temporarily, and bound to its interaction site only in a short stimulus-dependent

manner. In conclusion untargeted mass spectroscopy seems unlikely to be a very promising approach with the models proposed above.

Chromatin readers can fulfill different roles in different cell types based on their site of activity, which in turn depends on the localization of their target marks. These are in turn related to cell activity, cycle and most importantly in this respect, fate. A neuron has a different epigenetic code in the form of its histone acetylation, methylation and DNA methylation pattern than for example a liver cell (Maruyama et al. 2011). Part of these marks are actively involved in defining cell identity which therefore directly determines overall chromatin state (Srivastava et al. 2010; Sikder et al. 2020). It is important to keep this in mind especially when one studies BET chromatin readers via inhibition. To date BETs are mostly researched in relation to cancer and the effect of applying their inhibitors is usually observed in connection to this field (Fujisawa et al. 2017; Li et al. 2020). Consequently, most BET-related cancer experiments determine if an inhibitor like the often-referenced JQ1 prevent the transcription of oncogenes like myc in different cancer cell lines or tumor models. As described in the second part of Results Chapter 6 we hypothesized that JQ1 seems to have BET independent stimulative effects. Even if this was not the case (due to the reported high specificity of JQ1 and similar small molecule inhibitors for their respective pocket of target proteins) there seems to be a preference (but not exclusivity) for JQ1 targeting Brd4s BDs (Filippakopoulos et al. 2010). Since we could show that Brd2 is involved in spatial memory formation in mice and Brd4 is most likely essential for neuronal survival, it is possible that at least partial inhibition of all BETs over a longer period of time will have some unintended and potentially detrimental effects on overall cognitive performance and well-being of an organism. These hypothetical effects could potentially be masked by stimulative side effects, short application period or simply not immediately apparent if not directly tested for.

I would additionally strongly suggest the possibility that bromodomain inhibitors, if not structurally designed accurately (which might not be possible 100% due to high conservation of the bromodomain) and more importantly tested for their overall effect on the whole organism, could have unforeseen off-target effects. Additionally, to BETs, several HATs also possess BDs (Josling et al. 2012). Considering the here often referenced highly interconnected nature of chromatin modifications, one can easily imagine how cascades of unintended effects could be triggered by off-target BD-

inhibitor binding. First studies show that the application of the BET-inhibitor JQ1 on prostate cancer models not only has the opposite of the intended effect by promoting cancer invasion of other tissues, but also does this in an BET independent manner (Wang et al. 2020). This shows that even in models for the intended purpose, application of JQ1 may cause unforeseen and dangerous side effects. While cancer is a diverse field and one cannot expect one drug to work adequately on all diseases gathered under that term it is also true, that cancer cells are very prone to mutations. This makes it probable that a BET-inhibition based therapy might have two different effects on two different cancer strains existing in the patient at the same time due to independent effects on transcription.

In conclusion the data suggest, that while we have not understood BET chromatin-reader mode of action in relation to neuronal function and development in every detail, the absence of BET protein's transcription regulating effects do have a detrimental outcome on cognition, especially concerning memory formation and possibly recall in mice. It is very probable, at least in the case of the BETs studied here, that they also play an important role in the human brain - potentially related to transcriptional regulation of synaptic function or structure. This seems likely due to the high sequence conservation between species and the fact that BETs play a role in cancer phenotypes in mice as well as in humans (Jiang et al. 2020). We would suggest that, while the application of BET-inhibitors in cases of cancer or other life-threatening diseases seems reasonable, clinical studies should also screen for changes in mental state and memory performance of participants to ensure the applications of the respective drug are weighted against the side effects it might have. Development of drugs targeting single BET reader proteins as potential treatment for age-related memory impairments or the symptoms of dementia, even if very specific to an individual protein, seem unfeasible in light of the results generated during the course of this study. One has to consider, that the proteins in question could fulfill very different roles in different tissues as well as different cell types in the same tissue additionally to likely off-target effects.

The development and clinical testing of novel pharmaceuticals is extremely expensive and always faces the challenge of FDA approval, which generally requires proof of absence of detrimental side effects or a management thereof. Drugs with multiple unclear modes of action therefore have to overcome several significant hurdles with respect to approval, as is necessary to provide effective treatment

<https://www.fda.gov/drugs/development-approval-process-drugs>). The more reasonable approach would be to research if and how a certain BET (or other chromatin reader with such a high variety of interaction partners) affects transcriptional programs in a learning or neuronal stimulation paradigm and then identify a more suitable and, if possible, mono-functional downstream target in said transcriptional programs for initial verification and later possible chemical targeted inhibition. Alternatively, one could not limit focus to the role of BETs and could generally identify transcriptional changes in, for example, LTP-inducing stimulation experiments. Performed in a longitudinal way, the changes of mRNA expression in affected neurons observed in such experiments would provide a general overview of the transcriptional networks activated in memory formation. This could potentially allow for the design and testing of drugs targeting the inhibitory elements regulating these pathways to lower the stimulatory requirements for formation of LTP and therefore LTM. Since the inability to form new permanent memories out of STM is one of the first symptoms of forebrain and hippocampal dementias such as Alzheimer's disease (Naudin et al. 2014; Bastin et al. 2014) and is predated by synaptic loss which in turn is a factor in overall neuronal loss (Lowel and Singer 1992) it seems plausible that drugs with an LTP facilitating affect could serve as a remedy if not necessarily a cure for certain dementias, potentially slowing or even halting their progression.

5. SUMMARY

Transcriptional regulation (and translation) is directly linked to memory formation. The strengthening of synapses, which forms the basis of long-term memory, is dependent on the synthesis of new synaptic proteins, which in turn depends on the expression of the respective genes.

As such transcriptional regulation in neurons promises to provide potential targets for future drug-based interventions to alleviate the symptoms or even stop the progression of dementias such as Alzheimers Disease (AD). Previous studies have shed light on the existence of links between changes in the epigenetic code, which regulates transcription, upon aging, gene expression and memory (Peleg et al. 2010; Halder et al. 2016). Manipulation of the epigenetic code with pharmacological approaches can have beneficial effects in terms of affecting transcription of memory-related genes (Fischer et al 2007; Peleg et al. 2010).

Most drugs used for the manipulation of the epigenetic code come from the cancer field and target epigenetic writers and eraser, proteins that either add or remove chemical groups to or from chromatin. While these drugs do have proven effects on specific cancers and can be beneficial in studies in mouse models of neurodegeneration, the downstream modes of action are rather unclear due to the high number of different histone sites writer and eraser proteins target.

In a previous study we therefore used the small molecule inhibitor JQ1 which was developed to specifically inhibit a certain group of histone tail interaction partners, so called chromatin readers (Gilette et al. 2015; Sartor et al. 2015). These readers proteins called BET (bromodomain extra-terminal domain-containing) proteins, bind acetylated histone tail H4K12ac, a mark found to be linked to memory performance in mice and the decline thereof in aging (Peleg et al. 2010). We could show that JQ1 application did enhance memory performance and LTP in wild-type and AD model mice (Benito et al. 2017), which was contrary to what we expected from the previous data. Unfortunately, JQ1 does inhibit several BET family members including those expressed in the brain.

The goal of this thesis was to clarify if the inhibition of a specific BETs could potentially provide a pharmacological approach to treat memory-related diseases.

The aim was to identify the specific role that single, H4K12ac-targeting, BET members expressed in the brain played in the hippocampus and hippocampal-dependent memory tasks, as well as how their absence or overabundance affects transcription. For this purpose, I used BET cKO mice and primary cultures generated from embryonic brains, and over-expression constructs, in combination with next generation sequencing, bioinformatics, behavior, immunocyto- and immunohistochemistry, live cell imaging and code-based analysis thereof. Via RNAseq and immunocytochemistry I could show that the abundance of certain BETs not only has a direct impact on the expression of neuron-specific genes, but also that these changes are directly related to the expression and distribution of proteins essential for normal neuronal function. Contrary to Brd2, the postnatal knockout of the BET protein Brd4 was largely lethal; the only surviving mouse from several matings showed severe behavioral abnormalities indicative of neurological damage. Cell survival assays with primary hippocampal neurons supported this finding.

The KO of Brd2 in primary hippocampal neurons, led to a deregulation of synaptic gene expression and phenotypes indicative of lowered calcium signaling in the post-synapse. I performed two different calcium imaging approaches, analyzed with scripts I specifically coded to be accessible to other users for this purpose. Brd2 KO neurons did indeed have a lower amount of calcium signaling, consistent with a lack of the TRPC6 - channel protein that is essential for calcium storage refilling - in these neurons (Zhang et al. 2016). I could validate TRPC6 down-regulation on the protein level via immunocytochemistry in Brd2 KO neurons. The important perineuronal net protein aggrecan was also down-regulated in the nuclei of hippocampal neurons extracted from Brd2 cKO mice. This was in line with observations from behavioral tasks in which Brd2 cKO as well as Brd2 overexpressing animals showed (while overall healthy) impairments in spatial memory tasks.

In conclusion, the collected data strongly suggest that Brd2 and Brd4 do indeed play crucial roles in mouse neurons and in the brain but more importantly that neither their overabundance nor their absence has a positive effect on memory performance; the contrary is the case. While this underlines the importance of BETs in neurons and their potential importance for LTP formation, making for a promising field for further study in this context, it also suggests that BET inhibitors might not be as specific as expected. An initial fear conditioning experiment with Brd2 cKO animals suggests that the

memory enhancing effect of JQ1 and Brd2 inhibition seem to be unrelated. New studies in cancer models seem to support the assumption that JQ1 not only has off-targets (Yoa et al. 2015) but can lead to the activation of gene expression programs potentially detrimental to a patient's health (Wang et al. 2020). It seems therefore unlikely that inhibiting certain or several BETs represent a suitable approach for pharmacological intervention in dementias. While Brd2 at least clearly plays a role in the regulation of synaptic function, I would suggest to instead focus on the identification of more downstream targets of its activity to acquire drug targets with less potential side effects.

References

- Allen, N. J. and D. A. Lyons (2018). "Glia as architects of central nervous system formation and function." Science **362**(6411): 181-185.
- Anders, S., et al. (2012). "Detecting differential usage of exons from RNA-seq data." Genome Res **22**(10): 2008-2017.
- Bacsikai, B. J., et al. (1993). "Spatially resolved dynamics of cAMP and protein kinase A subunits in Aplysia sensory neurons." Science **260**(5105): 222-226.
- Bastin, C., et al. (2014). "Associative memory and its cerebral correlates in Alzheimers disease: evidence for distinct deficits of relational and conjunctive memory." Neuropsychologia **63**: 99-106.
- Benito, E., et al. (2017). "The BET/BRD inhibitor JQ1 improves brain plasticity in WT and APP mice." Transl Psychiatry **7**(9): e1239.
- Bindea, G., et al. (2009). "ClueGO: a Cytoscape plug-in to decipher functionally grouped gene ontology and pathway annotation networks." Bioinformatics **25**(8): 1091-1093.
- Bosiacki, M., et al. (2019). "Perineuronal Nets and Their Role in Synaptic Homeostasis." Int J Mol Sci **20**(17).
- Cavalleri, G. L., et al. (2007). "A multicenter study of BRD2 as a risk factor for juvenile myoclonic epilepsy." Epilepsia **48**(4): 706-712.
- Chen, V. S., et al. (2017). "Histology Atlas of the Developing Prenatal and Postnatal Mouse Central Nervous System, with Emphasis on Prenatal Days E7.5 to E18.5." Toxicol Pathol **45**(6): 705-744.
- Cheung, K. L., et al. (2017). "Distinct Roles of Brd2 and Brd4 in Potentiating the Transcriptional Program for Th17 Cell Differentiation." Mol Cell **65**(6): 1068-1080 e1065.
- Choi, J. H., et al. (2014). "Optimization of AAV expression cassettes to improve packaging capacity and transgene expression in neurons." Mol Brain **7**: 17.
- Crump, N. T., et al. (2021). "BET inhibition disrupts transcription but retains enhancer-promoter contact." Nat Commun **12**(1): 223.
- Devaiah, B. N., et al. (2016). "BRD4 is a histone acetyltransferase that evicts nucleosomes from chromatin." Nat Struct Mol Biol **23**(6): 540-548.
- Devaiah, B. N., et al. (2012). "BRD4 is an atypical kinase that phosphorylates serine2 of the RNA polymerase II carboxy-terminal domain." Proc Natl Acad Sci U S A **109**(18): 6927-6932.
- Devaiah, B. N., et al. (2012). "BRD4 is an atypical kinase that phosphorylates serine2 of the RNA polymerase II carboxy-terminal domain." Proc Natl Acad Sci U S A **109**(18): 6927-6932.
- Dey, A., et al. (2009). "Brd4 marks select genes on mitotic chromatin and directs postmitotic transcription." Mol Biol Cell **20**(23): 4899-4909.

- Dobin, A., et al. (2013). "STAR: ultrafast universal RNA-seq aligner." Bioinformatics **29**(1): 15-21.
- Ehrlich, I., et al. (2007). "PSD-95 is required for activity-driven synapse stabilization." Proc Natl Acad Sci U S A **104**(10): 4176-4181.
- Ennaceur, A. and J. Delacour (1988). "A new one-trial test for neurobiological studies of memory in rats. 1: Behavioral data." Behav Brain Res **31**(1): 47-59.
- Filippakopoulos, P., et al. (2010). "Selective inhibition of BET bromodomains." Nature **468**(7327): 1067-1073.
- Fischer, A., et al. (2007). "Recovery of learning and memory is associated with chromatin remodelling." Nature **447**(7141): 178-182.
- French, C. A. (2010). "NUT midline carcinoma." Cancer Genet Cytogenet **203**(1): 16-20.
- Fujisawa, T. and P. Filippakopoulos (2017). "Functions of bromodomain-containing proteins and their roles in homeostasis and cancer." Nat Rev Mol Cell Biol **18**(4): 246-262.
- Gandolfi, D., et al. (2017). "Activation of the CREB/c-Fos Pathway during Long-Term Synaptic Plasticity in the Cerebellum Granular Layer." Front Cell Neurosci **11**: 184.
- Garcia-Gutierrez, P., et al. (2014). "Pleiotrophin antagonizes Brd2 during neuronal differentiation." J Cell Sci **127**(Pt 11): 2554-2564.
- Garcia-Gutierrez, P., et al. (2012). "Association of bromodomain BET proteins with chromatin requires dimerization through the conserved motif B." J Cell Sci **125**(Pt 15): 3671-3680.
- Gilham, D., et al. (2021). "Bromodomain and Extraterminal Protein Inhibitor, Apabetalone (RVX-208), Reduces ACE2 Expression and Attenuates SARS-Cov-2 Infection In Vitro." Biomedicines **9**(4).
- Gillette, T. G. and J. A. Hill (2015). "Readers, writers, and erasers: chromatin as the whiteboard of heart disease." Circ Res **116**(7): 1245-1253.
- Gottschling, C., et al. (2019). "Elimination of the four extracellular matrix molecules tenascin-C, tenascin-R, brevican and neurocan alters the ratio of excitatory and inhibitory synapses." Sci Rep **9**(1): 13939.
- Gotzke, H., et al. (2019). "The ALFA-tag is a highly versatile tool for nanobody-based bioscience applications." Nat Commun **10**(1): 4403.
- Gupta, S., et al. (2010). "Histone methylation regulates memory formation." J Neurosci **30**(10): 3589-3599.
- Gyuris, A., et al. (2009). "The chromatin-targeting protein Brd2 is required for neural tube closure and embryogenesis." Biochim Biophys Acta **1789**(5): 413-421.

- Halder, R., et al. (2016). "DNA methylation changes in plasticity genes accompany the formation and maintenance of memory." Nat Neurosci **19**(1): 102-110.
- Houzelstein, D., et al. (2002). "Growth and early postimplantation defects in mice deficient for the bromodomain-containing protein Brd4." Mol Cell Biol **22**(11): 3794-3802.
- Houzelstein, D., et al. (2002). "Growth and early postimplantation defects in mice deficient for the bromodomain-containing protein Brd4." Mol Cell Biol **22**(11): 3794-3802.
- Hsu, S. C., et al. (2017). "The BET Protein BRD2 Cooperates with CTCF to Enforce Transcriptional and Architectural Boundaries." Mol Cell **66**(1): 102-116 e107.
- Huang, P., et al. (2021). "Identification of New Transcription Factors that Can Promote Pluripotent Reprogramming." Stem Cell Rev Rep.
- Hyun, K., et al. (2017). "Writing, erasing and reading histone lysine methylations." Exp Mol Med **49**(4): e324.
- Jiang, G., et al. (2020). "General mechanism of JQ1 in inhibiting various types of cancer." Mol Med Rep **21**(3): 1021-1034.
- Johanning, F. W., et al. (2015). "Ryanodine Receptor Activation Induces Long-Term Plasticity of Spine Calcium Dynamics." PLoS Biol **13**(6): e1002181.
- Josling, G. A., et al. (2012). "The role of bromodomain proteins in regulating gene expression." Genes (Basel) **3**(2): 320-343.
- Kandel, E. R. (2001). "The molecular biology of memory storage: a dialogue between genes and synapses." Science **294**(5544): 1030-1038.
- Khakh, B. S. and B. Deneen (2019). "The Emerging Nature of Astrocyte Diversity." Annu Rev Neurosci **42**: 187-207.
- Khakh, B. S. and M. V. Sofroniew (2015). "Diversity of astrocyte functions and phenotypes in neural circuits." Nat Neurosci **18**(7): 942-952.
- Kiani, C., et al. (2002). "Structure and function of aggrecan." Cell Res **12**(1): 19-32.
- Korb, E., et al. (2015). "BET protein Brd4 activates transcription in neurons and BET inhibitor Jq1 blocks memory in mice." Nat Neurosci **18**(10): 1464-1473.
- Lalonde, R. and C. Strazielle (2011). "Brain regions and genes affecting limb-clasping responses." Brain Res Rev **67**(1-2): 252-259.
- Lamprecht, M. R., et al. (2007). "CellProfiler: free, versatile software for automated biological image analysis." Biotechniques **42**(1): 71-75.
- Layouni, S., et al. (2010). "BRD2 and TAP-1 genes and juvenile myoclonic epilepsy." Neurol Sci **31**(1): 53-56.

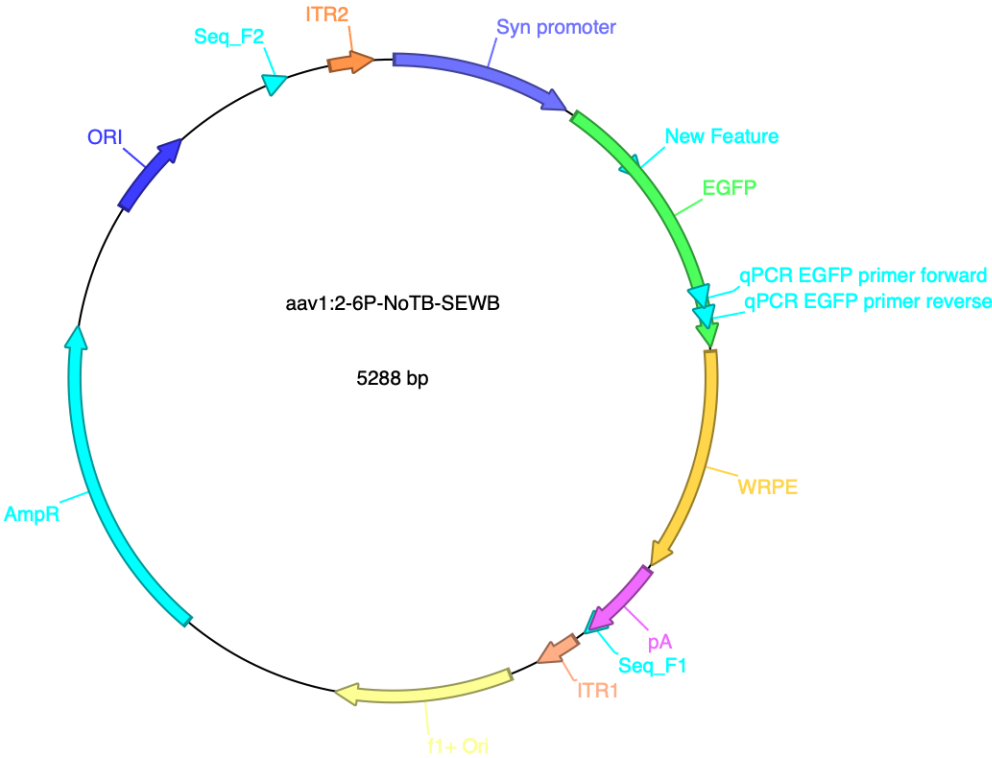
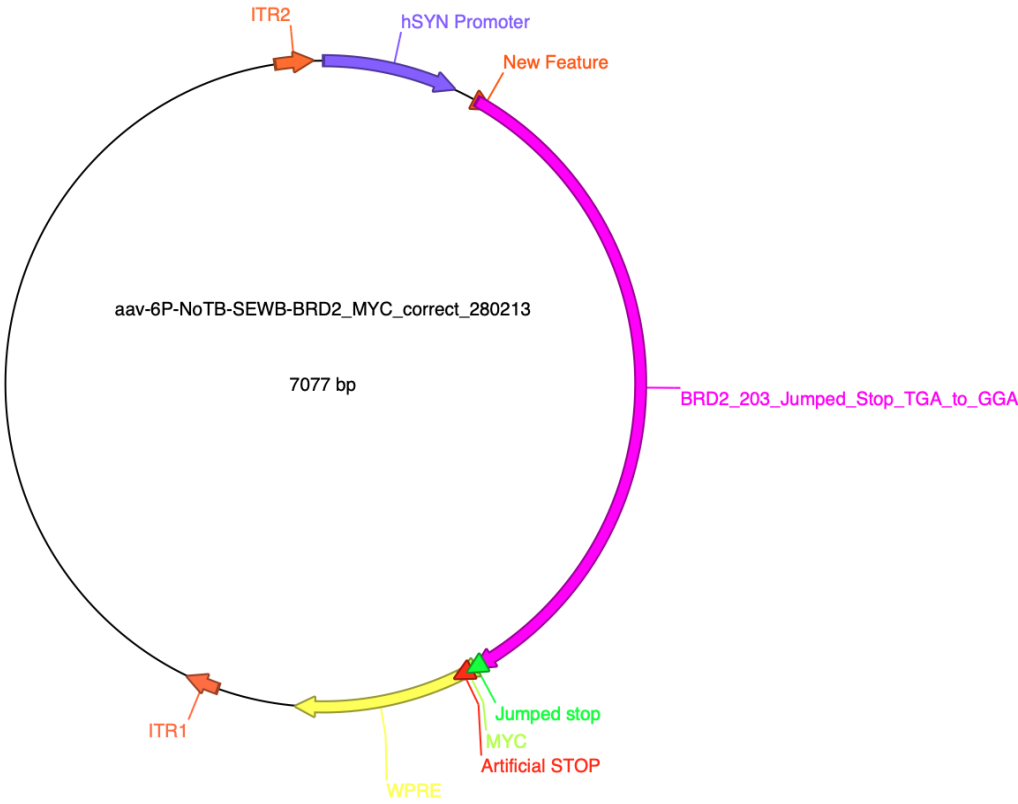
- Leal, G., et al. (2014). "BDNF-induced local protein synthesis and synaptic plasticity." Neuropharmacology **76 Pt C**: 639-656.
- LeRoy, G., et al. (2008). "The double bromodomain proteins Brd2 and Brd3 couple histone acetylation to transcription." Mol Cell **30**(1): 51-60.
- Li, F., et al. (2019). "BET inhibitor JQ1 suppresses cell proliferation via inducing autophagy and activating LKB1/AMPK in bladder cancer cells." Cancer Med **8**(10): 4792-4805.
- Li, K., et al. (2020). "Clinical and prognostic pan-cancer analysis of m6A RNA methylation regulators in four types of endocrine system tumors." Aging (Albany NY) **12**(23): 23931-23944.
- Li, Y., et al. (2020). "Natural antisense transcripts of MIR398 genes suppress microR398 processing and attenuate plant thermotolerance." Nat Commun **11**(1): 5351.
- Lin, S. C. and D. E. Bergles (2004). "Synaptic signaling between neurons and glia." Glia **47**(3): 290-298.
- Lise, M. F., et al. (2006). "Involvement of myosin Vb in glutamate receptor trafficking." J Biol Chem **281**(6): 3669-3678.
- Lorenz, S., et al. (2006). "Association of BRD2 polymorphisms with photoparoxysmal response." Neurosci Lett **400**(1-2): 135-139.
- Love, M. I., et al. (2014). "Moderated estimation of fold change and dispersion for RNA-seq data with DESeq2." Genome Biol **15**(12): 550.
- Lowel, S. and W. Singer (1992). "Selection of intrinsic horizontal connections in the visual cortex by correlated neuronal activity." Science **255**(5041): 209-212.
- Malenka, R. C., et al. (1988). "Postsynaptic calcium is sufficient for potentiation of hippocampal synaptic transmission." Science **242**(4875): 81-84.
- Martin, K. C., et al. (1997). "Synapse-specific, long-term facilitation of aplysia sensory to motor synapses: a function for local protein synthesis in memory storage." Cell **91**(7): 927-938.
- Maruyama, R., et al. (2011). "Epigenetic regulation of cell type-specific expression patterns in the human mammary epithelium." PLoS Genet **7**(4): e1001369.
- Masliah, E., et al. (1990). "Quantitative immunohistochemistry of synaptophysin in human neocortex: an alternative method to estimate density of presynaptic terminals in paraffin sections." J Histochem Cytochem **38**(6): 837-844.
- Matthews, R. T., et al. (2002). "Aggrecan glycoforms contribute to the molecular heterogeneity of perineuronal nets." J Neurosci **22**(17): 7536-7547.
- Mattioli, F. and L. Penengo (2021). "Histone Ubiquitination: An Integrative Signaling Platform in Genome Stability." Trends Genet **37**(6): 566-581.

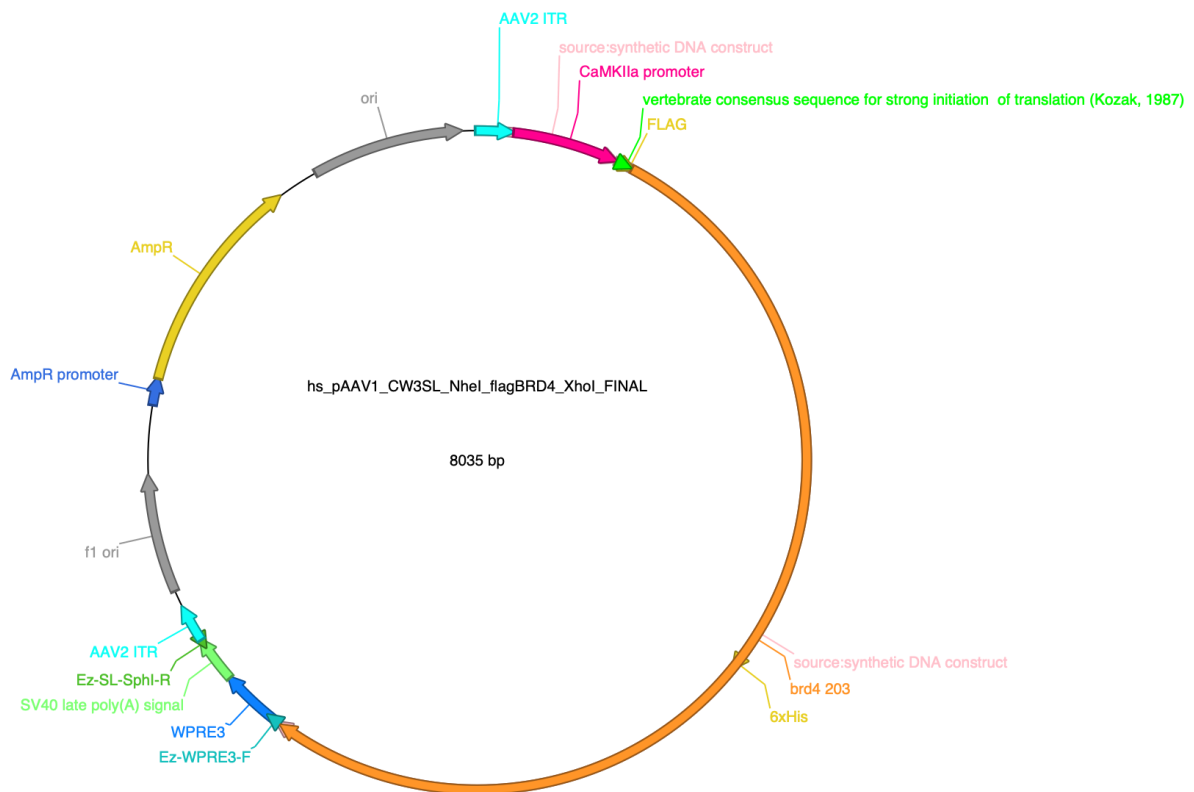
- Mayford, M., et al. (1996). "Control of memory formation through regulated expression of a CaMKII transgene." Science **274**(5293): 1678-1683.
- McClure, C., et al. (2011). "Production and titering of recombinant adeno-associated viral vectors." J Vis Exp (57): e3348.
- McHugh, T. J., et al. (1996). "Impaired hippocampal representation of space in CA1-specific NMDAR1 knockout mice." Cell **87**(7): 1339-1349.
- Moore, L. D., et al. (2013). "DNA methylation and its basic function." Neuropsychopharmacology **38**(1): 23-38.
- Morris, R. G. M. (1981). "Spatial localization does not require the presence of local cues." Learning and Motivation **12**(2): 239-260.
- Mueller, F., et al. (2013). "Quantifying transcription factor kinetics: at work or at play?" Crit Rev Biochem Mol Biol **48**(5): 492-514.
- Mueller, F., et al. (2013). "Quantifying transcription factor kinetics: at work or at play?" Crit Rev Biochem Mol Biol **48**(5): 492-514.
- Muller, S., et al. (2011). "Bromodomains as therapeutic targets." Expert Rev Mol Med **13**: e29.
- Nagayoshi, T., et al. (2017). "Hippocampal calpain is required for the consolidation and reconsolidation but not extinction of contextual fear memory." Mol Brain **10**(1): 61.
- Nakamura, Y., et al. (2007). "Crystal structure of the human BRD2 bromodomain: insights into dimerization and recognition of acetylated histone H4." J Biol Chem **282**(6): 4193-4201.
- Naudin, M., et al. (2014). "Long-term odor recognition memory in unipolar major depression and Alzheimers disease." Psychiatry Res **220**(3): 861-866.
- Nicodeme, E., et al. (2010). "Suppression of inflammation by a synthetic histone mimic." Nature **468**(7327): 1119-1123.
- Okuno, H. (2011). "Regulation and function of immediate-early genes in the brain: beyond neuronal activity markers." Neurosci Res **69**(3): 175-186.
- Peleg, S., et al. (2010). "Altered histone acetylation is associated with age-dependent memory impairment in mice." Science **328**(5979): 753-756.
- Pellow, S., et al. (1985). "Validation of open:closed arm entries in an elevated plus-maze as a measure of anxiety in the rat." J Neurosci Methods **14**(3): 149-167.
- Quezada, E., et al. (2021). "BET bromodomain inhibitors PFI-1 and JQ1 are identified in an epigenetic compound screen to enhance C9ORF72 gene expression and shown to ameliorate C9ORF72-associated pathological and behavioral abnormalities in a C9ALS/FTD model." Clin Epigenetics **13**(1): 56.
- Robichaux, M. A. and C. W. Cowan (2014). "Signaling mechanisms of axon guidance and early synaptogenesis." Curr Top Behav Neurosci **16**: 19-48.

- Robison, A. J. and E. J. Nestler (2011). "Transcriptional and epigenetic mechanisms of addiction." Nat Rev Neurosci **12**(11): 623-637.
- Sakib, M. S., et al. (2021). "Intranuclear immunostaining-based FACS protocol from embryonic cortical tissue." STAR Protoc **2**(1): 100318.
- Sartor, G. C., et al. (2015). "Epigenetic Readers of Lysine Acetylation Regulate Cocaine-Induced Plasticity." J Neurosci **35**(45): 15062-15072.
- Shang, E., et al. (2009). "Double bromodomain-containing gene Brd2 is essential for embryonic development in mouse." Dev Dyn **238**(4): 908-917.
- Shannon, P., et al. (2003). "Cytoscape: a software environment for integrated models of biomolecular interaction networks." Genome Res **13**(11): 2498-2504.
- Sikder, S., et al. (2020). "Regulation of epigenetic state by non-histone chromatin proteins and transcription factors: Implications in disease." J Biosci **45**.
- Slaker, M. L., et al. (2016). "A standardized and automated method of perineuronal net analysis using Wisteria floribunda agglutinin staining intensity." IBRO Rep **1**: 54-60.
- Sorg, B. A., et al. (2016). "Casting a Wide Net: Role of Perineuronal Nets in Neural Plasticity." J Neurosci **36**(45): 11459-11468.
- Srivastava, S., et al. (2010). "Regulation of cellular chromatin state: insights from quiescence and differentiation." Organogenesis **6**(1): 37-47.
- Stephens, A. S., et al. (2011). "Internal control genes for quantitative RT-PCR expression analysis in mouse osteoblasts, osteoclasts and macrophages." BMC Res Notes **4**: 410.
- Stilling, R. M. and A. Fischer (2011). "The role of histone acetylation in age-associated memory impairment and Alzheimer's disease." Neurobiol Learn Mem **96**(1): 19-26.
- Sullivan, J. M., et al. (2015). "Autism-like syndrome is induced by pharmacological suppression of BET proteins in young mice." J Exp Med **212**(11): 1771-1781.
- Tao-Cheng, J. H. (2019). "Stimulation induces gradual increases in the thickness and curvature of postsynaptic density of hippocampal CA1 neurons in slice cultures." Mol Brain **12**(1): 44.
- Thanawala, M. S. and W. G. Regehr (2013). "Presynaptic calcium influx controls neurotransmitter release in part by regulating the effective size of the readily releasable pool." J Neurosci **33**(11): 4625-4633.
- Ueno, H., et al. (2018). "Expression of aggrecan components in perineuronal nets in the mouse cerebral cortex." IBRO Rep **4**: 22-37.
- Ueno, H., et al. (2018). "Expression of aggrecan components in perineuronal nets in the mouse cerebral cortex." IBRO Rep **4**: 22-37.

- Umehara, T., et al. (2010). "Structural basis for acetylated histone H4 recognition by the human BRD2 bromodomain." J Biol Chem **285**(10): 7610-7618.
- Wang, L., et al. (2020). "Small molecule JQ1 promotes prostate cancer invasion via BET-independent inactivation of FOXA1." J Clin Invest **130**(4): 1782-1792.
- Wang, R., et al. (2012). "Bromodomain protein Brd4 associated with acetylated chromatin is important for maintenance of higher-order chromatin structure." J Biol Chem **287**(14): 10738-10752.
- Wang, X., et al. (2013). "Distribution of CaMKIIalpha expression in the brain in vivo, studied by CaMKIIalpha-GFP mice." Brain Res **1518**: 9-25.
- Wasiak, S., et al. (2020). "BET protein inhibitor apabetalone (RVX-208) suppresses pro-inflammatory hyper-activation of monocytes from patients with cardiovascular disease and type 2 diabetes." Clin Epigenetics **12**(1): 166.
- Wilton, D. K., et al. (2019). "Neuron-Glia Signaling in Synapse Elimination." Annu Rev Neurosci **42**: 107-127.
- Yang, Z., et al. (2005). "Recruitment of P-TEFb for stimulation of transcriptional elongation by the bromodomain protein Brd4." Mol Cell **19**(4): 535-545.
- Yao, W., et al. (2015). "The BET bromodomain inhibitor, JQ1, facilitates c-FLIP degradation and enhances TRAIL-induced apoptosis independent of BRD4 and c-Myc inhibition." Oncotarget **6**(33): 34669-34679.
- Zhang, H., et al. (2016). "Store-Operated Calcium Channel Complex in Postsynaptic Spines: A New Therapeutic Target for Alzheimer's Disease Treatment." J Neurosci **36**(47): 11837-11850.
- Zhou, Z., et al. (2020). "A Bromodomain-Containing Protein 4 (BRD4) Inhibitor Suppresses Angiogenesis by Regulating AP-1 Expression." Front Pharmacol **11**: 1043.

Appendix





Access to scripts used in this thesis:

<https://drive.google.com/drive/folders/1Y0R6LO6hcdAI6ydh2Un29yMF13X0dIYI?usp=sharing>

Acknowledgements

I want to first and foremost thank my supervisor Prof. Andre Fischer for giving me the opportunity to continue my master's project and do a PhD in his lab. I learned a lot in my time here, scientifically and otherwise, much more than I imagined I would.

Special thanks go also to the members of my thesis committee Prof. Dr. Tiago Outeiro, for good questions and even better advice and Dr. Camin Dean for her invaluable advice and help with the calcium imaging and other experiments. I would also like to thank the members of my extended examination board Prof. Ralf Heinrich, Prof. Thomas Dresbach and Dr. Jan Clemens for agreeing to take time out of their busy schedules to participate in what will probably be yet another zoom meeting of which everyone had quite enough at this point.

Additional thanks go to:

Eva Benito my old supervisor for teaching me soooooo much about science and lab work in addition to being a dear friend, working as your minion probably quadrupled my skillset in just a few months.

The old guard, Christian as a coconspirator for crazy mass spec experiments, Magda for being Magda, Hendrik for being an overall awesome friend, colleague, always reliable and helpful, not many people are, Vincenzo for advice well given, Gaurav for his passion of explaining ones and zeros to clueless master students, Tea for inspiring scientific discussion and a demonstration how many empty moldy coffee mugs one person can carry back to the kitchen in one go, I miss working with you guys.

Ricardo for, among other things, his help in many things scientific but especially for the help with visualizing the GO data. Robert for suffering through AAV production with me and being very generous with the contents of his snack drawer. Sascha for completely overpaying me with chocolate in exchange for some simple primer design and an awesome picture of a raven. Our animal caretakers, especially Jacqueline and Lea, for the effective cooperation, the helpful advice and setting up the terminated matings without which the CC experiments and therefore big parts of this thesis would have been impossible. Sakib not only for nuclei sorting and RNA extraction but also for answering all my annoyingly specific ChIPseq questions. Susi for her awesome work in general and especially for making sure the sequencings run smoothly. Tal for ECM imaging in exchange for just a few bars of dark chocolate, best deal ever. Ulli and Daniel for keeping the lights on and the institute running. The GGNB office for putting up with my tardiness and always being helpful. My graduate school for exciting scientific discussion and Prof. Dresbach again for leading these and taking care of us. My students Delane and Julia who were incredibly willing to learn and will bring it far. But especially Hanna for her great pilot work on some experiments that made it into this thesis and a steady flow of cat related memes to my inbox during the writing of this thesis.

All of my extended family whom I haven't seen in forever but of course especially my mother for being an overall awesome human being, believing in me when I did not, and well, just everything. My father for kindling my interest in how the natural world works from an early age on. Explaining the principle of energy to light conversion to a ten-year-old who asked why flames have different colors might have overdone it a bit, but no worries I got it when I started using fluorescence microscopes a good decade later. I wish you could read this dad.

And of course, everyone I forgot.

Curriculum Vitae

Henning Schroeder

Personal Information

Date of birth: 12.03.1987
Place of birth: Aix-en-Provence
Citizenship: German

Education:

2017 - present PhD candidate within the program Cellular and Molecular Physiology of the Brain at the Georg-August University of Göttingen.

Thesis title: The influence of epigenetic alterations on synaptic function and memory. Supervisor Prof. Dr. André Fischer, Dep. of Psychiatry and Psychotherapy, University Göttingen

2013 - 2017 M. Sc. Degree in Neurobiology, Thesis at the German Center for Neurodegenerative diseases (DZNE), Dept. Epigenetic Mechanisms in Dementia), Göttingen, Germany.

Thesis title: The role of BET chromatin readers in neuroepigenetics and cognition. Supervisor Prof. Dr. André Fischer, Dep. of Psychiatry and Psychotherapy, University Göttingen

2008 - 2012 B. Sc. Degree in Biology, Thesis at the Johann-Friedrich-Blumenbach Institute for Zoology and Anthropology, Dept. of Cellular Neurobiology, Georg-August-University Göttingen, Germany.

Thesis title: The regulation of reproductive behavior in female locusts via FMRamide and NO levels in the Corpora allata. Supervisor Prof. Dr. Ralf Heinrich, Dept. of Cellular Neurobiology, University Göttingen

Publication:

Benito E, Ramachandran B, **Schroeder** H, Schmidt G, Urbanke H, Burkhardt S, Capece V, Dean C, Fischer A. The BET/BRD inhibitor JQ1 improves brain plasticity in WT and APP mice, *Transl Psychiatry*. 2017 Sep 26;7(9).